UNIVERSITÄTSKLINIKUM HAMBURG-EPPENDORF

Zentrum für Diagnostik und Institut für Neuropathologie

Ärztlicher Leiter und Direktor Prof. Dr. med. Markus Glatzel

Establishing a neuron-astrocyte co-culture system to model non-cell autonomous mechanisms of neurotoxicity and synaptotoxicity in the context of Alzheimer's disease

Dissertation

zur Erlangung des Grades eines Doktors der Medizin der Medizinischen Fakultät der Universität Hamburg.

vorgelegt von:

David Wasilewski aus Berlin

Hamburg 2020

wird von der Medizinischen Fakultät ausgefüllt)

Angenommen von der
Medizinischen Fakultät der Universität Hamburg am: 22.02.2021

Veröffentlicht mit Genehmigung der
Medizinischen Fakultät der Universität Hamburg.

Prüfungsausschuss, der/die Vorsitzende: Prof. Dr. Hans-Jürgen Kreienkamp

Prüfungsausschuss, zweite/r Gutachter/in: Prof. Dr. Markus Glatzel

CONTENT

1. INTRODUCTION

1.1 Dementia and Alzheimer's disease

Alzheimer's disease (AD) is the most prevalent form of dementia in elderly individuals and accounts for approximately 60-70% of all dementia patient cases (1, 2). AD incidence will significantly increase in the upcoming decades given a growing proportion of the elderly population worldwide. Based on recent estimates of the Alzheimer's Disease International federation on global prevalence data and other reports, in 2030 the total number of people afflicted with dementia will measure approximately 66-76 million and by 2050 reaching 115-136 million, respectively (2-4). Despite this, it is only recently that AD is treated as a major public health priority sparking a marked increase in research funding (5-6). AD as such, is a chronic neurodegenerative condition accompanied by progressive and irreversible memory decline (i.e. amnestic dementia) and impairment of several cognitive domains (e.g. attention, executive functions, visual perception), ultimately interfering with daily activities and functioning (5-8). Macroscopically, on autopsy evaluation, gross neuropathologic features of brains derived from AD patients are typically suggestive of diffuse and symmetrical cerebral cortical atrophy often associated with ventricular enlargement and atrophy of subcortical white matter tracts (1, 3). Late-onset AD is a multifactorial disease, whereas early-onset AD was found to harbor distinct pathogenic mutations in genes inherited in an autosomal dominant fashion, e.g. amyloid precursor protein (APP) or presenilin 1 and 2 (PSEN1/2) (9-12). Importantly, these alterations inherent to the early-onset form lead to a malfunctioning within the APP processing pathway. APP is a protein ubiquitously found in the CNS and under physiological conditions converted into the amyloid-β (Aβ) peptide (9-13). In the context of pathological conditions however, Aβ can aggregate over time as it is occurring in AD resulting in accumulation of extracellular Aβ plaques in the neuropil and adjacent vasculature (8, 13-15). This laid the foundation for the so-called Aβ hypothesis in AD (2, 3, 11-17). Importantly, soluble, non-fibrillar or diffusible Aβ species, known as Aβ42 oligomers, are believed to play a key role during AD pathogenesis, through modulation of a variety of pathophysiological processes through-out the disease course. This implies progressive synaptic injury, which is believed to constitute an early event in the disease being present in individuals with mild cognitive decline years before clinical diagnosis of AD (13-19). For example, loss of synaptic proteins such as Synaptophysin (Syn) in comparison to brain sections from cognitive normal controls was demonstrated earlier (15, 16). Similarly, specific brain regions such as temporal lobe regions including the entorhinal cortex and the CA1 hippocampal region are known to be affected early in AD showing signs of volume loss,

followed by adjacent areas such as structures of the limbic system or isocortical areas (18-20). Notwithstanding, the detailed cellular and molecular mechanisms involved in Aβ-related synaptotoxicity remain ill-defined (1, 2, 21-24). Aβ42 species, can act in a ligand-like manner and are thought to account for neurotoxic and synaptotoxic effects, e.g. interfering with long-term potentiation (LTP) in *ex vivo* studies with hippocampal organotypic slice cultures and in *in vivo* studies with rats, respectively (23, 24). LTP at synapses accounts for synaptic plasticity and is regarded as the molecular and electrophysiological underpinning of learning and memory (23-26). Experimental data suggest that Aβ42-related effects contribute to synaptotoxicity through a vast array of molecular targets and pathways. These include membrane lipids, receptor or channel proteins activating downstream signaling events via second messengers, resulting in modification of the cytoskeleton, modulation of the production of inflammatory mediators and cell death signaling etc. (26-29). In several recent *in vivo* studies direct, low-dose and repetitive orthotopic microinjections of synthetic Aβ peptides into rodent brains resulted in learning and memory deficits (30-33). Disease features inherent to more progressive AD stages involve chronic deposition of extracellular Aβ aggregates (senile plaques) and formation of intra-neuronal neurofibrillary tangle conformers, predominantly in the neocortex. Ultimately, aggregation of hyperphosphorylated Tau protein results in overt neurotoxicity with concomitant microscopic changes including neuronal cell loss (21, 26, 27, 34). Intriguingly, abundant evidence including epidemiological, neuropathological as well as pre-clinical observations suggest that neuroinflammation could be a disease element promoting AD development and progression - independently of the Aβ hypothesis (35-38). Here, in pre-clinical AD models both astrocytes and microglia were shown to produce a variety of pro-inflammatory cytokines indicating that chronic neuroinflammation is apparent even before full-blown disease features develop (38-46).

1.2 Modeling Alzheimer's disease *in vitro*

Given its unknown etiology, accelerated research effort is of paramount importance in the light of a rising AD incidence, its significant socio-economic impact and current lack of disease-modifying treatment modalities (6, 46, 47). Aside from the abundance of pre-clinical studies on AD, there has been a steadily increasing number of clinical trials testing novel treatments to tackle AD - though, with a highly unsatisfactory success rate. For instance, from 2002 until 2012, in 413 trials a total number of 214 compounds have undergone clinical

testing overall resulting in one FDA approval in the year 2003 (46, 47). In addition to that, recently published data from several larger phase-III clinical trials probing either Aβ immunotherapy (Bapineuzumab, Solanezumab, Aducanumab) or the use of small molecule inhibitors (SMIs) directed either against γ-secretase (Semagacestat, Tarenflubil) or β-site amyloid precursor protein cleaving enzyme 1 (BACE-1) (Verubecestat, Atabecestat, Lanabecestat) unequivocally resulted in disappointment results (48-53). Along these lines, continuing collaborative effort of both pre-clinical and clinical researchers of the National Institute on Aging-Alzheimer's Association Research Framework intended to define diagnostic criteria or a research framework for preclinical stages of AD as well clinical stages of AD, i.e. mild cognitive impairment and dementia, emphasizing the fact that AD needs to be treated as a continuum with an onset typically decades before overt dementia ensues (54-57). Keeping the aforementioned failures in mind, conceptual advances in defining pre-syndromal AD and apparent limitations of the Aβ hypothesis, future trials will mandate careful planning in conjunction with extensive analyses of pre-clinical research data, ultimately testing the "right target and right drug at the right stage" (58). In this regard, existing shortages of appropriate pre-clinical models leave the exact disease onset, linearity of disease events, involved mechanistic drivers of both disease onset and progression in human AD, unknown (14, 26, 27). This in turn, hampers translation of research findings, i.e. probing potential targets for disease-modifying therapy or testing biomarkers for preemptive diagnosis of AD (14, 59). *In vivo* AD models include transgenic mouse strains, in which human genes are over-expressed, e.g. WT human APP or familial familial AD-associated APP or a combination of these (13). To a certain degree, these models mimic specific AD features such as Aβ plaque deposition or Aβ-induced synaptotoxicity. Yet, they often fail to recapitulate other disease features, e.g. the typical cognitive deficits associated with AD, neuronal cell loss or the presence of NFT (13, 60). Conversely, *ex vivo* and *in vitro* models can complement *in vivo* experiments based on several aspects which can be listed as follows:

1) E*x vivo* and *in vitro* models recapitulate aspects of disease such as Aβ-mediated neurotoxicity in AD.
2) Reduction in biologic complexity allows to manipulate cells or cell types independently of their intricate brain tissue environment encountered *in vivo*, rendering interpretation of experimental results more straightforward.

3) The relative control and stability over experimental conditions in *in vitro* or *ex vivo* assays renders them amenable to experimental manipulations allowing testing of compounds or drugs at larger scale and with higher throughput.

4) *Ex vivo* and *in vitro* models show relatively higher cost-effectiveness in comparison to *in vivo* studies.

5) Use of *ex vivo* and *in vitro* models is associated with decreased time to termination of a given experiment, i.e. the time to obtain experimental readouts from an experiment.

6) *Ex vivo* and *in vitro* models facilitate reduction of mouse experiments (principle of 3 R's) depending on the experimental set-up and scientific question (13, 59, 60).

In vitro studies in neuroscience and neurodegeneration frequently involve the use of a variety of cell-based systems ranging from established cell lines (e.g. HEK293, SH-SY5Y or PC12 cells) to primary mouse neurons, 2-D or 3-D co-culture systems, *ex vivo* organotypic hippocampal slice cultures and more recently the use of patient-derived induced pluripotent stem (iPS) cells to obtain differentiated CNS cells or even „brain organoids" (59-62). Cell lines derived from tumor tissue such as the neuroblastoma cell line SH-SY5Y or immortalized hippocampal neuronal cell lines (e.g. HT4 or HT22 cells) exhibit limited neuronal characteristics (i.e. lack of neuronal morphology and differentiation such as well-defined axons, dendrites or synapses, expression of neuronal markers and presence of a post-mitotic cell state) (63-65). Nevertheless, they have been used by numerous groups to study certain aspects of molecular and cellular processes related to neurotoxicity and neuroprotection *in vitro* since they are easily available, affordable and simple in handling (59, 63-65). In parallel, the improvement of *in vitro* primary dissociated cell culture techniques of murine (mouse or rat) hippocampal or cortical neurons throughout the last two decades, offered researchers a constant and cost-effective supply of neuronal cells for *in vitro* studies enabling researchers to model aspects of AD at least to a certain degree (59, 66-70) (*see 2.7*). As a matter of fact, all aforementioned techniques and methods inherently harbor advantages and disadvantages (59, 70, 71). Primary hippocampal or cortical mouse neuronal cultures display hallmarks of neuronal morphology and function similarly to those observed *in vivo* (72). Methods such as iPS cells from diseased patients, cell lines or slice cultures can all be: 1) relatively costly and time-consuming especially in the case of iPS models, 2) prone to bias or variability as in the particularly in the case of iPS cells but also established cell lines, which may accumulate mutations and underlie selective pressures or reduced sensitivity to toxic insults, or 3) not amenable to higher throughput exploitation and

so forth (61, 62, 71). Preparations of primary cells are commonly subjected to low-density plating onto glass surfaces (e.g. glass coverslips) where they display some phenotypic features of neurons (e.g. well-developed neurites, extensive connections and spines) allowing researchers to visualize and investigate processes of subcellular protein localization and dynamics as well as protein trafficking, cell signaling pathways, but also neurite outgrowth, axon regeneration, synaptogenesis and synaptic plasticity, etc. by either using pharmacological, forward and backward genetics as well as electrophysiological approaches (66-69, 71-74). At high densities, they usually serve for biochemical analyses such as Western blotting (73, 74).

1.3 Aim of the work

Early alterations in AD remain ill-defined and are likely associated with alterations at the level of dendritic spines as well as neuroinflammatory processes. So far, there is a lack of simple, yet validated *in vitro* models to study cellular and molecular events that may be relevant in early AD. The goal of this thesis was to establish and optimize an *in vitro* platform of primary mouse neurons following a bottom-up approach to model the process of neuronal synaptic degeneration in the context of AD. Based on a relatively well-described protocol originally published by Banker et al., our assay offers a facile and reproducible protocol, where primary neurons are co-cultured with primary astrocytes providing paracrine support, enabling proper *in vitro* differentiation of neurons (74, 75). Importantly, this model overcomes some of the difficulties of complex *in vivo* studies as it provides separate access to two main cell types of the CNS, while it still retains some complexity allowing experimental manipulations in a dish. Accordingly, we aimed to characterize our system by modeling astrocyte-mediated neuronal changes by addressing the following key aspects:

1) Characterizing acutely dissected CNS tissue and resulting primary CNS cultures in regard to survival and cell-specific marker expression of astrocytes and neurons the co-culture assay.
2) Tracking neuronal growth and differentiation in co-cultures, thus determining the optimal time window for experimental manipulations.
3) Comparison of co-cultured neurons with neurons in monocultures in terms of neuronal health status and morphometric indices.

4) Probing the impact of experimental manipulation - including Aβ42-related effects and effects of LPS - on both astrocytes and neurons to model non-cell autonomous effects on neurotoxicity and synaptotoxicity.

1.4 Primary *in vitro* cultures

1.4.1 Primary astrocyte cell cultures

1.4.1.1 Functions, morphology and markers of astrocytes

Astrocytes represent the major class of non-neuronal glial cells within the CNS with a species-specific and a brain-region-dependent astrocyte-to-neuron ratio (76, 77). Throughout the last decade, a conceptual shift occurred in how astrocytes are viewed. Traditionally, astrocytes have been seen as a relatively homogenous cell population acting primarily as supporting cells to neurons providing structural and metabolic support (classically referred to as „glue cells„) (79). Moreover, it is established that astrocytes contain heterogeneous cell subsets endowed with distinct modulatory functions in CNS development, regeneration, neuronal circuit function by accounting for tripartite synapse formation, synaptogenesis, synaptic remodeling as well as neurovascular coupling, blood-brain barrier formation and maintenance (78-80). Apart from their physiological roles, astrocytes react to virtually any type of CNS insult or injury, playing an important role in neurodegenerative diseases, e.g. AD, Parkinson's disease, amyotrophic lateral sclerosis, stroke, subarachnoid hemorrhage, intracerebral hemorrhage, traumatic brain injury and spinal cord injury, as well as in primary and secondary brain tumors (81-90). Different methodological approaches enabled researchers to further assess morphology, function or phenotype of astrocytes, as well as their transcriptional landscape under both physiological and pathological conditions (90). Characterization of astrocyte phenotypes *in vivo* as well as *in vitro* is usually conducted with immunolabelling techniques such as IF and IHC. Here, increased expression of the intermediate filament protein and pan-astrocytic marker glial fibrillary acidic protein (GFAP) has emerged as a hallmark of reactive astrogliosis (79, 90-92). Intriguingly, astrocytes can acquire an activated phenotype - generally referred to as reactive astrocytes (RAs) - characterized by hypertrophy, marked up-regulation of prototypical RA markers, namely GFAP, S100B, expression of various pro-inflammatory mediators and axon-repelling extracellular matrix proteins including other features (90-92). Nevertheless, GFAP does not meet the criteria of a universal astrocyte marker neither from

a physiological, nor a pathological standpoint. Under *in vivo* conditions in healthy CNS tissue astrocytes remain largely undetected by antibodies to GFAP. Moreover, astrocytes display heterogeneity and loco-regional differences in GFAP expression (76, 77, 93). Research in AD has been shifting steadily from a neuro-central perspective - with the Aβ hypothesis taking center stage - towards a more comprehensive picture of the disease incorporating other elements such as neuroinflammation, altered lipid metabolism, neurovascular processes, neuronal circuit-related derangements. Accordingly, appreciation and interest in the contribution of distinct CNS cell subsets such as different types of microglia, astrocytes, and other cell types is increasing (27, 39, 93, 94). This goes hand in hand with the aforementioned disappointing AD trials (52, 53). Accordingly, growing *in vitro* and *in vivo* evidence points towards an active role of astrocytes in AD disease progression (27, 93-95). On neuropathology specimens of post-mortem human tissue increased astrocytic GFAP levels as a sign of astrocyte reactivity appears even before the onset of clinical symptoms, and it proportionally increases with Braak stage (96). RAs seem to be focally distributed in association with Aβ plaques with signs of engulfed intracellular Aβ deposits, which has been thought to pose a neuroprotective barrier compartimentalizing toxic deposits, similarly the encapsulation of the damaged tissue mediated by astrocytes in ischemic stroke (97, 98). This seems to be in accordance to other observations, where crossing of the AD transgenic APP/PS1 mouse model together with a line with a GFAP -/- Vimentin -/- background results in disrupted cytoskeleton of RAs without presence of reactive gliosis and a concomitant exacerbation of Aβ burden in AP- P/PS1 GFAP -/- Vimentin -/- animals (98). Another protective effect is thought to involve one the well-established functions of astrocytes in AD, including Aβ catabolism, i.e. the uptake and degradation of Aβ *in vitro*; a this scavenger function was shown to be diminished in the case of ApoE-/- astrocytes (99, 100). The exact contribution of astrocytes in AD remains to be defined, as astrocytes likely display a spatio-temporal and context-dependent spectrum of beneficial and detrimental effector functions. Regarding this, research showed that there is no plaque load difference between the APPswe/PS1dE9 double-transgenic AD mouse model (APP/PS1), APP/PS1-GFAP -/- and APP/PS1-GFAP -/- Vimentin -/- (97, 99). Additionally, several studies indicated that *in vitro* cultured astrocytes derived from AD models or Aβ42-treated astrocytes may lose neuronal supporting functions (100-105). In this regard, Lian et al. recently demonstrated that pro-inflammatory NF-kappaB/complement 3 (C3)/C3 receptor signaling results in neurotoxic and synaptotoxic effects due to altered calcium homeostasis in neurons via binding of astrocyte-secreted molecule C3 on the C3 receptor of neurons, thus accounting for dysregulated

neuron-astroglia cross-talk in the context of AD (94). Apart from complement factors, other pro-inflammatory cytokines increased in AD specimens of humans and AD mouse models are thought to be at least in part secreted by astrocytes including IL-1β, IFN-γ, TNF-α and TGF-β (104, 105). Although with the advent and continuous improvement of *in vitro* astrocyte cultures, the use of primary astrocytes *in vitro* to probe the role of their contribution of AD has some limitations (106-111). The relative ease and reduction of *in vivo* complexity by means of culturing astrocytes together with other CNS cells (co-culture) can facilitate identification of potential pathways and interactions between astrocytes and other cells, such as neurons in the presence of Aβ pathology or various different disease situations (106). Here, it is worthwhile to mention an important caveat of *in vitro* culturing of murine astrocytes involves non-physiological serum-containing medium as well as 2D-culturing conditions which are not encountered by quiescent astrocytes in the brain. Age dependency of murine primary cells (prenatal vs. postnatal) and the fact that murine astrocytes were shown to harbor distinct genomic and functional traits to human ones are additional factors that have to be considered when drawing conclusions from *in vitro* studies (88, 107, 108).

1.4.1.2 Other glial cells as a potential resource of contamination in primary astrocyte cultures

A potential problem of primary astrocyte cultures lies in the presence of other cell types derived from the same tissue, which have not been depleted during culture. Most publications using *in vitro* primary astrocyte cultures typically follow a protocol where rodent astrocytes can be purified from mixed CNS cultures derived from rodent neonatal cortical or hippocampal tissue using a mechanical shaking-off approach. This is based on CNS-cell-type specific and selective adhesive capacities found *in vitro* (106-108, 112). Thereby, a relatively high purity of astrocytes can be achieved devoid of main contaminants, i.e. contaminating glial cell types such as microglia, oligodendrocytes, oligodendrocyte precursor cells (OPCs) or non-glial meningeal fibroblasts and ependymal cells (74, 75, 108). Several prospective techniques have been introduced to enrich and isolate primary astrocytes involving immunopanning or fluorescence activated cell sorting (FACS)-based approaches. Resultant neuronal cultures typically contain a much lower fraction of contaminating non-neuronal cells (106-108). Additionally, these approaches are not as time-consuming and allow to avoid some of the supra-physiological culture conditions of the regular astrocyte isolation and culture protocol by McCarthy and de Vellis (including

activation of astrocytes due to serum, the 2-D-surface with selection and expansion of the proliferative astrocytic cell fraction) (74, 75, 106-114). Normally, the majority of contaminating cells is deprived by the de Vellis approach using plastic surfaces and simple shaking off procedures before experiments based on selective *in vitro* adhesive capacities of astrocytes in comparison to other CNS cells or use of proliferation inhibitors (108, 111, 112). Astrocyte purity is usually assessed by means of IF co-staining for GFAP while Hoechst dye is used for counterstaining of all cell nuclei (79, 113, 114).

1.4.2 Primary neuronal cell cultures

1.4.2.1 Principles of culturing primary neurons and neuronal markers

Dispersing cells from CNS tissues such as the rodent hippocampus and seeding cells to obtain primary dissociated neurons is a widely used and invaluable tool in various neuroscience-related fields. Respective protocols have improved significantly since the 1970s (113, 115). Since this work is primarily focusing on neurons from mice, primary cultures from other species are not covered here. In case of primary hippocampal neurons, studies provided a wealth of morphological and physiological information owing to some advantages of hippocampal neurons over neurons from other CNS sites (74). Firstly, important biological and behavioral functions linked to the hippocampal and parahippocampal region including spatial and contextual learning as well as memory are based on the well-described connection between molecular and cellular processes in hippocampal neurons and their corresponding effects on processes such as neurogenesis and behavioral phenomena (116, 117). Secondly, hippocampal neuronal cultures yield a relatively homogenous cell population with a simple architecture, yet, well-defined in shape reminiscent to neurons *in vivo* with an axon and numerous dendrites forming synaptic connections undergoing five distinct developmental stages *in vitro* (74, 118). This is in contrast to cortical neurons which display by far a more heterogeneous cell population. Thirdly, culturing hippocampal neurons represents an economic, easy and simple method (74, 75, 119, 120). However, many factors can significantly influence quality and outcome of cultures as well as downstream applications and experiments depending on 1) whether embryonal or postnatal tissue is dissected, 2) which type of enzymatic tissue digestion protocol is used, 3) at which density neurons are seeded, 4) which cell culture media is used, 5) what type of coating is used for glass coverslip surface and so forth (121, 122). For instance, culturing mouse postnatal p0-1 neurons is known to be more challenging than the

culture of embryonic mouse or rat neurons given the higher plasticity and resistance of immature, embryonal neurons against the harsh conditions during tissue preparation and associated axonal shearing damage as embryonal neurons do not express as many adhesive molecules as mature, postnatal neurons (68, 74, 75). Herein, some authors argued against the use of embryonal neurons to study neuronal phenotypes linked to age-related neurodegenerative diseases such as AD, as postnatal tissue more faithfully match these conditions which however is more difficult to work with and maintain *in vitro* (67, 68). Working rigorously under defined culture conditions is an additional fundamental aspect of culturing neurons where most protocols avoid the use of serum-containing media (122-124). First of all, serum-based culture conditions contribute to experimental variability with a myriad of undetermined factors that can be found in serum and that differ from batch to batch in their concentration (122-125). Moreover, serum-based culture conditions are highly artificial given that they contain factors which are normally not present in CNS tissue, whereas serum-free media including commercial serum-supplements such as B27 and N2 offer chemically more defined conditions for neuronal cultures (88, 107, 124, 125). Apart from reducing variability of culture conditions, serum-free cultures avoid potential toxic effects of components within the serum (122, 126, 127). Importantly, in the case of single cell suspensions that are not subjected to prospective isolation of neurons as with FACS, resulting neuronal cultures typically contain a much higher contaminating non-neuronal cell fraction (128). Serum-free conditions help to curb expansion of mitotic, non-neuronal cells including astrocytes but also other types of glial cells (79, 128-130). In every primary neuronal culture, determination of the optimal seeding density poses one of the most debated problems and is probably the decisive factor accounting for overall quality and maintenance of primary neurons (128). Generally, low-density cultures are used to evaluate morphology, neurite outgrowth and dendritic spines or spine-related processes, whereas high-density cultures commonly serve for electrophysiological or biochemical analyses (74, 75, 128-130). For selective identification of freshly dissected and *in vitro* cultured neuronal cells in a non-sorted, mixed CNS culture background, several IF markers have proved to be useful. For example, a common marker is microtubule-associated protein 2 (MAP2), which is expressed especially in dendrites of both hippocampal and cortical neurons with detailed phenotypic characterization of neuronal structures as evidenced by IF using MAP2-specific antibodies (74, 75, 130). As delineated above, phenotype and behavior of neurons largely depend on plating density and quality of cultures. One reason for this observation is certainly that processes such as neuronal maturation, differentiation and synapse formation partly

underlie direct cell-cell (juxtacrine) interactions (129). Additionally, neurons in culture generally rely on growth factors, metabolites and other soluble factors for survival, proper growth, and differentiation, which are largely produced by adjacent glial cells (paracrine interactions) (74, 75). Based on some of the pitfalls of primary neurons, several possibilities exist to optimize growth and differentiation to model disease in a dish, which will be discussed below in more detail.

1.4.2.2 Neuronal Morphology - Dendritic spines, spine classification, and synaptic plasticity

As stated earlier, primary neuronal cultures can serve as a powerful tool to study isolated neurons, out of the context of their complex CNS environment. Since neurons cultured *in vitro* develop some main features reminiscent of neurons *in vivo*, dissection of molecular and cellular processes including dendrite and spine development, synaptogenesis, subcellular processes is possible (74, 118). Neurons are composed of a soma (cell body), a dendritic arbor with a myriad of extensions (referred to as dendrites or neurites) and an axon. Dendritic spines are defined as small protrusions that can be found on neurites enabling them to sequester and compartmentalize excitatory signals of the CNS, which mostly involve glutamergic excitatory inputs (131-133). Likewise, dendritic spines account for the postsynaptic component of excitatory synapses and form approximately one-to-one connections with pre-synaptic terminals. Hence, it is believed that spine density reflects synapse density (133-135). Dendritic spines contain a scaffold of actin filaments and are not static, but inherently dynamic in their 3D structure and volume by virtue of their activation-dependent synaptic plasticity. Consequently, they are regarded as anatomical correlates for synaptic transmission and plasticity, memory storage, motivation and behavioral phenomena (69, 135). Along these lines, changes in neuronal morphology, particularly at the dendritic spine level are widely accepted as salient functional features of neurons (135). In the context of neurodegenerative disorders and other CNS pathologies, morphological or numerical (qualitative or quantitative) changes at different levels (i.e. soma, dendrites and particularly dendritic spines) are believed to lead to concurrent impairment of neuronal function and/or loss of synaptic function, respectively (27, 38, 134, 135). Hence, analysis of different morphological neuronal readouts might provide vital insights into the correspondent mechanisms and pathways underlying these alterations in disease (136, 137). The basic morphological appearance of dendritic spines includes the spine head and neck, which connects both shaft and head. Moreover, spines can be sub-classified into thin, stubby and

mushroom-shaped spines (116, 130, 131). Novel, more sophisticated imaging modalities such as two-photon laser scanning microscopy enabled researchers to visualize longitudinally spine transitions, (i.e. spine formation, maintenance and loss phase) and assess functions of dendritic spines in relation to factors such as density, maturity and distance from the cell soma (116, 131). Exact mechanisms governing spine dynamics and its role in neurodegenerative diseases remain to be fully determined. Although, dendritic spines can be readily identified by using confocal laser scanning fluorescence microscopy the theoretical resolution (diffraction) limit of approximately 200 µm restricts imaging of spine plasticity. More sensitive systems such as stimulated emission depletion (STED) microscopy provide an improved imaging modality and a more reliable and precise mode of imaging (69). Manual analysis and quantification of neuronal morphology is labor-intensive and time-consuming, but also prone to intra- and inter-observer bias (136). As a consequence, different semi-automatic and automatic software tools have been developed to detect spines in 2D or 3D and annotate spine characteristics (134, 135). Standard approaches in dendritic spine analysis involve either data based on morphological (imaging), molecular or biochemical studies (i.e. qRT-PCR, Western blot). Generally, a so-called neuronal cell-fill marker is required for imaging of dendritic spines to visualize the whole neuron including its dendrites. This can be achieved by transfection of *in vitro* cultured neurons with a reporter gene such as eGFP or tdTomato (68, 74). Alternatively, several groups made use of IF staining of neurons with the MAP2 as a selective neuronal dendrite marker, thus avoiding transfection of neurons maintaining culture protocols simple and reducing artificial stressors and negative consequences on the viability of neurons. Thus, throughout this work, IF staining of MAP2 was chosen as an adequate cell-fill marker of hippocampal neurons as well as a marker of neuronal health status, similar to previous research (74, 75, 94, 118). MAP2 can later serve as a trace marker for analysis of synaptic puncta when using the freehand selection tool in the program for synaptic puncta analysis (SynPAnal) (135). Synaptophysin (Syn) is an integrated membrane glycoprotein accounting to a major part to the structural composition of synaptic vesicles and is a widely used pre-synaptic marker. Although Syn harbors neither excitatory, nor inhibitory functions, it was shown to regulate activity-dependent synapse formation in *in vitro* cultured hippocampal neurons. Positivity for Syn is apparent when synapses are already established thus serving as a late differentiation marker for neurons (136-139). For staining of dendritic spines Syn was used, to obtain density and intensity of Syn-positive (Syn+) puncta associated with the MAP2-positive (MAP2+) signals corresponding to the dendritic tree, similar to Lian et al. (94). More detailed

information on how synaptic puncta were analyzed will be provided in the method section below.

1.4.3 Neuron-astrocyte co-cultures

1.4.3.1 Applications and benefit of co-cultures systems

Considering the wealth of publications involving primary neurons, it is common that neurons subjected to experiments are often not properly differentiated with cells dying-off after several days *in vitro*. This in turn can influence outcome of experiments (74, 75, 116). A marked improvement of long-term survival, overall neuronal health, onset of growth and differentiation *in vitro* has been achieved by the use of conditioned medium (CM) derived from astrocytes (aCM) or by co-culturing of neurons and astrocytes as compared to neurons which were neither treated with aCM, nor co-cultured with astrocytes (124, 141, 142). This is based on the observation that neurons under *in vitro* conditions depend on paracrine neurotrophic support, specifically provided by astrocytes, as other cell types do not recapitulate the beneficial effect of neuron-astrocyte co-cultures. This system seemingly mimics some of the specific reciprocal, interactions *in vivo* encompassing a wide range of different soluble factors such as lipids, thrombospondins, and glypicans (143). Importantly, juxtacrine interactions between neurons and astrocytes are not involved, as both are separated and cultured in the same media (74, 75). Hence, neuron-glia co-cultures are an established *in vitro* model to probe the reciprocal interactions of these cell types underlying neurite outgrowth, synapse formation and transmission (74, 75) (***Fig. 1***). Co-cultures are of value in other fields such as drug and neurotoxicity testing and aid in reducing animal studies - whenever feasible (144-147). In fact, seeding density is application-driven. Activity-dependent changes or biochemical assays are reliant on higher neuron densities, whereas morphological and imaging-related studies require low-density cultures to prevent overgrowth of primary cultures and fasciculations of neighboring dendrites (75).

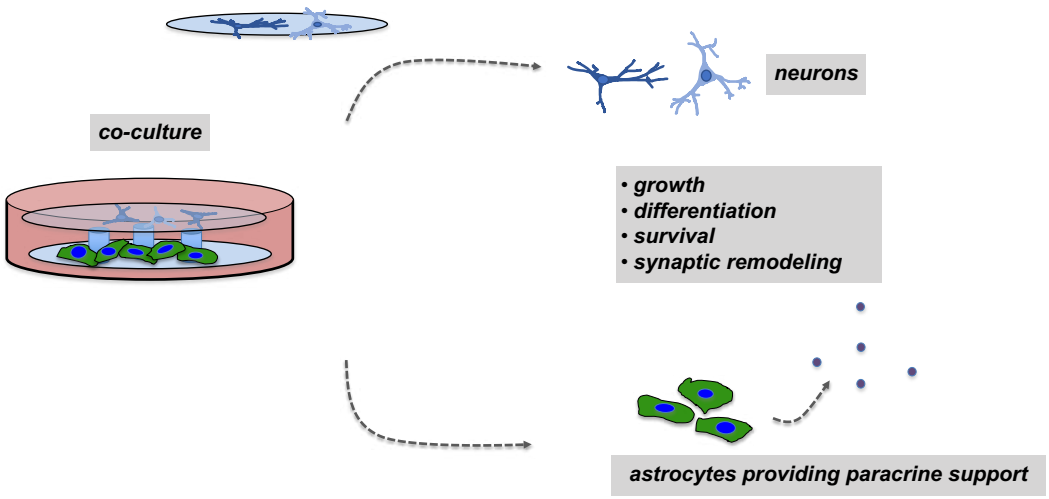

Fig. 1 The principle of the Banker sandwich *in vitro* co-culture assay: Astrocyte feeder cells plated at the bottom of a multi-well plastic dish containing a glass coverslip is the internal part of the neuron-astrocyte „sandwich" co-culture model allowing paracrine support of co-cultured neurons suspended over the feeder cells, resulting in proper neuronal growth and differentiation *in vitro*.

Particularly, in the latter case, neuronal preparations and culture protocols can be associated with insufficient long-term viability and differentiation including misshaped, or atrophic neurons) (74, 115, 124, 129, 141, 142). Interestingly, Yang et al. stated in their recent study that low-density cultures of neuronal cells could be spurred in their growth and development by adding media of older, more mature neuronal cultures (116). Accordingly, data from cell culture experiments suggest that not only paracrine support by means of CM from astrocyte feeder cells but also autocrine (neuronal) support may provide proper environmental cues and factors that enhance proliferation and development of neuronal cultures (74, 116). Possible variations of paracrine support cultures avoiding co-cultures with direct cell-cell contact have been introduced for *in vitro* culturing of primary neurons, including co-culturing neurons with a) mixed primary co-cultures, b) pure primary astrocyte cultures (referred as to astrocyte feeder cells) or c) use of CM derived from mixed primary cultures, d) use of aCM or e) CM derived from primary neuronal cultures) (75, 116, 124, 141-143). In the present work a modified version of the well-known protocol of *in vitro* neuron-astrocyte co-cultures (also referred to as neuron-astrocyte "sandwich" co-cultures) was established. This co-culture model is an experimental assay where postnatal (p0-1) primary mouse hippocampal neurons are grown in defined, serum-free conditions on the underside of a glass coverslip suspended over a layer of primary mouse astrocytes (74, 75). Initially, this assay was performed with embryonal rat neurons and first described by Banker

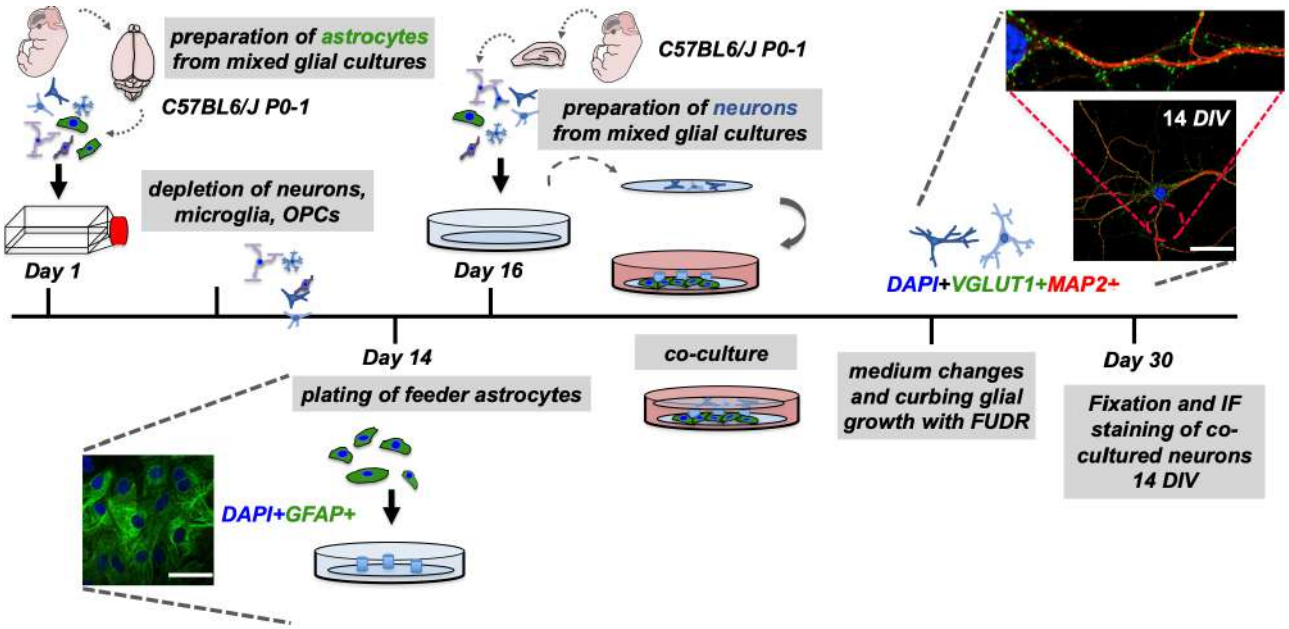

Fig. 2 Workflow of the neuron-astrocyte co-culture assay: This graphical abstract depicts the modified „Banker" assay developed in this thesis adapted from Banker et al. involving two different preparations to obtain mixed CNS cell cultures. The protocol allows to co-culture a layer of feeder cells on a lower coverslip together with an inverted upper coverslip containing mainly neuronal cells. Cells were stained *via* IF and correspondent representative images were taken with Leica SP5 (Leica, Wetzlar, Germany), scale bar = 50 um.

and colleagues (74, 112, 117). Neurons cultured in this manner become polarized and establish axonal and dendritic arbors, where dendrites are studded with *bona fide* spines and functional synaptic connections, respectively (74). (***Fig. 1 and 2***). Primary mouse neurons plated on a glass coverslip which is inverted and hanged over the astrocyte feeder layer - with the wax dots serving as a physical barrier between feeder layer and neurons - can be cultured at least two weeks *in vitro* resulting in properly differentiated dendritic projections and dendritic spines (74, 75). Hence, our modified two-coverslip „sandwich„ co-cultures provides a simple modular assay offering a platform for experimental manipulations of neurons and/or astrocytes allowing to study dendritic spine-related neuronal (cell-autonomous) but also astrocytic (non-cell-autonomous) processes, e.g. impact of astrocytes on dendritic spine development and degeneration (74, 75, 144, 145, 148, 149).

1.4.4 Experimental manipulations of primary CNS cultures

1.4.4.1 Pre-treatment of primary astrocytes for induction of astrocyte reactivity

Primary neuronal cultures provide a valuable experimental tool in multiple areas of neuroscience research including research on AD (75). For example, an experimental set-up to probe aspects of the Aβ hypothesis with *in vitro* primary neurons commonly involves the external administration of synthetic Aβ species, particularly solubilized Aβ42 or the use of CM with naturally secreted Aβ oligomers derived from established and transfected cell lines

(e.g. CHO cells) expressing transgenes such as the human APP (67, 73, 147). Further, transgene expression of APP or Tau in primary neurons via viral transfection using adenoviral vectors was recently introduced to induce increased Aβ production and secretion in neurons in a more efficient and physiological manner with accelerated toxic effects due to Tau overexpression (73). In addition to that, multiple pro-inflammatory factors including cytokines were shown to be linked to an increase in the APP production in different models (i.e. in the mouse brain *in vivo*, in cell lines as well as primary cultures of astrocytes) (150-151). In fact, there is a well-accepted notion that AD is accompanied by chronic inflammation involving for instance activation of astrocytes and microglia as well as activation of complement factors and inflammasomes. At the same time, low-grade systemic inflammatory conditions such as periodontitis represent independent risk factors for AD (151, 152). A common practice in research on AD and neuroinflammation is to induce chronic inflammation both in the *in vivo* and *in vitro* setting with administration of the endotoxin LPS activating inflammatory signaling pathways, either via intraperitoneal injections in mice or addition of LPS into media of cell cultures. LPS can induce a reactive phenotype in astrocytes, often referred to as RAs leading to an increase in APP expression (42-45, 151). Furthermore, in their recent study Liddelow et al. described (in analogy to M1 and M2 macrophages and microglia found in different neuroinflammatory conditions) different phenotypes of astrocytes termed A1 and A2 astrocytes with LPS being an inducer of A1 astrocytes (79, 83). While A1 astrocytes are believed to exert neurotoxic effects with high expression of genes of the complement cascade such as C3, A2 astrocytes have been shown to exert neuro-protective effects via upregulation of neurotrophic and synaptogenic factors (79, 83). Nevertheless, the classification into A1 and A2 astrocytes is still under debate, yet it will promote investigation of disease-specific phenotypes of astrocytes in the future (83). In this work, we used Aβ42 (with Aβscr as its correspondent negative control) and LPS (with water as its correspondent negative control) to model aspects of AD including Aβ- and LPS-mediated effects on astrocytes including indirect effects on neurons. In doing so, treatment with Aβ42 or LPS over 24 h served for induction of A1 astrocytes (i.e. induction of a RA phenotype). After treatment, media in which astrocytes were cultured, were changed to fresh media without LPS or Aβ42. Lastly, differentiated cultured for 14 *DIV* neurons were inverted over pre-treated astrocytes to assess the impact of RAs on neuronal morphology and phenotype focusing specifically on synaptic puncta.

1.4.5 Methods used for morphological characterization and quantification of co-cultured neurons

Common morphometric measurements of neurons found in publications across sub-disciplines include different approaches to quantify soma size, neurite length, outgrowth and complexity, as well as synaptic puncta density including spine classification. The aim of this work was to obtain multiple readouts from a given experiment of the introduced co-culture model, offering a simple and fast multi-parametric measurement (multiplexing) of the health status of co-cultured neurons in the context of experimental manipulations (153-155).

1.4.5.1 Soma size

Amongst different readouts of neuronal morphometry, soma size provides an additional means through which morphological characterization and quantification of given phenotypes of CNS cells is possible, as for instance, in neurodegenerative diseases such as Rett syndrome (154). Here, soma size was examined manually in confocal 1024 x 1024-pixel images (zoom = 1,2x) by outlining the soma in the red channel visualizing MAP2+ neuronal somata and dendrites. As delineated above, MAP2+ is a cell-fill marker of neurons, i.e. highlighting soma and dendrites and faithfully depicts neuronal morphology (74). During manual outlining of neuronal somata using ImageJ software, dendrites were omitted.

1.4.5.2 Integrated density and corrected total cell fluorescence

To quantify changes of fluorescence intensity of a given cell marker of interest (e.g. signal intensity of MAP2 or synaptic markers such as Syn) relative to the untreated group of samples IntDen or corrected total cell fluorescence (CTCF) served as readouts. Color threshold was set and maintained constant for each neurons and astrocytes analyzed for each of the three independent experiments. Mean gray values per image or outlined area were calculated *via* ImageJ. IntDen could be obtained by measured grey value with outline surface area (156-163). According to previous publications, fluorescence intensity values as a readout reflect protein content and can be expressed as IntDen or CTCF, where the background mean gray value (BMGV) is incorporated resulting in the following calculation: CTCF = (integrated density - (area of selected cell * mean fluorescence of background)) (162-166).

1.4.5.3 Sholl analysis

In 1953, Sholl developed a technique enabling reliable quantification of indices of axon length and neurite branching complexity (164). Sholl analysis is accessible as a plug-in either for ImageJ14 programmed in Java and bundled in Fiji15, a distribution of ImageJ providing a platform for analysis of 2D or 3D images of fluorescence-labeled cells. Characterizing neuronal morphology and quantifying neurite branching in a physiologic or a disease context provides a valuable means to screen compounds, that display potential neuroprotective and neurotoxic activity, respectively (164, 165). Sholl analysis is commonly used to characterize and quantify effects of genetic and pharmacological manipulations on CNS cell types, but can also be applied to study retinal vasculature, angiogenesis and mammary duct sprouting (166). The resulting Sholl profile based on a cell-fill marker (in this study MAP2) depicts the branching pattern of dendrites and axons by plotting the number of branches as a function of the distance from a defined location, most commonly the center of a cell, namely the soma. Consequently, the number of MAP2+ neurites that intersect with those drawn circles are plotted as a function of radial distance from the soma (166, 167). Drawbacks of Sholl analysis include labor-intensive image processing, even in case of programs allowing semi-automated analyses since pre-processing of digital images is inevitable (166, 167). Here, we conducted analysis of linear Sholl plots of our primary neurons. Polynomial regression can be used describe relationships between the number of intersections and distance to the soma. According to Ferreira et al. the following key indices can be extracted from linear Sholl plots (166) (***Fig. 3***):

- Critical value (Nm): The maximum of the polynomial function, an indicator of maximal branching.
- Critical radius (rc). The distance at which the Critical value occurs.
- Mean value of the polynomial function (Nav): Implies the average number of intersections between the starting radius and enclosing radius

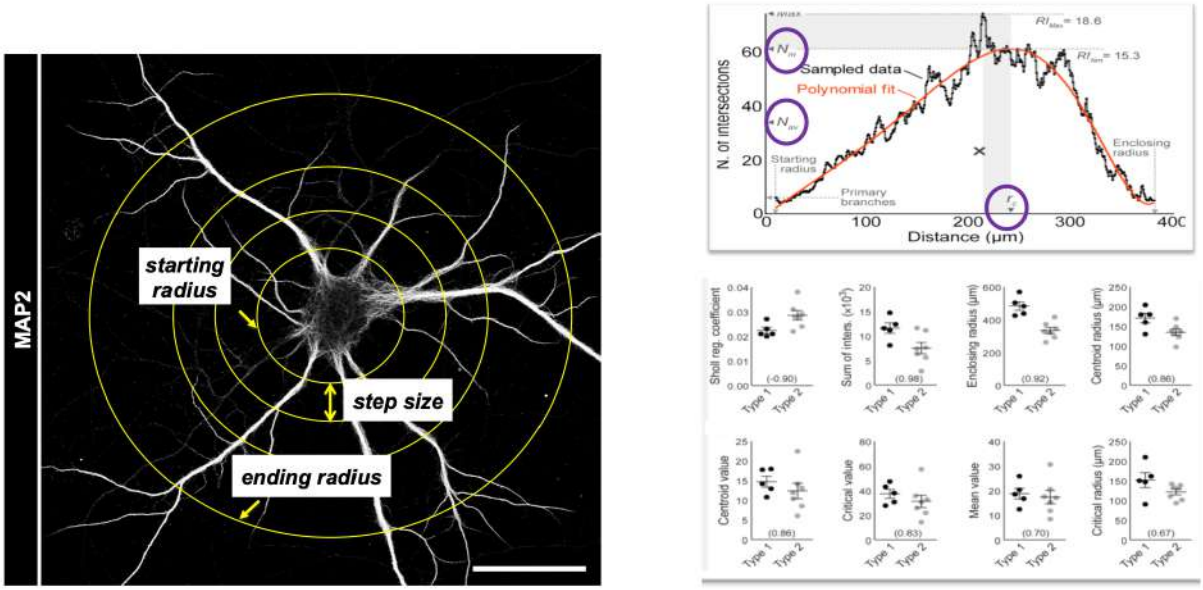

Fig. 3 Sholl plotting and Sholl-based morphometric values: A representative picture of a co-cultured hippocampal neuron (14 *DIV*) stained for MAP2 (used as a cell-fill marker) by means of IF with superimposed concentric circles used for Sholll analysis (**left**). Sholl plotting similar to Ferreria et al., Nature Methods, 2014 with Sholl plot and resulting Sholl metrics displayed (**right**) (taken and adapted from Ferreria et al., Nature Methods, 2014). Images were taken with Leica SP5 (Leica, Wetzlar, Germany), scale bar = 50 um.

1.4.5.4 Synaptic puncta analysis

Imaging of spine alterations is an informative and common readout in neuroscience (137, 168). Since synaptic puncta attributes (e.g. changes in density, size and intensity) are linked to function of synaptic signal transduction, neuronal circuits and synaptic plasticity, but also synaptotoxicity, there is a wealth of existing image software packages performing analysis of synaptic puncta. However, the concurrent analysis often turns out to be a time-consuming and labor-intensive task (168-169). In view of the need for more reliable and time-saving analysis, Danielson and Lee developed Synaptic Puncta Analysis, henceforth referred to as SynPAnal, a software written with JAVA to perform unbiased, semi-automatic quantification of synaptic puncta (here Syn+ puncta) in 2D confocal laser scanning microscopy images of IF labelled neurons (137). SynPAnal measures fluorescence intensity, and morphometric analyses of neurons including dendrite length, spine density, and dimensions as well as classification of spine types based on puncta detection at multiple thresholds and semi-automatic dendrite tracking. Finally, SynPAnal was shown to provide a timesaving, valid and effective means to study localization and distribution of synaptic associated proteins in dendritic spines and will be employed in this thesis as one key method to analyze the effect of experimental manipulation on neuronal cells (74, 75, 137, 168).

2. MATERIAL AND METHODS

2.1 Materials and Reagents

For more details refer to the protocol described in section neuron-astrocyte co-cultures. Whenever possible and specified in a data sheet, catalog number (Cat#), product number (Product#) or reference number (Ref#) are listed of each product or model number (Model#) in case of laboratory equipment.

Autoclave, Technoclav50, ibs Tecnomara, Fernwald, Germany
Binocular stereomicroscope, Bresser Advance ICD, Bresser, Rhede, Germany
Biophotometer Plus, Eppendorf, Hamburg, Germany
Cell culture incubator, safe cell UV, Panasonic, Kadoma-Osaka, Japan
Cell culture incubator, Heraeus CO2 incubator, Fisher Scientific, Pittsburgh, PA, USA
Centrifuge 5810/5810 R, Eppendorf, Hamburg, Germany
Centrifuge Eppendorf F45-24-11 and 5417R, Eppendorf, Hamburg, Germany
Confocal microscope TCS SP5, Wetzlar, Germany
Confocal microscope TCS SP8, Wetzlar, Germany
Countess™ II Automated Cell Counter, Thermo Scientific, Waltham, MA, USA
4°C fridge, Liebherr Profi line, Liebherr, Bulle, Switzerland
Inverted microscope, Nikon Eclipse TS100, Zeiss, Oberkochen, Germany
Inverted microscope, Axiovert S100, Minato-Tokyo, Japan
Lamp KL 1500 LCD, Schott, Mainz, Germany
Loading balance, Sartorius CP3202S, Data Weighing Systems, Inc., Wood Dale, IL, USA
Magnetic stirrer with heating, RCT basic IKAMAG, IKA-Werke, Staufen, Germany
Mixer, IKA MS3 digital, Model# ms3d, Fisher Scientific, Schwerte, Germany
pH Meter, Schott Gerate CG 840 pH Meter, Schott, Mainz, Germany
Pipetboy, Pipeteboy Acu 2, Inegra Biosciences, Hudson, NH, USA

Printer, P93D, Mitsubishi, Tokyo, Japan
Staining rack, Thomas Scientific, Cat# 8542E40, Swedesboro, NJ, USA
Thermo Scientific -86°C freezer, tsx series, Model# tsx60086v, Thermo Scientific, Waltham, MA, USA
Vortexer, Vortex Genie 2, Scientific Industries, Bohemia, NY, USA

Table 1: Lab equipment

BD Luer-Lok tip 20 mL syringe, Cat# 309650, Becton Dickinson, Franklin Lakes, NJ, USA
Cell strainer von BD Biosciences, Cat# 352350, Becton Dickinson, Franklin Lakes, NJ, USA
Cellstar 50 mL Tubes, Cat# 227261, Greiner Bio-one, Krensmünser, Austria
Cellstar 15 mL Tubes, Cat# 188271, Greiner Bio-one, Krensmünser, Austria
Countess cell counting chamber slides, Cat# C10283, Thermo Scientific, Waltham, MA, USA
Facial tissues, 2-ply, Cat# 07730012, Tapira Plus, Heidenheim, Germany
Microscope round cover glasses #1,5 12 mm Menzel-Gläser 1000 Deckgläser/cover slips, Cat# 11846933, Fisher Scientific part of Thermo Scientific, Waltham, MA, USA
Microscope round cover glasses #1,5 mm (for co-cultures subjected to MTT assay), Cat# 72296-05, Science Services, München
Nunclon Delta Surface, sterile 12 well cell cultures plastic dish, Cat# 150628, Thermo Scientific, Waltham, MA, USA
PARAFILM M, Cat# P7793, Sigma, Saint Louis, MO, USA
Corning universal fit pipet tips, 1-200 uL, Cat# CLS4860, Corning, NY 14831, USA
Plastic pipette tips, Corning universal fit pipet tips, 1-200 uL, Cat# CLS4867
Safe-lock Eppendorf tubes 1,5 mL, Cat# 2025-12-28, Eppendorf, Germany, Hamburg
Serological pipette 5 mL, Cat# 86.1253.001, Sarstedt, Nürnbrecht, Germany

Serological pipette 15 mL Cat# 86.1254.001, Sarstedt, Nürnbrecht, Germany
Serological pipette 50 mL, Cat# 356525, Durham, USA
Tip stack pack 10 uL pipette tips, Cat# 70.1130.460, Sarstedt, Nümbrecht, Germany
Tip stack pack 20 uL pipette tips, Cat# 70.760.502, Sarstedt, Nümbrecht, Germany
Tissue culture dish 60, standard with grid, Ref# 83.3901.002, Sarstedt, Nürnbrecht, Germany
Tissue culture flask T75, Cat# 83.3911.002, Sarstedt Nürnbrecht, Germany
Tissue culture dish, Nunclon delta surface, Cat# 150628, Thermo Scientific, Waltham, MA, USA
Cell strainer von BD Biosciences, Cat# 352350, Becton Dickinson, Franklin Lakes, USA

Table 2: Disposable synthetic and plastic material

Aβ42, Aβ42-TFA, Cat# A-42-T-1, GenicBio, Shanghai, China
Aβscr, Aβ-scrambled, Cat# A-42-S-1, GenicBio, Shanghai, China
Anti-FSP antibody, produced in rabbit, Cat# ABF32, Millipore, Burlington, MA, USA
Anti-GFAP antibody, produced in mouse, Cat# MAB360, clone GA5, Millipore, Burlington, MA, USA
Anti-GLAST antibody, produced in rabbit, Cat# ab416, Abcam, Cambridge, UK
Anti-MAP2 antibody, produced in mouse, Cat# M9942, Sigma, Saint Louis, MO, USA
Anti-Iba1 antibody, produced in rabbit, Cat# 019-19741, Wako Pure Chemical Industries, Osaka, Japan
Anti-MABN50 Olig2, produced in mouse, Cat# MABN50, Millipore, Burlington, MA, USA
Anti-MAB345 O4, produced in mouse, Cat# MAB245, Millipore, Burlington, MA, USA
Anti-smooth muscle actin antibody, produced in rabbit, Cat# ab5694, Abcam, Cambridge, UK
Anti-synaptophysin antibody, produced in rabbit, Cat# ab32594, Abcam, Cambridge, UK

Anti-VGAT antibody, produced in rabbit, Cat# 131 022, Synaptic Systems, Göttingen, Germany
Anti-VGlutT1 antibody, produced in rabbit, Cat#135 302, Synaptic Systems, Göttingen, Germany
Bovine serum albumine, Cat# A9647-50G, Sigma, Saint Louis, MO, USA
B-27 Serum-Free Supplement (50X) liquid, Cat# 17504-001 or 17504-044, Gibco, CA, Carlsbad, USA
CellTiter 96 Non-radioactive Cell Proliferation Assay, Cat# S G4000 and G4100, Promega, Madison, WI, USA
Cytosine ß-D-arabinoside, Cat# C1768-100MG, Sigma, Saint Louis, MO, USA
DAPI Fluoromount-G, SouthernBiotech, Cat# 0100-20, Birmingham, AL, USA
Destilled water from UKE water supply device, 2. OG, Campus Forschung, Hamburg, Germany
DMSO >/= 99%, Sigma Aldrich, Cat#M81802 Aldrich, Sigma, Saint Louis, MO, USA
Donkey anti-rabbit Alexa 555, Cat# 31572, Thermo Scientific, Waltham, MA, USA
Donkey anti-rabbit Alexa 488, Cat# A21206, Thermo Scientific, Waltham, MA, USA
DPBS 1x no calcium, no magnesium, no phenol red, 500 mL, Gibco, Cat# 14190144, Carlsbad, CA, USA
DNase I grade II, from bovine pancreas, Cat# 10104159001, ROCHE, Basel, Switzerland
Dumont no. 5 forceps: Cat# 11252-23, Fine Science Tools, Heidelberg, Germany
Eppendorf Research plus pipette, 10, 100, 1000 uL, Cat# Z683825, Hamburg, Germany
Ethanol (EtOH), 100%, Cat# 100983, Merck Millipore, Burlington, MA, USA
Fetal Bovine Serum (FBS), 500 mL, Cat# 10270-106, Gibco, Carlsbad, USA
5-Fluoro-2'-Deoxyuridine (FUDR), Cat# F0503-100MG, Lot# 110M1212V, Sigma, Saint Louis, MO, USA

D-(+)-Glucose solution, 45% in H_2O, sterile-filtered, BioXtra, suitable for cell culture, G8769, Sigma aldrich
GlutaMAX™-I supplement, Gibco, Cat# 35050-038, Carlsbad, CA, USA
HEPES buffer, 1M pH 7,3: Cat# 15630-080, Thermo Scientific, Waltham, MA, USA
HBSS 10X with Calcium and Magnesium, without Phenolred, Cat# 14065056, Thermo Scientific, Waltham, MA, USA
Natriumtetraborat (Borax), Riedel-deHaen, Cat# 11648, RdH Laborchemikalien GbH & Ko KG, Germany
Neurobasal, Cat# 21103-049, Invitrogen, Carlsbad, CA, USA
ParaffinShandon™ Paraffin, Cat# 501006, Thermo Scientific, Waltham, MA, USA
Paraformaldehyde (PFA) 16% solution, EM Grade Cat# 15710, Electron Microscopy Sciences, Hatfield, PA, USA
Penicillin Streptomycin (Pen Strep), 100 mL, Cat# 15140-122, Gibco, Carlsbad, USA
Poly-L-Lysine hydrobromide 25 mg, Cat# p2636-25MG, Lot# SLBP4080V, Sigma, Saint Louis, MO, USA
Primocin, Cat# ant—pm-1, Lot# PML38-04A, Invivogen, San Diego, CA, USA
0.05% Trypsin-EDTA (1x), 100 mL, Cat# 25300-054, Lot# 1801701, Gibco, Carlsbad, USA
2.5% Trypsin (10x), 100 mL, Cat# 15090-046, Lot# 1797254, Gibco, Carlsbad, USA

Table 3: Reagents including antibodies

2.2 Animals and primary cell cultures

All research procedures involving animals were according to and approved by the animal care and ethics committee of the UKE. Primary astrocyte and neuronal cultures were derived from male or female p0-1 C57BL/6J mice (Charles Rivers, Wilmington, MA, USA) as described by Kaech and Banker (74) (***Fig 2***).

2.3 Specific steps of our modified neuron-astrocyte „sandwich„ co-culture assay

The following section will provide our protocol with slight modifications of the original Banker protocol specifying its distinct steps in a sequential manner (***Fig. 2***).

1. **Preparation of plastic multi-well plates and glass coverslips**
2. **Preparation of reagents and media**
3. **Propagation and expansion of astrocyte feeder cells**
4. **Seeding of astrocyte feeder cells onto lower glass coverslips**
5. **Preconditioning of astrocyte feeder cells**
6. **Coating of neuronal (upper) glass coverslips**
7. **Preparation and seeding of mixed primary CNS cells onto upper glass coverslips**
8. **Inversion of the neuronal (upper) coverslip over the feeder layer**
9. **Maintenance of co-cultures including monitoring, medium changes and treatment**

1. Preparation of 12-well plates and glass coverslips

One important modification introduced in this study that differs from the classic Banker protocol for neuron-astrocyte co-cultures consists in the incorporation of a second glass coverslip, that is placed in the bottom of a well of a 24 well plate (12 mm in diameter for 24 well plates and 18 mm in diameter for 12-well format). Hence, the model in this study does not only involve an upper (neuronal) coverslip being suspended over the feeder layer, but also a lower (astrocytic) coverslip at the bottom of the well (***Fig. 1, 2***). Importantly, on top of the lower coverslips paraffin wax dots were plated in a triangular fashion before plating of astrocytes serving as a spacer or physical barrier between the two cell types and glass coverslips, respectively (***Fig. 1, 2, 4***) (74). Whereas glass coverslips for neurons (upper coverslip) require special treatment before use including nitric acid-based treatment and banking at 200°C, coverslips used for astrocytes did not require any treatment (74). The rationale for this is the importance of proper attachment to glass surface cell in case of neurons to facilitate their growth and differentiation *in vitro*. Conversely, astrocytes are known to adhere to glass coverslips without special treatment of glass surfaces (68, 74). To attach paraffin wax dots onto glass coverslips placed in wells of a multi-well plates, a sufficient amount of paraffin pellets was melted in a glass container over a heating plate. Work under sterile conditions and with good pace are crucial. Optimal temperature to

produce roundly shaped paraffin wax dots adhering to the plate was found to be at 110°C (***Fig. 4***) Temperatures below that can lead to insufficient adhesion of paraffin wax dots, which can potentially lead to detachment later during cell culture. At the same time, paraffin should not be too hot in order to avoid spreading of the paraffin over the surface of the plastic dish (74). Finally, plastic dishes with coverslips inside the wells of a multi-well plate were covered with wax dots and plates were irradiated with UV light under the bench for at least 30 min. Plates were kept under sterile conditions until use for experiments. Again, for

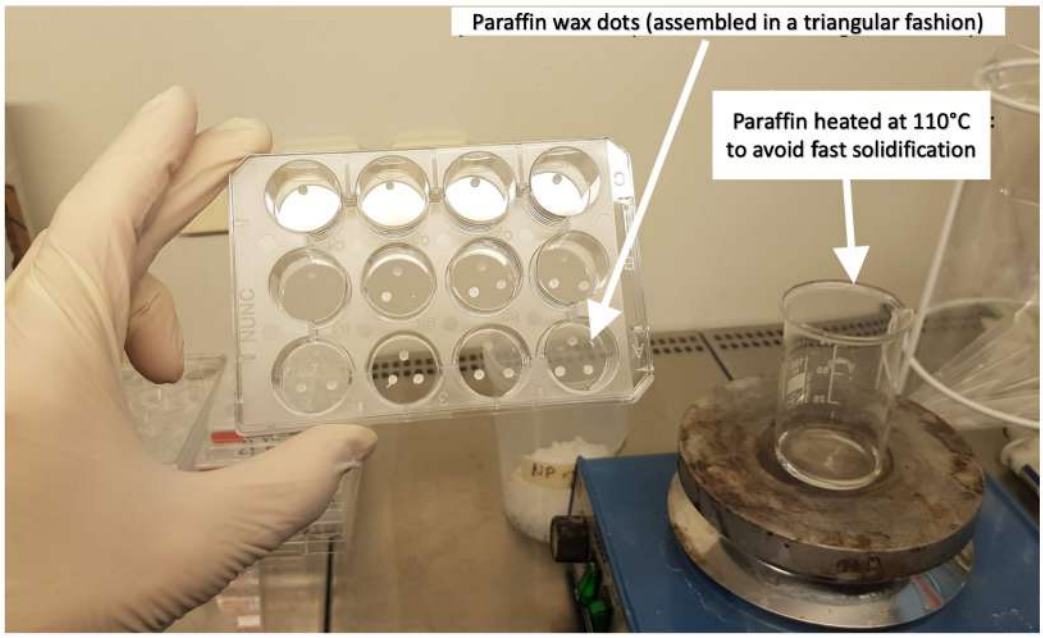

Fig. 4 Assembling triangular parrafin wax dots on glass coverslips in wells of a 12-well plastic dish: To establish a physical barrier between lower layer and upper layer of sandwich co-cultures, glass coverslips placed at the bottom of multi-well plastic dishes were equipped with paraffin wax dots assembled in a triangular fashion with subsequent plating of astrocytes on prepared glass coverslips (i.e. lower layer or lower coverslip).

coverslips that serve for future upper coverlips, a special pre-treatment was mandatory involving nitric acid treatment and backing of the glass coverslips. Glass coverslips were placed into ceramic racks, rinsed with ddH20, placed in 65% nitric acid for at least 18h to roughen the surface of glass coverslips allowing improved attachment conditions for neuronal cells (68, 74). Subsequently, the glass coverslips were rinsed three times for 3 min with ddH2O, placed in 96% EtOH for 30 min and again rinsed three times for 3 min with ddH2O 5 min and lastly placed under the hood to dry and irradiate with UV for at least 30 min. Finally, treated and dried coverslips were baked at 200°C for at least four hours. Coverslips and plates were kept under sterile conditions (74).

2. Preparation of reagents and media

Dissection medium (DM) as well as astrocyte growth medium, henceforth referred to as glial growth medium (GGM) were prepared according to previous protocols (67, 70, 74) (***Table***

4). All agents for dissection of mouse tissue and cell culture were subjected to filter-sterilization with 0.22 µm filter devices under the bench. Throughout work proper

Medium or solution	Components
Dissection medium (DM) (stored at 4°C)	HBSS 1x (HBSS 10x 1:10 in MiliQ water) + 1% P/S + 10 mM Hepes (from 1M stock solution, i.e. 1:100 dilution) + 0,6% of 45% Glucose solution, store at 4°C up to 14 days
Glial growth medium (GGM) (stored at 4°C)	DMEM + 0,6% v/v glucose (from 45% glucose solution, sterile) + 1% P/S + 10% FBS, store at 4°C up to 4 weeks
poly-L-lysine (PLL) (stored at -20°C)	borate buffer (1,24 g boric acid + 1,90 g of borax + 400 mL H2O, final pH 8,5, final volume 400 mL (stirred some hours to dissolve and filter-sterilized) + polylysine hydrobromide (P2636-25mg, Sigma) at a a concentration of 25 mg/25 mL) in borate buffer, aliquoted
neuronal maintenance medium (NMM) (stored at 4°C)	Neurobasal 50 mL + 1% 200 mM Glutamax with a final concentration of 2 mM, i.e. 500 uL/50 mL medium + 2% (v/v) B27 serum supplement, i.e. 1 mL/50 mL medium + 1% P/S, store at 4°C 1 month, only 50 mL aliquots of NMM were produced and storage was not longer than 10-12 days

Table 4: Media and solutions for primary cultures

technique and preventive measures against contamination were applied (e.g. desinfection of surfaces with 70% EtOH, wearing gloves and a face mask) (***Fig. 5***). Additionally, for each day of dissection of pups the following equipment, materials and reagents should be at hand (***Fig. 5***): Cell culture incubator 36.5°C and 5% CO2 laminar flow hood, water bath at 37°C, dissection microscope, which was not incorporated into the laminar flow hood, but outside of the hood. Thus, mouse tissue dissection occurred under semi-sterile conditions. Further, autoclaved fine-tipped dissection tools, and 50 mL vials filled with DM and with 70% EtOH for intermediate cleaning of dissection tools throughout the procedure of tissue handling and dissection had to be prepared in advance to every dissection (***Fig. 5***). To avoid overt tissue hypoxia and damage, dissected tissue should be kept chilled in an icebox, which should be prepared in advance. Further, 15 mL and 50 mL sterile falcon tubes, plastic pipettes, 60 mm cell culture dishes, 75cm2 plastic tissue culture flasks, 4x p0-1 C57BL/6J #2020 mouse pups, fresh Trypsin 2,5% (10x), DNase I 1mg/mL, cell counter (Countess II Automated Cell

Counter, Thermo Scientific, Waltham, MA, USA), Trypan blue, cell strainer with 70 µm mesh should be available before onset of dissection (***Fig. 5***).

3. Propagation and expansion of astrocyte feeder cells

Primary mouse cortical astrocytes were derived from mixed CNS cultures from p0-1 dissected C57BL/6J mouse brains (dissection #1, two weeks before neuronal dissection, i.e. dissection #2). All surfaces were wiped down and autoclaved dissection tools were kept in 70% EtOH after unpacking, immediately before use they were rinsed with DM. Sterile 60 mm cell culture dishes were prepared under the bench and filled each with cold filtered DM, kept on ice as normally multiple brains were dissected at dissection day and subjected to the protocol (***Fig. 5***). Dissection tools were stored in 50 mL vials filled with 70% EtOH, and for each part of the dissection (skin, skull, brain) different dissection tools were used and stored separate vials to minimize the risk of contamination (***Fig. 5)***. A towel was then moistened with 70% EtOH to carefully wipe head and neck of each pup. Right away, pups were decapitated. The head was immersed for a few seconds in 70% EtOH by putting it into a cap of a 50 mL plastic falcon. Sterile plastic caps from 15 or 30 mL falcons were stored in a bag for this specific step to avoid excessive use of plastic to save resources. After two subsequent washes in 70% EtOH heads were transferred immediately to a new 60 mm dish

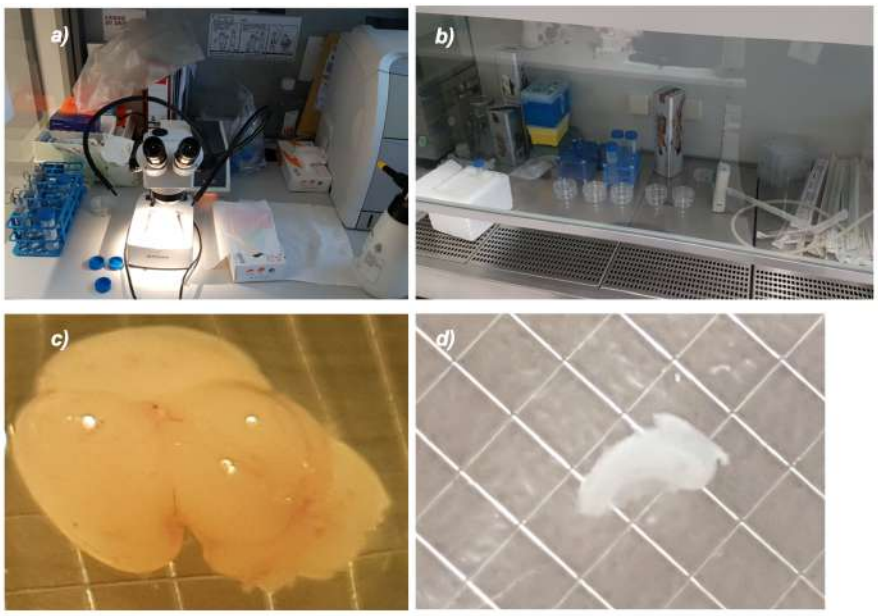

Fig. 5 Dissection of cortical and hippocampal mouse tissue to obtain mixed primary CNS cultures for downstream neuron-astrocyte co-cultures: a) and b) show the semi-sterile workplace outside the bench and sterile work place inside the bench during mouse tissue dissection at dissection day, whereas c) demonstrates an extracted mouse brain and d) a hippocampal tissue slice about to be subjected to enzymatic treatment and trituration to obtain a single-cell suspension of hippocampal cultures.

filled with chilled DM. Next, the skin flap of the skull was removed using dissection tools. To reduce the chance for a contamination each of the different structures (i.e. skin, skull, and

brain) were handled with different dissection tools (**Fig. 5**) Next, a cut along the sagittal suture line was performed and the skull was removed in a similar fashion as done with the skin flap using bended forceps. Finally, the brain was extracted using curved forceps and placed into a 60 mm dish with chilled DM. Under a binocular microscope, hemispheres with the correspondent rostral cerebellum were separated by cutting along the inter-hemispheric suture using curved forceps (***Fig. 5***). Curved forceps served for removal of meninges and visible blood vessels associated with the choroid plexus. Insufficient removal of meninges and choroid plexus will likely lead to contamination with meningeal fibroblasts and endothelial cells (68, 74). Both, cerebellum and diencephalon were removed and discarded. Accordingly, per mouse two halves of the original cortex and two hippocampi were obtained and placed in a 15 mL falcon with chilled DM and placed on ice. Generally, tissue from 4 mice was pooled to obtain a sufficient amount of cells for both cortical and hippocampal cultures. From this step onwards, sterile conditions under the bench were maintained. Under the bench tissue was transferred with a 5 mL Pasteur pipette into a 15 mL falcon tube. Freshly dissected tissue was kept in 15 mL falcons on ice. After tissue reconstitution, 2 mL of DM including tissue pieces were transferred into a 60 mm dish. Total volume of DM should reach 4,5 mL DM with 0,5 mL pre-warmed 2,5% Trypsin added. The resulting mixture was incubated at 37°C for 15 min in the cell incubator at horizontal agitation with 400 rpm. 60 mm dishes were covered with parafilm to avoid evaporation and potential changes in concentrations of the enzyme during incubation) (74, 75). After 15 min of enzymatic tissue digestion with Trypsin, 100 µL of sterile 1mg/mL DNase I was added into the 60 mm dish, which then was gently swirled. After approximately 1 min 5 mL of GGM was added to quench the enzymatic reaction. In case of dissection #2 (to seed cells for the neuronal coverslip) neuronal maintenance medium (NMM) was used instead of GGM to avoid serum-containing conditions during neuronal dissection). Gentle trituration with a blue 1000 µL pipet (10 times) was followed by transfer of the mixture (10 mL total volume) into a new 15 mL vial. A centrifugation step (5 min at 1000 rpm) followed. Trituration is regarded by many researchers as a key step as it minimizes variations in the yield and viability of primary CNS cells (74, 75). Next, supernatant was decanted to obtain a small pellet. Using a 5 mL plastic pipette 2 mL of GGM was added. Gentle trituration was performed with a fire-polished glass pipette (7 times). After tissue was able to sink and reconstitute, tissue was subjected to another trituration step (7 times). Additional 2 mL of GGM were added to the cell suspension as a wash step followed by 5 min centrifugation at 1000 rpm. Again, the resulting supernatant was decanted and the pellet resolved in 2 mL GGM. A 70 µm cell strainer was

placed over a 50 mL vial. The surface of the cell strainer was incubated with 500 µL of GGM 1 min before smashing cells through the cell strainer (pre-equilibration of the membrane). Subsequently, the cell suspension was mixed by gently pipetting up and down 3 times. Cells were then smashed through the cell strainer and the 15 mL falcon washed with an additional volume of 500 mL of GGM, which were transferred onto the cell strainer with the 50 mL vial. Another fresh 1000 µL pipette tip was used to aspirate the remaining cell suspension from the bottom side of the cell strainer to salvage cells that still adhered to the surface of the cell strainer). Two halves of cortices yield approximately 1.200.000/mL in a total volume of 4 mL (***Fig. 5, 6***). The cell suspension was then plated into a T75cm2 plastic flask, which was filled up to 12,5 mL of GGM according to previously published protocols (74, 94, 116). Next day, medium was changed with an intermittent wash step with DPBS 1x (74, 75, 112). Mixed CNS cultures were monitored with medium changes and one wash step every 5-7 days. Potential contaminating cell types such as microglia or OPCs were removed as described previously by de Vellis (74, 75). Briefly, before plating primary astrocytes for co-culture experiments onto plates prepared with coverslips and wax dots in advance, mixed CNS cell cultures were subjected to overnight shaking at 500 rpm at 37°C to reduce the amount of microglia (108).

4. Seeding of astrocyte feeder cells onto lower glass coverslips

Plating of astrocyte feeder cells originating from the first dissection (dissection #1) was issued 48 hours before “neuronal” dissection (dissection #2). First, the T75 cm2 flask with mixed primary CNS cells was put on an orbital shaker for at least 24 hours to get rid of contaminating non-astrocytic cells (75). Briefly, before plating T75 cm2 flask was subjected to a mechanical shaking off by repetitively exercising force against the ground of the flask 10x times (75). Subsequently, the T75 cm2 flask was washed 1x with DPBS1x and trypsinized for 10-15 min. Trypsin was removed by spinning down 1000 rpm for 5 min. 80.000 astrocytes were plated per well of a 24-well plate on top of a 12 or 18 mm coverslip equipped with 3 wax dots (lower coverslip) (***Fig. 2, 4, 5***).

5. Pre-conditioning of astrocyte feeder cells

Medium was changed 24 h after plating (i.e. 24 h before neuronal dissection) from GGM to NMM with a total per-well-volume of 1 mL), which marks the onset of pre-conditioning of the NMM medium, where later neurons will be co-cultured. Pre-conditioning facilitates growth and maturation of neurons upon initiation of co-cultures (74) (***Fig. 1, Fig. 2***).

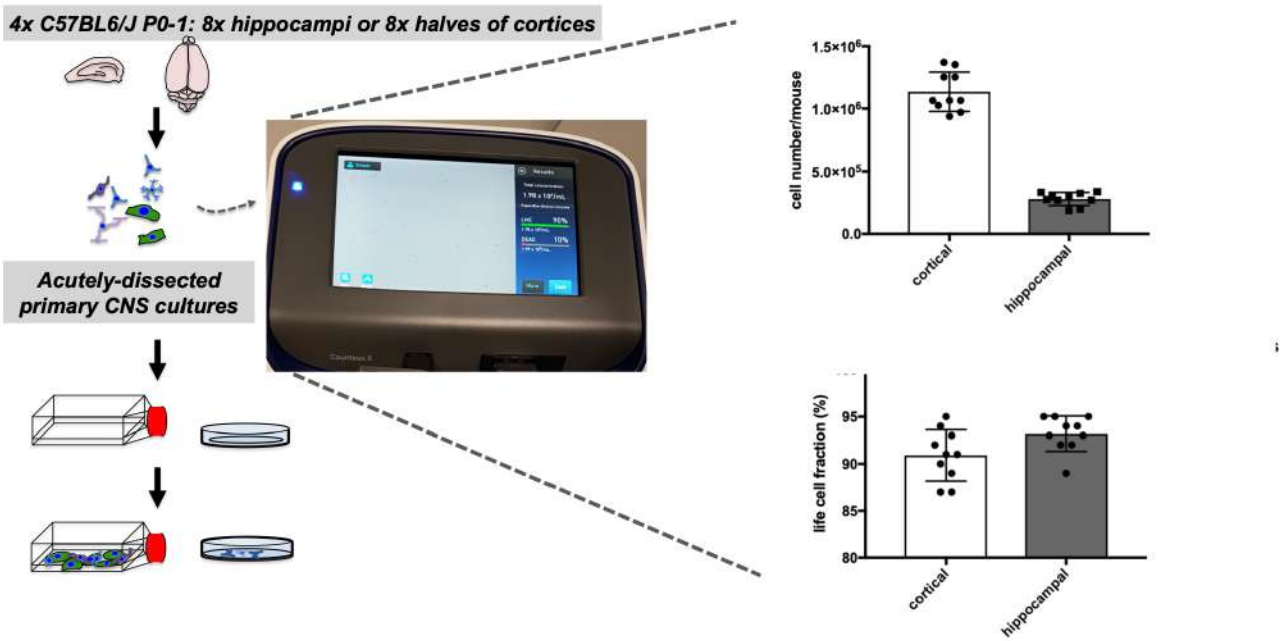

Fig. 6 Assessment of cell viability and cell number of viable cells upon acute dissection: Single cell suspension derived from acutely dissected mouse brains (N = 10 mice) subjected to a protocol (including enzymatic digestion, trituration and centrifugation steps) were assessed using the Thermo Scientific Countess II cell counter. Data analysis was performed using GraphPad Prism 8 (GraphPad Software Inc, La Jolla, CA).

6. Coating of neuronal (upper) glass coverslips

To ensure optimal adhesion of freshly dissected neuronal cells on glass, coverslips were placed in wells of a separate multi-well dish (12-well or 24-well plate) and each coverslip was treated with PLL at least 24 hours before neuronal dissection. PLL was dissolved at 1 mg/mL in 0.1 M borate buffer, which was prepared according to Beaudoin et al. III. pH was set to 8.5 (1,9 g borax + 1,24 g boric acid in 400 mL H2O) and filter-sterilized (68, 74). Approximately 1 mL PLL solution was added to each coverslip, to assure that each glass coverslip within a well was fully covered by PLL solution. Drying of coated coverslips should be avoided. PLL solution was removed with three washes using DPBS1x shortly before plating the neurons. DPBS1x was left just until the plating (68, 74).

7. Dissection and plating of mouse neurons

For the second “neuronal” dissection (dissection #2), working steps were similar to that of astrocytes preparation explained above. However, serum-free NMM was used according to established protocols (***Table 4***) (74) In case of work with transgenic mice where genotyping is mandatory, hippocampi or cortices from mice should not be pooled. Cell counting was accomplished semi-automatically by using Countess™ II Automated Cell Counter (Thermo Scientific, Waltham, MA, USA). Here, digital images are taken in one focal plane of the loaded cell suspension stained with Trypan blue dye and its software analyzes binary 1-bit

images. Cell count is based on the Trypan blue dye exclusion method, in which only membranes of dead cells are readily penetrated by the Trypan blue dye allowing exclusive labelling of dead cells. Semi-automated viable cell counting was preferred over the manual mode of cell counting for the sake of time and increase in accuracy by reducing counting variability (data not shown). Plating of cells was adapted according to needs, e.g. 200.000 cells/well were plated for Western blotting (WB) experiments (data not shown), whereas 50.000 or 25.000 cells were regarded as optimal for imaging of high-density and low-density cultures, respectively). Typically, four mice with hippocampi dissected and pooled together yield approximately 500.000 cells/mL in 4 mL of a total volume (***Fig. 6***), whereas two cortices yield 1.200.000 cell/mL in 4 mL of total volume. Cell viability was evaluated semi-automatically using a cell counter based on Trypan blue exclusion and should normally range between 85-90% (***Fig. 6***). One hour after seeding neuronal cells onto Poly-L-lysine-coated (100 µg/mL end concentration) 12 mm-glass coverslips, coverslips were flipped and inverted over the astrocyte feeder layer plated previously onto different wells of distinct 24-well plastic dish. Co-cultures were regularly monitored and maintained for two weeks in a humidified atmosphere of 5% CO2 at 37°C before experimental manipulation as well as immunostaining or cell lysis. Medium changes of the co-cultures were performed every four days, with the first medium change including the thymidylate synthase inhibitor 5-Fluoro-2'-Deoxyuridine (FUDR) at a concentration of 10 µM to deplete other mitotic cell types such as microglia, oligodendrocytes, fibroblasts and to dampen glial proliferation in the upper coverslips. Cytosin ß-D-arabinoside (AraC), also referred to as Cytarabin is often used for curbing glial overproliferation, however in comparison to FUDR, increased neurotoxicity was associated with the use of AraC (data not shown) (74). Three independent cultures were used for all *in vitro* experiments.

8. Inversion of the upper coverslip with seeded neurons over the feeder layer

One hour upon plating of freshly dissected cells onto PLL-coated glass coverslips, coverslips were inverted and hanged over the feeder layer (74, 75). Now, wax dots of the lower coverslip can function as spacers and ensure proper separation between upper and lower coverslip. In our experience, one hour to-inversion-time seems superior to 3 hours to-inversion-time in terms of time and glial contamination of the upper coverslip later on (no data shown; 74).

9. Maintenance of co-culture including monitoring, medium changes and treatment

After inversion of the upper coverslip and commencement of co-culture, daily monitoring of the co-cultures was necessary (***Fig. 7, 8***). Furthermore, media needed to be changed every four days removing 50% of medium under of each well of the 12-well plates with co-cultures under the bench by using a 1000 µL pipette. Right after withdrawing a proportion of old media, the same amount of fresh NMM was added. Here, it is key to add a mitotic inhibitor in the very first medium change of the co-culture, whereas subsequent medium changes did not include a mitotic inhibitor. FUDR was regularly used at a concentration of 10 µM. AraC at a concentration of 2 µM can serve as an alternative - however, we observed better results with FUDR (no data shown). Additionally, it is more neurotoxic according to the current literature (68, 70, 74, 75).

2.4 Oligomeric Aβ peptide preparation and pre-treatment of astrocytes with Aβ42 and LPS

Oligomeric Aβ - either Aβscr as an internal (negative) control or Aβ42 serving as the treatment - was used to model Aβ-related effects as done in a multitude of other studies focusing on synaptotoxicity (33, 173). In this study neurons were not directly exposed to Aβ species but co-cultured with Aβ-treated astrocytes to probe indirect (non-cell-autonomous) synaptotoxic effects. 2mM stock solutions of Aβ42 or Aβscr were purchased (GenicBio, Shanghai, China) and prepared according to Falker et al. (174). Briefly, commercial Aβscr or Aβ42 were dissolved in 110 µL ultra-filtered Dimethyl sulfoxide (DMSO) with a subsequent centrifugation step 5000 x g 1 min, to obtain 2 mM stock solutions. Corresponding aliquots were stored in a -80°C deep freezer and thawed immediately before next use in follow-up experiments. Careful pipetting of the appropriate volume was assured during preparation of aliquots and during experiments. The working concentration was 2 µM for both Aβscr or Aβ42 a concentration, which is similar to previous reports. Based on literature research, Aβ42 at a concentration of 2 µM should not influence significantly neurotoxicity, but preferentially synaptotoxicity in co-cultured neurons (173). LPS was prepared according to Liddelow et al., and different concentrations were tested with 100 ng/mL as the final LPS concentration for the experiments (83).

2.5 Immunofluorescence staining and microscopy

For fluorescence microscopy (Axiovert S100) as well as confocal imaging (SP5) involving IF with double immunolabelling was performed with a focus on following markers: astrocyte-

associated markers (GFAP, Glast), fibroblast markers (S100A4, FSP, α-SMA), microglia-associated markers (Iba1) (data not shown), oligodendrocyte markers (Olig2 or O4) (data for O4 not shown) or neuronal markers (MAP2, Tau, Synaptophysin, Vglut1) (data for Tau not shown) were used in different combinations with at least one astrocyte marker.

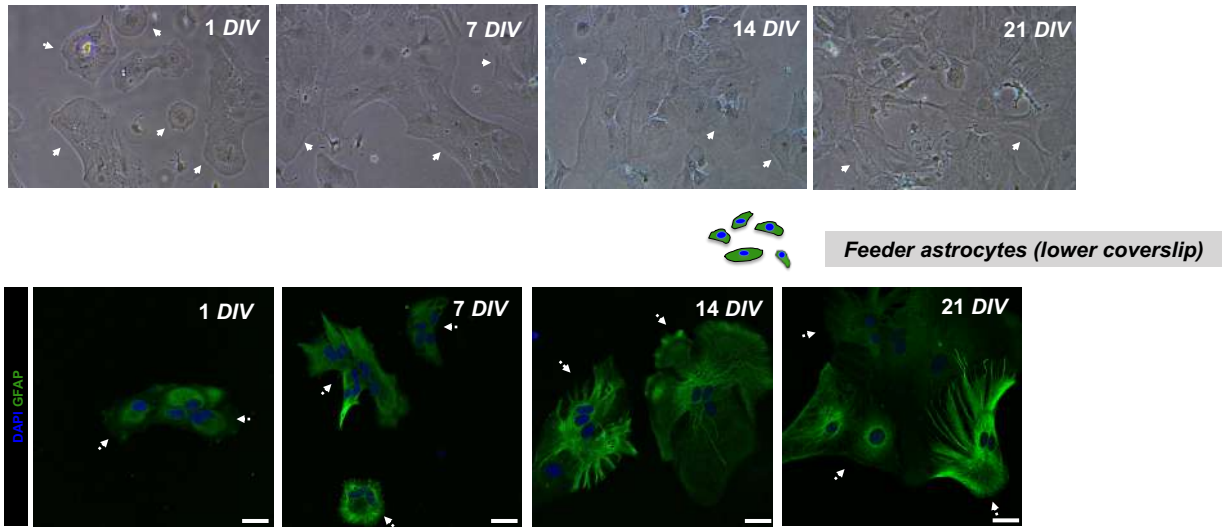

Fig. 7 Co-cultured astrocytes monitored over 3 weeks *in vitro:* Monitoring the evolution of feeder cells in sandwich co-cultures trough serial widefield imaging of primary mouse cortical astrocytes in co-cultures and confocal microscopy images of fixed and IF stained cortical astrocytes. Images were taken with an inverted widefield microscope (Nikon Eclipse TS100, Zeiss, Oberkochen, Germany) and Leica SP5 (Leica, Wetzlar, Germany), scale bar =

After 24 h of treatment, the upper coverslip with adherent neurons was removed from the cognate wells of co-culture plates and removed with a forceps and placed into a cognate labelled well of a new 12-well plate with pre-warmed DPBS1x. Co-culture medium was removed and remaining coverslips with the astrocytes were carefully rinsed with pre-warmed DPBS1x. Subsequently, DPBS1x of each well was aspirated carefully and pre-warmed 4% p-formaldehyde (w/v) and 4% sucrose (w/v) fixation solution were added with 10 min incubation time (at RT on agitation). Gentle aspiration and three washing steps with DPBS1x assured removal of the fixation solution. After three washes in DPBS1x, cells were permeabilized by incubating in DPBS1x containing 0.3% Triton X-100 for 10 minutes at RT. Coverslips were pre-incubated in blocking solution (DPBS1x containing 1% bovine serum albumin (w/v) (Sigma-Aldrich, Saint Louis, MO, USA)) for one hour. Subsequently, blocking solution containing the primary antibody of choice was used for incubation of the coverslips over 18 hours. Next day, three washing steps in PBS followed before secondary antibodies conjugated to either Alexa Fluor 488 or 594 were used and incubated for 2 hours in the dark. Final washing steps involved three washes in DPBS1x in the dark. Coverslips were shortly dried and gently mounted avoiding bubbles on microscopy slides for nuclear counterstaining with 4',6-Diamidino-2-phenylindole (DAPI) Fluoromount-G (SouthernBiotech, Birmingham, AL, USA). Antibodies were used as following: for IF stainings of neurons anti-Syn 1:250 (Synaptic Systems, Göttingen, Germany), anti-Vgat1 1:250 (Synaptic Systems, Göttingen,

Germany), anti-MAP2 1:500 (Saint Louis, MO, USA) were used. All other antibodies were used at concentrations of 1:1000, e.g. for astrocyte IF stainings anti-GFAP was used at a concentration of 1:1000 (Millipore, Burlington, MA, USA). Images were stored as TIFF files, measuring 1024 x 1024 pixels with a 63x immersion oil lens objective and a numerical aperture of 1.2 (N.A. = 1.2) using a Leica TCS SP5 confocal laser scanning microscope (Leica Microsystems, Mannheim, Germany) equipped multiline Argon, diode 561-nm, HeNe 595-nm and HeNe 633-nm visible lasers. The emitted fluorescence was detected after excitation with Ar laser at different wavelengths λ, either λ = 352 nm for DAPI, λ = 488 nm for Syn and λ = 647 nm for MAP2. Briefly, random fields with neurons were imaged, with a zoom = 1.5, maintaining equal settings for all neurons of each of the three independent

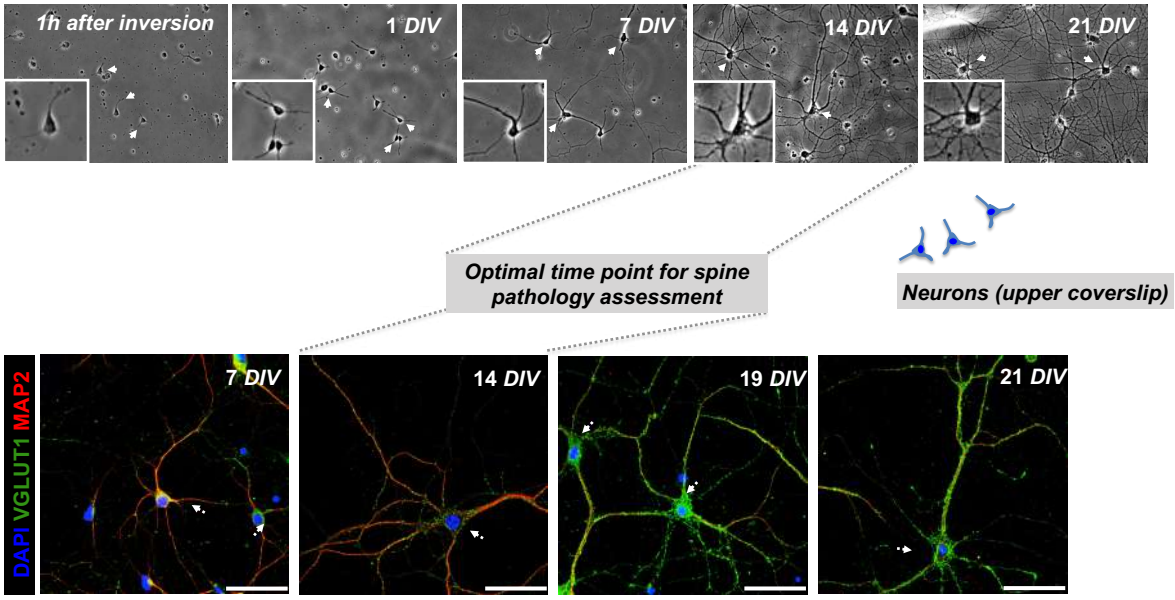

Fig. 8 Co-cultured neurons monitored over 3 weeks *in vitro:* Monitoring the evolution of neuronal cells in sandwich co-cultures by means of serial widefield images of primary mouse hippocampal neurons in co-cultures as well as confocal microscopy images of fixed and IF stained hippocampal neurons. Images were taken with an inverted widefield microscope (Nikon Eclipse TS100, Zeiss, Oberkochen, Germany) and Leica SP5 (Leica, Wetzlar, Germany), scale bar = 50 um.

experiments. No stack images were taken, as spine classification based on 3D data was not feasible. Furthermore, this allowed increasing the throughput in image acquisition. On average, for each of the 3 independent experiments 15 neurons per experimental condition were analyzed.

2.6 Image analysis

To obtain the integrated density (IntDen) or CTGF values of markers of interest specific to neurons or astrocytes raw confocal and fluorescence images stored as TIFF files had to be converted into and stored as 8-bit images. Alternative to CTCF, in case encircling of single cells with the free-hand selection tool single cells was not possible IntDen per field served as a final readout. At first, confocal or fluorescence images were processed via

ImageJ (bundled with Java 1.8.0_172), split into single channels and images. For instance, in case of neurons, images were split into red channel (MAP2) and green channel (Syn). Sholl analysis was using the advanced Sholl analysis plugin of Fiji software, where the geometric center (i.e. soma) was manually set and marked using the point tool in Fiji and the image was analyzed with the Fiji plugins Bitmap Sholl Analysis (169, 175). All Sholl analyses were carried out with a starting radius of 12 µm progressing with 10 µm intervals to a maximum radius of 120 µm, lower threshold was set to 0 and upper threshold to 128. All neurons of each group were subjected to same settings. SynPAnaL served for synaptic puncta analysis. Here, three randomly-chosen, non-overlapping dendritic segments per neuron were analyzed for quantification of synaptic puncta (137). Synaptic puncta were recognized as puncta positive for the presynaptic marker Syn showing specific signal enrichment and proximity to the dendritic marker MAP2 similarly to other studies in the field (67, 96). Spine number and intensity were normalized with an in-built calibration tool provided by SynPAnal to the measured length of a given dendritic segment that was tracked with the free-hand selection tool in SynPAnal in order to give the number of synaptic puncta per 100 µm, the density of puncta per µm2, intensity of synaptic puncta per length of 100 µm or per area in µm2.

2.7 MTT assay

The 3-(4,5-Dimethylthiazol-2-yl)-2,5-diphenyltetrazolium bromide (MTT) assay is a calorimetric method for *in vitro* cell culture experiments serving as a readout of cell viability - or more accurately the metabolic activity of the mitochondrial dehydrogenase in living cells (176, 177). MTT as such is a water-soluble, yellow-colored dye (tetrazolium salt) that can be enzymatically reduced to purple formazan product dye by the mitochondrial dehydrogenase in living cells. The latter can be quantified through a microplate reader with a spectrophotometer as the concentration of the formazan dye in solution (its relative absorbance) is directly proportional to the amount of metabolically active cells (176, 177). The MTT assay has limitations and yields no morphological information, still its convenience and rapid performance with a simple two-staged protocol makes it a widely used assay for compound testing in different cell systems (178, 179). Effects of 2,5 µM Aβ42 or LPS treatment on astrocytes were probed by performing the CellTiter 96® Non-radioactive Cell Proliferation Assay (Promega, Madison, WI, USA) according to manufacturer's instructions (180). Astrocytes were treated for 24 hours. Next, after 4h incubation at 37°C, MTT solution

was replaced with 100 µL DMSO and vigorously mixed. The absorbances at 550 nm and 650 nm were measured using a microplate reader (Molecular Devices, CA, USA). The percent cell viability was determined by comparing the absorbances between control conditions and vehicle-treated control.

2.8 Statistics

All experiments were repeated at least three independent times (N =/> 3) with distinct culture series of co-cultured hippocampal neurons originating from different animals, constantly having at least technical duplicates for each experiment. Data analysis and visualization was performed either with Graphpad Prism 8 (GraphPad Software Inc, La Jolla, CA). Data were represented as mean ± SD if not otherwise specified. Ordinary one-way ANOVA followed by a post-hoc Tukey‘s test. A probability of $p < 0.05$ was considered statistically significant, whereas p values of higher than 0.05 were considered as nonsignificant. Nonsignificant results were not indicated within bar blots for the sake of readability and clarity of the data.

3. RESULTS

The result part will here not include our modified protocol as such since we already refer to the technical details and troubleshooting details of our modified Banker assay in the material and methods part.

3.1 Assessment of yield and viability of acutely dissected primary CNS cultures

Tissue dissection and digestion are crucial when establishing primary CNS cell cultures and should provide an effective means to obtain a sufficient amount of viable primary cells. After enzymatic tissue digestion, several centrifugation steps and trituration of tissue pieces, the resulting primary CNS cell suspension was assessed in terms of cell amount and viability by using the Countess II Automated Cell Counter (Thermo Scientific, Waltham, MA, USA) before being used for downstream applications (***Fig. 6***). The protocol is essentially the same for the first dissection (feeder astrocytes) and the second dissection (for neurons plated on the upper coverslip), differences only exist in regard to usage of media and the surface used for cell plating, i.e. plastic surfaces (in case of astrocytes) or poly-L-lysine-coated, nitric acid treated and backed glass coverslips (in case of neurons) (***Fig. 2, 4***) (70, 74). The mean number of primary cortical CNS cells dissected per brain was 1.135.500 +/- 49797, whereas in the case of hippocampal tissue the number was 279.125 +/- 16543 per mouse per brain (i.e. per 2 hippocampi). The mean life cell fraction in case of cortical tissue 90,09 +/- 0,8622 % and in case of hippocampal tissue the mean life cell fraction was 93,2 +/- 0,5925 % (***Fig. 6***).

3.2 Co-cultured astrocytes monitored and co-cultured over 3 weeks *in vitro*

As for upper coverslip with neurons in „sandwich„ co-cultures, lower coverslips with feeder cells were monitored over a time of 3 weeks in order to show the presence of GFAP+ astrocytes that are crucial for providing paracrine (trophic) support to neurons (74, 75). To prove astrocyte differentiation state of feeder cells, IF double staining for different markers were used, such as GFAP, Glast, αSMA, FSP and Olig2 for quantification of the relative amount of GFAP+ cells within the population of cells plated cells the feeder layer (***Fig. 7, 8***). Importantly, feeder cells showed in its majority positivity for the pan-astrocyte marker GFAP without signs of gross contamination with other cells, degeneration, cell death or overt reactivity during their use for „sandwich„ co-cultures. This is concordant to previously published reports and protocols (74-76). Over time, we observed a steady growth of feeder cells reaching sub-confluent to confluent levels typically at 14 days (***Fig. 7***).

3.3 Co-cultured neurons exhibit signs of maturity at *14 DIV* offering an optimal time point for experimental manipulations

We monitored co-cultured neurons in neuron-astrocyte co-cultures with lower (astrocytic) coverslip and upper (neuronal) coverslip. Phase-contrast imaging and IF staining at 7, 14, 19 and 21 *DIV* of the upper and lower coverslips demonstrated continuous growth and differentiation with increasing age of the co-cultures. Importantly, after plating as early as One hour, before inversion of the upper (neuronal) coverslip over the astrocyte feeder layer, phase-contrast imaging of neurons consistently showed neurons attaching to the glass forming small minor neurites, similar to developmental stage 2 according to Banker et al. (74). After 7 days in culture, neurites have grown steadily with some of neurites becoming longer than the remaining ones, resembling axons (***Fig. 8***). Further co-culture of neurons shows signs of maturity *in vitro* as of 14 *DIV* with increased soma size, neurite thickness and branching (***Fig. 8***). In accordance with that, IF images of correspondent neurons at 14 *DIV* showed properly differentiated neurons with MAP2+ neurites and Syn+ synaptic puncta - again similarly shown as in previous studies (74, 75, 118). In many cases dendritic and axonal branches formed crossings or intersections, thus even in low-density-culture settings neurons adjacent to each other may develop extensive interconnections. This observation was especially true for older cultures, which renders subsequent analysis of neuronal morphology including analysis of dendrites or dendritic spines troublesome. Consequently, 14 *DIV* was regarded as the optimal time point for experimental manipulations in order to model the impact of experimental manipulations on fully differentiated neurons in co-cultures (***Fig. 8***).

3.4 Sandwich co-cultures are devoid of contaminating cells

Relatively pure feeder astrocytes devoid of contaminating cells such as microglia, oligodendrocytes, fibroblasts are crucial to study phenotype of astrocytes and its impact on co-cultured neurons (70, 74, 75). Therefore, IF staining of the lower coverslip with different markers of other CNS cells were performed. For example, astrocytes, defined as GFAP+DAPI+ cells, accounted for of 89,5819 +/- 10,6135% cells in the feeder layer, whereas the relative amount of cells without evidence of GFAP positivity, i.e. αSMA+DAPI+

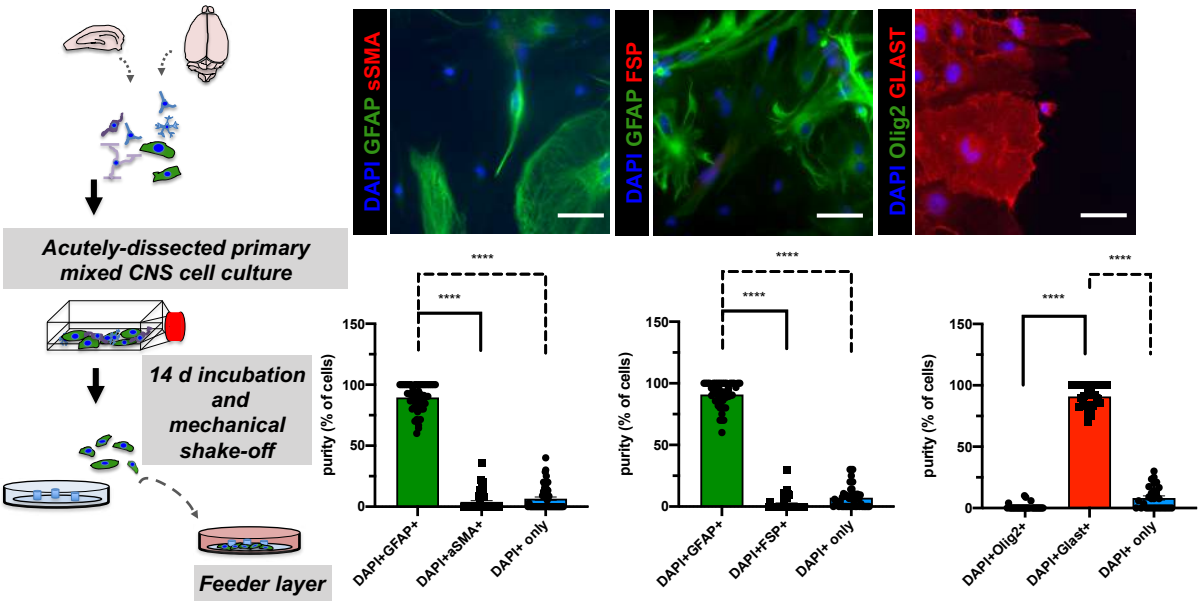

Fig. 9 Purity of feeder astrocytes*:* Characterization of the purity of feeder cells by staining mixed CNS cultures for different cell markers - either aSMA or FSP (fibroblast markers) or Olig2 (late OPC marker) (N = 4 mice). Data analysis was performed using GraphPad Prism 8 (GraphPad Software Inc, La Jolla, CA), statistical comparison was performed using ordinary one-way ANOVA followed by a post-hoc Tukey's test. Data is shown as mean ± SEM. Images were taken with a fluorescence microscope (Axiovert 200, Carl Zeiss, Göttingen, Germany), scale bar = 50 um.

cells or DAPI+ only cells was 3,9429 +/- 7,4126% and 6,6150 +/- 9,6779%, respectively (***Fig. 9***). In experiments of the same tissue preparations, GFAP+DAPI+ cells accounted for 90,8778 +/- 9,8411% of cells, whereas DAPI+FSP+ cells were found in only 2,9 +/- 5,3653% and DAPI+ only cells in 7,1268 +/- 8,6089%. Additionally, cells showing positivity for late OPC markers by means of Olig2 expression accounted only for 8,1997 +/- 9,1761% of cells within the feeder cell population. Similar values were found in Iba1+ and O4+ cells, where the mean cell fraction of GFAP- cells was constantly below 10-20% (data not shown).

3.5 FUDR treatment allows to curb the GFAP+ proliferating glial cell fraction in co-cultures

In order to probe consequences of experimental manipulations on neuronal health status and morphology including dendritic spines a relative high purity of neuronal cells (on the upper coverslip) was mandatory. Overgrowth of the upper layer with glia, especially astrocytes or microglia and their direct influence on neurons may hinder interpretation and analysis of downstream neuronal readouts (74, 75) (***Fig. 9***). Thus, upper coverslips with mixed primary CNS cultures seeded were subjected to IF staining for neuron-specific markers such as MAP2 or β-III-Tubulin which enables to evaluate the relative purity of neurons (percentage of β-III-Tubulin+ cells) among the total cell population seeded on top of the upper coverslip (***Fig. 2, 10***). In terms of medium changes, slight adjustments in the

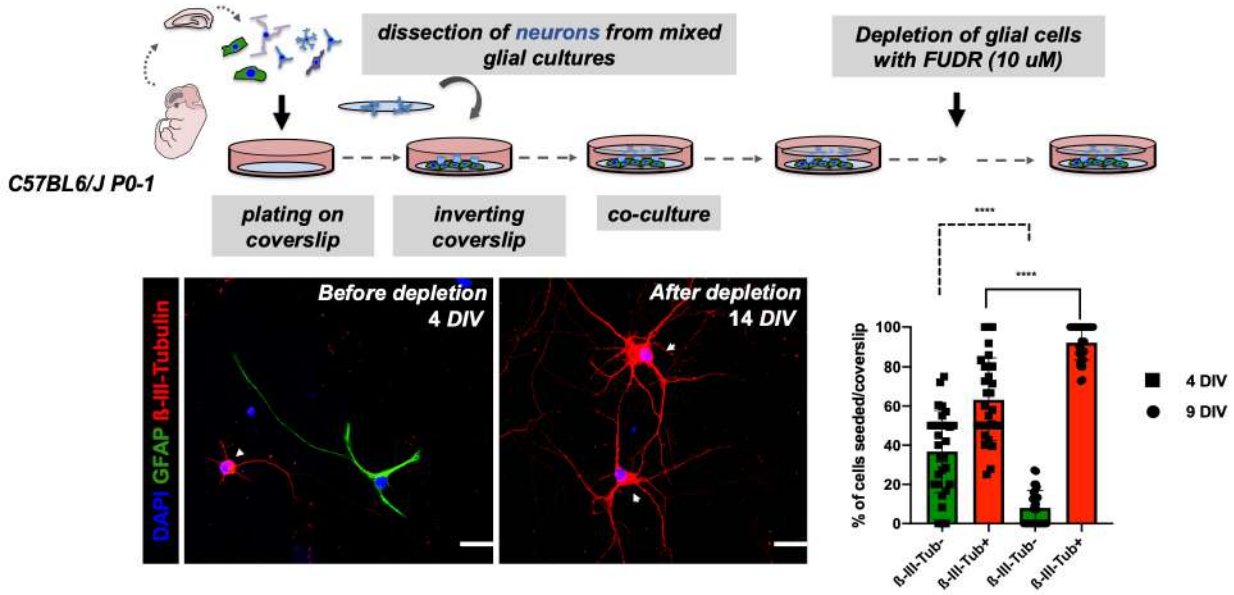

Fig. 10 Depletion of glial cells in the neuronal layer (upper coverslip) of the sandwich co-culture: Independent rounds of preparations (N = 3 mice) comparing frequency of primary neurons and astrocytes in the upper coverslips at 4 *DIV* and 14 *DIV*. Fixed cells were stained for glial (GFAP) or neuronal markers (ß-III-Tubulin or MAP2) *via* IF. Data analysis was performed using GraphPad Prism 8 (GraphPad Software Inc, La Jolla, CA), statistical comparison was performed using an ordinary one-way ANOVA followed by a post-hoc Tukey's multiple comparison test. Data is shown as mean ± SEM. Images were taken with Axiovert 200 (Carl Zeiss, Göttingen, Germany) or Leica SP5 (Leica, Wetzlar, Germany) microscopes, scale bar = 50 um.

protocol were made including not only the frequency of medium changes as well as the relative amount of old culture medium withdrawn and new volume added. Additionally, the first medium change with NMM after setting up the co-cultures was issued regularly after 3 days involving a single-dose treatment with 10 µM of the thymidylate synthase inhibitor and mitotic inhibitor FUDR to curb proliferation and growth the dividing primary cell fraction in co-cultures (75). Conversely, the medium changes of NMM later on did not involve addition of FUDR in order to avoid adverse effects on neuronal metabolism. Mean percentage of ß-III-Tubulin+ neurons per field of a given coverslip at 4 *DIV* was 63,2389 +/- 21,0176%, whereas at 14 *DIV* it was 92,0187 +/- 8,8579%. In contrast, at non-neuronal GFAP+ DAPI+ astrocytes accounted for 36,7611 +/- 21,0176% and 7,9812 +/- 8,8579% of all DAPI+ cells at 4 *DIV and* 14 *DIV,* respectively (***Fig. 10***).

3.6 Neuron-astrocyte co-cultures are superior to neuron monocultures with respect to neuronal growth and differentiation

After establishment and characterization of the neuron-astrocyte co-culture system, a direct comparison was undertaken between neurons in co-cultures versus neurons in monocultures. Both types of neuronal cultures were compared at 9 *DIV* in terms of several

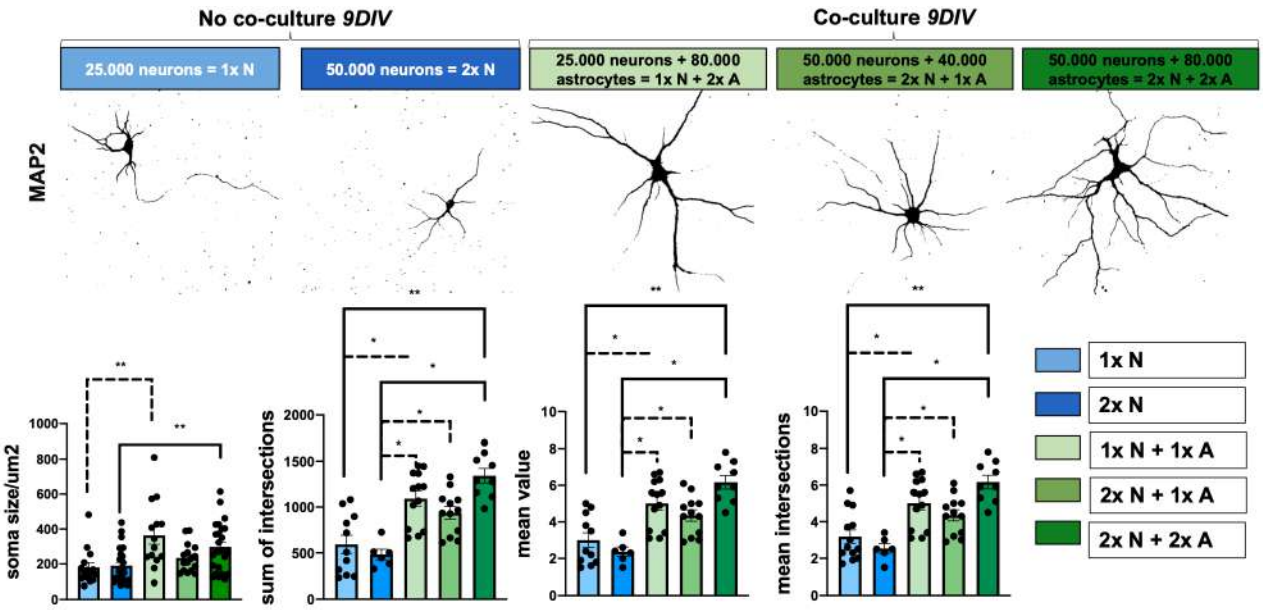

Fig. 11a Comparison of morphometric indices in neurons with vs. without co-cultures: Sholl analysis of neurons without co-cultured astrocyte feeder cells and neurons co-cultured with astrocytes at 9 *DIV*. Fixed cells were stained for the neuronal cell-fill marker MAP2. Data analysis was done using GraphPad Prism 8 (GraphPad Software Inc, La Jolla, CA) and statistics using an ordinary one-way ANOVA followed by a post-hoc Tukey's multiple comparison test. Data is shown as mean ± SEM. Images were taken with a fluorescence microscope (Axiovert 200, Carl Zeiss, Göttingen, Germany), scale bar = 50 um.

readouts of neuronal morphology reflecting overall neuronal health status under *in vitro* conditions, which were as follows: soma size, IntDen of the neuronal marker MAP2 and the synaptic marker Syn by means of IF, which in turn correlate with protein production of correspondent markers, as well as dendritic complexity by means of Sholl metrics) (***Fig. 11a, 11b***) (181, 182). By comparing both type of neuronal cell cultures at the same time point the effect of paracrine interactions and trophic support provided by astrocyte feeder cells could be assessed. Hence, this approach would provide insights as to whether the modified Banker protocol involving „sandwich„ co-cultures of neurons and astrocytes adds a benefit for investigations of primary mouse neurons *in vitro*. Therefore, different seeding densities of neurons in monocultures or in co-cultures were prepared (***Fig. 11a, 11b***). Soma size in um2 in neurons in monocultures seeded at a density of 25.000 neurons/well (1x N) showed a mean soma size of 180,7070 +/- 101,5301 um2, neurons plated at the double density (2x N) showed a soma size of 190,1960 +/- 97,7438 um2, whereas co-cultured neurons showed significantly higher mean values of soma size (***Fig. 11a***). In contrast between the group of co-cultured neurons (1x N co-cultured with either 80.000 astrocytes (2x A), 2x N co-cultured with 1x A and 2x N co-cultured with 2x A) there was no significant difference in the mean neuronal soma size (***Fig. 11a***). In regard to Sholl analysis, mean intersections was analyzed via the Sholl plugin and showed again significantly increased

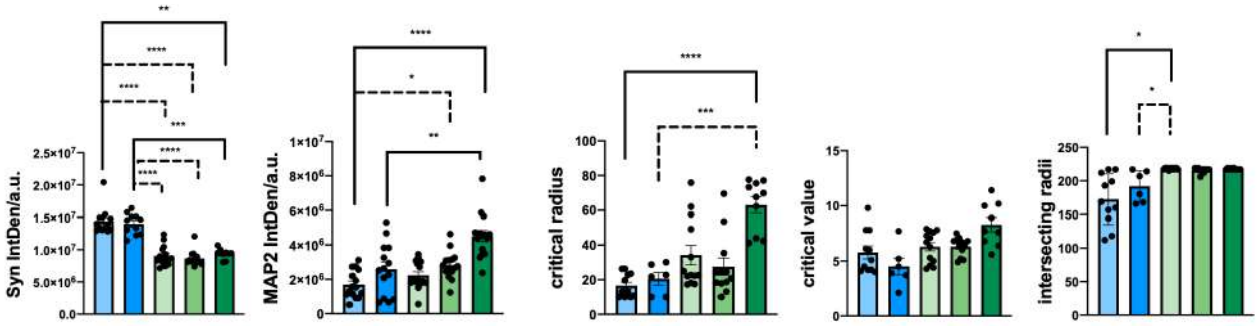

Fig. 11b Comparison of morphometric indices in neurons with vs. without co-cultures: Sholl analysis of neurons without co-cultured astrocyte feeder cells and neurons co-cultured with astrocytes at 9 *DIV*. Fixed cells were stained for the neuronal cell-fill marker MAP2 *via* IF. Data analysis was performed using GraphPad Prism 8 (GraphPad Software Inc, La Jolla, CA), statistics were performed using an ordinary one-way ANOVA followed by a post-hoc Tukey's multiple comparison test. Data is shown as mean ± SEM (continuation of 11a)

mean number of intersections of co-cultured neurons as compared to monocultures. 1x N had 3,1846 +/- 1,3189 mean intersections, 2x N 2,5333 +/- 0,6470, whereas 1x N co-cultured with 1x A showed 5,0153 +/- 1,3440 mean intersections, 2x N co-cultured with 1x A 4,3500 +/- 1,0492 and 2x N co-cultured with 2x A showing with 6,1667 +/- 1,1034 the highest number of mean intersections. Likewise, the sum of intersections with 593,1820 +/- 328,8418 and 481,6670 +/- 138, 9239 for 1x N and 2x N monocultures was significantly lower as compared to the values reached in co-cultured neurons: 1x N co-cultured with 2x A showing 1092,3800 +/- 296,4193 sum of intersections, 1x N co-cultured with 1x A 938,167 +/- 236,8746 and 2x N co-cultured with 2x A showing 1342,22 +/- 238,6329 sum of intersections (***Fig. 11a***). Furthermore, so-called key metrics according to the technical paper of Ferreira and colleagues were analyzed as they derive from a polynomial function that can be plotted after running the Sholl analysis plugin and use of a built-in heuristic algorithm in the Sholl analysis plugin approximating the polynomial function from a linear Sholl plot, thus improving local variations of sampled data (169). Interestingly, results of the key metrics were similar to the results above. Significant changes in the mean value were observed between neurons either subjected to monocultures or co-cultures: For 1x N and 2x N monocultures was significantly lower as compared to the values reached in co-cultured neurons: 1x N showed a mean value of 3,0000 +/- 1,3505, 2x N a value of 2,3667 +/- 0,6345. Conversely, 1x N co-cultured with 2x A showed a Nav of 5,0154 +/- 1,3440, 1x N co-cultured with 1x A a mean value of 4,3500 +/- 1,0715, 2x N co-cultured with 2x A showing a mean value of 6,1666 +/-1,1034 (***Fig. 11a***). Whereas other key metrics based on the Sholl analysis tool, such as critical radius and intersecting radii were in line to the results above. In contrast, another key metric, the so-called critical value, showed no significant differences between monocultured and co-cultured neurons (***Fig. 11b***). In addition, the key metrics, signal intensity of the dendritic marker MAP2 and the synaptic marker protein Syn were assessed

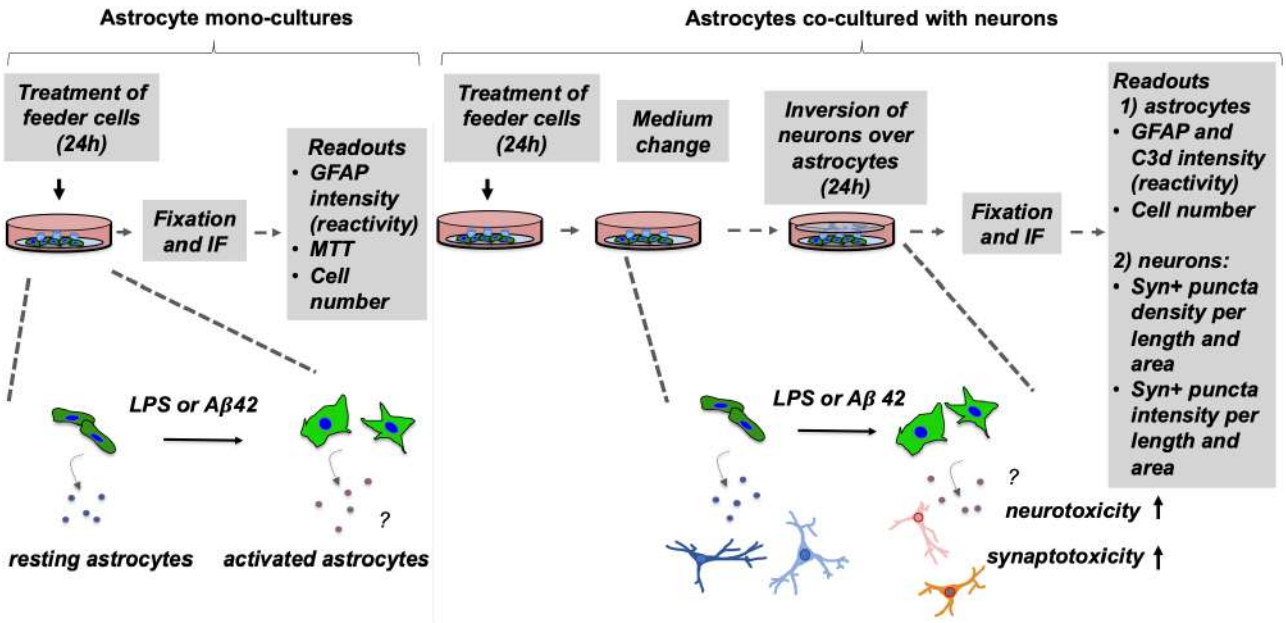

Fig. 12a Experimental setting of reactive astrocyte induction and co-culture with neurons: Astrocyte mono-cultures were subjected to different treatment conditions, fixed and in the end stained for reactive astrocyte markers such as GFAP and C3d by means of IF. Additionally, pre-treated astrocytes were co-cultured with fully-differentiated neurons (14 *DIV*) with downstream readouts for both astrocytes and neurons (see graphical abstract).

by means of IntDen values. Here, co-cultured neurons generally showed higher MAP2 signal intensity values as compared to neuronal monocultures. However, IntDen for Syn was higher in monocultured neurons (***Fig. 11b***).

3.7 Induction of reactive astrocytes in primary astrocyte cultures through treatment with Aβ42 or LPS to model non-cell autonomous effects in AD

Since the co-culture system is modular with two layers of cells (upper and lower coverslip), paracrine, non-cell autonomous effects and mechanisms of neurotoxicity and synaptotoxicity can be studied. Each of the cell layer contains a relative pure population of cells, namely primary cortical astrocytes in the case of the lower coverslip at the bottom of the „sandwich„ co-culture and primary hippocampal neurons in the upper coverslip. Given the increasing appreciation of gliosis in different CNS diseases, numerous studies made use of astrocyte-neuron co-cultures to study the impact glial cells might have on neurodegeneration including neurotoxicity and synaptotoxicity (33, 184-186). We aimed at assessing the effect of toxin-exposed astrocytes on neurons using our established assay by pre-treating astrocytes either with Aβ42 or LPS or Aβscr and water as the correspondent control, respectively. This is based on previous reports demonstrating a conversion of astrocytes into a reactive state through both Aβ42 and LPS (90, 187, 188). Similarly, there are several published reports suggesting that Aβ42 may also activate astrocytes resulting in loss of neuroprotective capacities and even acquirement of neurotoxic and synaptotoxic

capacities (189-191) (***Fig. 12a***). In our setting, the first step included direct treatment of primary astrocytes without any neuronal co-culture, where astrocytes were exposed to 24 hours treatments either with Aβ42 or LPS. There was no significant difference in the number of cells between the different treatment conditions suggesting that treatment did not significantly influence astrocyte proliferation (***Fig. 12b***). However, GFAP IntDen of astrocytes was significantly elevated in Aβ42-treated astrocytes with 5,0685*10^7 +/- 11045240,84 arbitrary units (a.u.) as compared to the correspondent control condition Aβscr with 3,4956*10^7 +/- 11960517,06 a.u.. In contrast, there was a non-significant elevation of GFAP signal intensity upon treatment with LPS with 3,5846*10^7 +/- 14517849,33 a.u. as

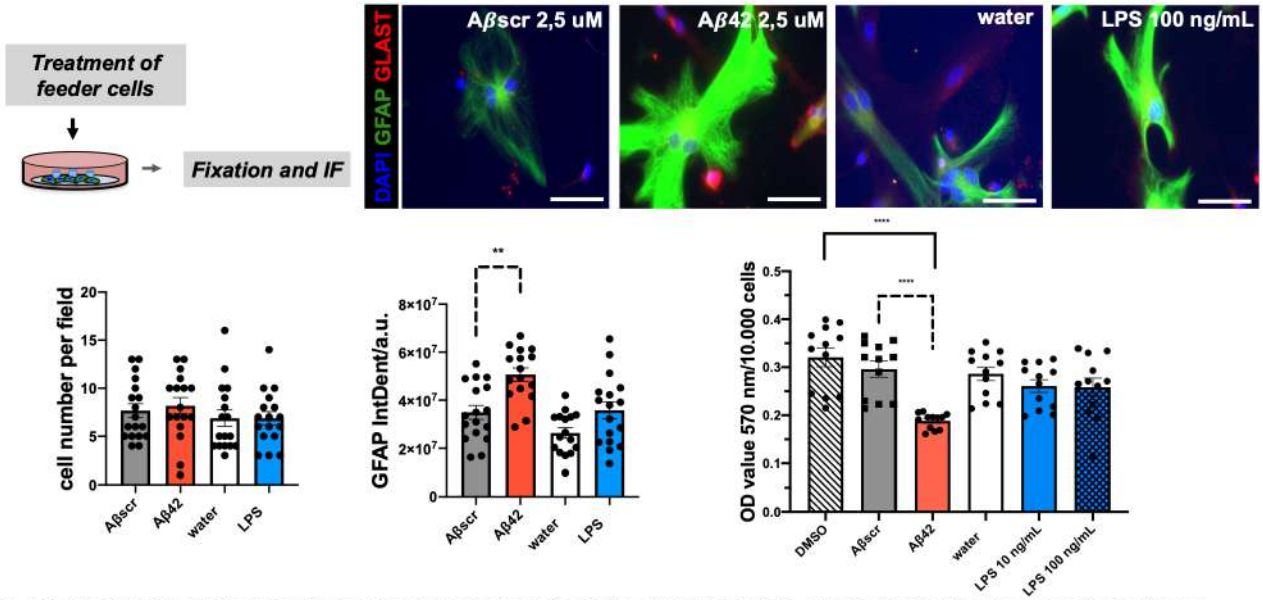

Fig. 12b Direct treatment of astrocytes over 24h (for induction of reactive astrocytes): Mono-cultures of astrocytes were subjected to different treatment conditions. Upon termination cells plated on glass coverslips were fixed and stained for IF. Data analysis was done with GraphPad Prism 8 (GraphPad Software Inc, La Jolla, CA), statistical comparison was performed with an ordinary one-way ANOVA followed by a post-hoc Tukey's multiple comparison test. Data is shown as mean ± SEM. Images were taken with a fluorescence microscope (Axiovert 200, Carl Zeiss, Göttingen, Germany), scale bar = 50 um.

compared to their correspondent control condition 2,6356*10^7 +/- 8720571,991 a.u. (***Fig. 12b***). In line with that observation, MTT assay of primary astrocytes with the same treatment conditions led to a significant decrease of the OD value upon treatment with Aβ42 at a concentration of 2,5 uM, whereas, again, no significant differences in the OD values were detected between water and LPS treatment of astrocytes (***Fig. 12b***). Next, treated astrocytes were assessed for Aβ42 uptake through IF staining for the astrocyte-specific marker GFAP and 6E10 antibody, which is specific to human Aβ42. As a consequence,

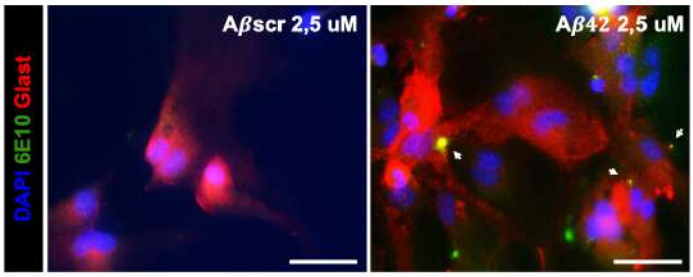

Fig. 12c Aß42-treated astrocytes show signs of Aβ**42 uptake:** Astrocytes in mono-cultures were exposed to treatment for 24h at concentrations of 2,5 uM for either Aβ**42 or** Aβ**scr. Upon termination** cells on coverslips were fixed and stained by means of IF staining using antibodies directed against Glast and 6E10, an Aβ42-specific antibody. Images were taken with a fluorescence microscope (Axiovert 200 (Carl Zeiss, Göttingen, Germany), scale bar = 50 um.

treated and fixed primary cortical astrocytes would be detected by 6E10 anti-human Aβ42 antibody, whereas control astrocytes would not show positivity for Aβ42 (***Fig. 12c***).

3.8 Pre-treated astrocytes maintain their phenotype in co-cultures with neurons

Next, astrocytes were subjected to the same treatment protocol as described above (pre-treatment), but additionally media were changed after 24 hours of treatment (either with water vs. LPS or with Aβscr versus Aβ42) and lastly neurons (co-cultured over 14DIV with other naive feeder cells) were inverted over the pre-treated astrocyte feeder cells (***Fig. 12a***). The resulting co-cultures were maintained for 24 hours and both coverslips were subsequently fixed and subjected to IF staining with astrocytes being stained for GFAP and C3a, both markers for RAs and neurons were stained for MAP2 and Syn. Similar to the

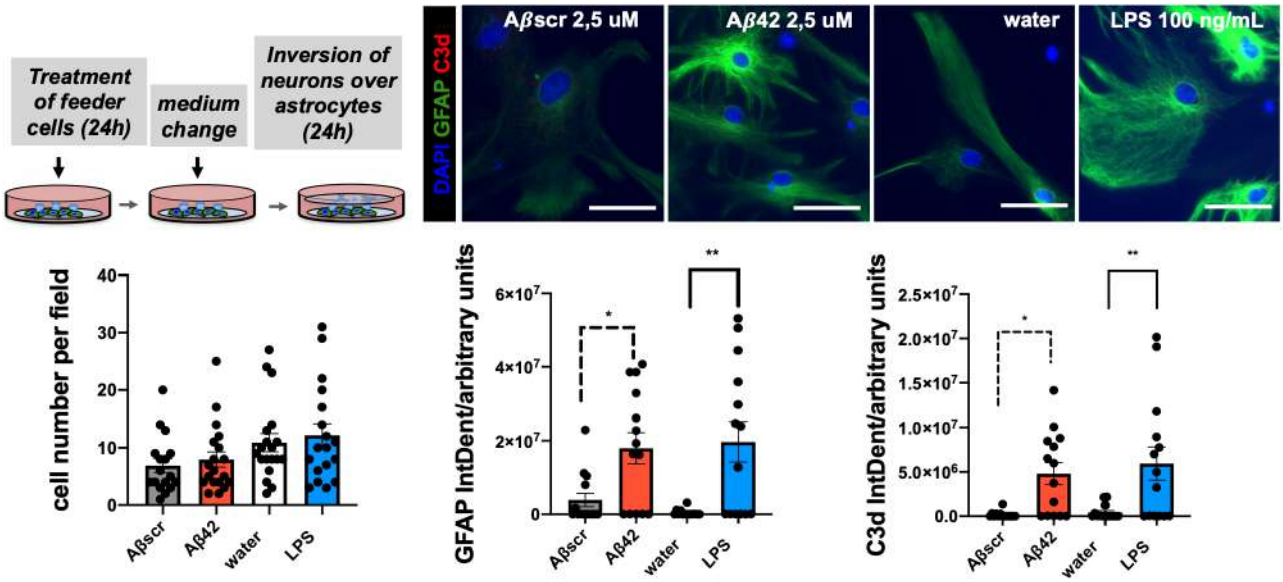

Fig. 13 Pre-treatment and subsequent co-culture of astrocytes: Astrocytes were subjected to pre-treatments for 24h, media were replaced, subsequently differentiated neurons were inverted over pre-treated astrocytes and co-cultured for 24h. After termination, cells were fixed. IF staining was done for reactive astrocyte markers, i.e. GFAP (green channel) or C3d (red channel). Data analysis was performed using GraphPad Prism 8 (GraphPad Software Inc, La Jolla, CA), statistical comparison was performed using an ordinary one-way ANOVA followed by a post-hoc Tukey's multiple comparison test. Data is shown as mean ± SEM. Images were taken with Axiovert 200 (Carl Zeiss, Göttingen, Germany), scale bar = 50 um.

previous results no significant difference in cell number was observed between the different experimental conditions. However, in regard to the GFAP intensity and C3d intensity values significant differences between control and treatment condition were detected. Aβ42-treated astrocytes showed a mean GFAP signal intensity of 1,7987*10^7 a.u. and Aβscr-treated astrocytes a mean value of 3,9020*10^6 a.u., whereas LPS-treatment of astrocytes was associated with a GFAP intensity value of 1,9695*10^7 a.u. and water-treated astrocytes showed a mean value of 414684 a.u. (***Fig. 13***).

3.9 Co-culture of pre-treated primary astrocytes with neurons is associated with synaptotoxic effects

Next, the impact of pre-treatment of astrocytes on neuronal dendritic spine pathology of co-cultured neurons was analyzed. Corresponding readout for assessing putative synaptotoxic effects Aβ treatment involved Syn+ synaptic puncta (clusters), a common readout which was previously introduced and employed by different groups (66, 94). Analysis of Syn+ synaptic puncta of designated neuron areas, i.e. 3 dendritic segments per neuron with at least five neurons per experiment, was done in a semi-automatic fashion with SynPAnal with its built-in dendritic area-drawing and thresholding tool. Comparing Syn+ synaptic puncta of co-cultured neurons either treated with pre-treated or naive astrocytes (see above) over 24 h demonstrated a significant difference in the mean number of synaptic puncta per 100 µm

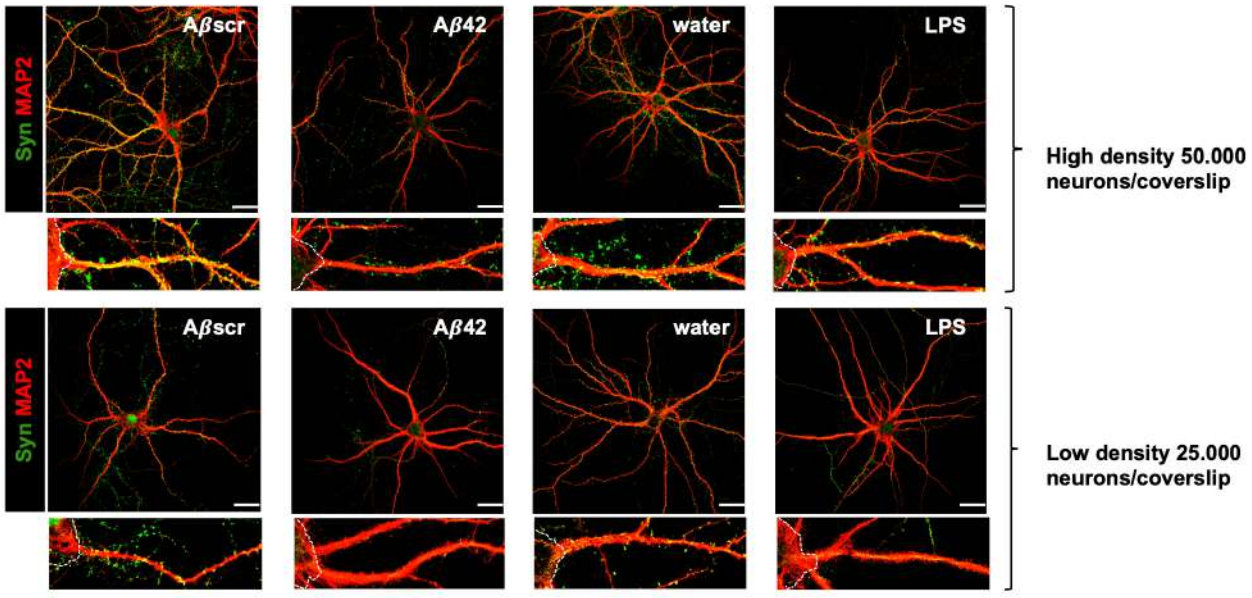

Fig. 14a Probing the effect of astrocytes on synaptic puncta in neurons co-cultured with pre-treated astrocytes: Neurons were exposed 24h to paracrine interactions emanating from pre-treated astrocytes in co-culture. Subsequently, neurons were stained by means of IF and Syn+ synaptic puncta were analyzed with SynPAnal. Data analysis was performed using GraphPad Prism 8 (GraphPad Software Inc, La Jolla, CA), statistical comparison was performed using two-way ANOVA followed by a post-hoc Student's t-test. Data is shown as mean ± SEM. . Images were taken with a confocal microscope Leica SP5 (Leica, Wetzlar, Germany), scale bar = 50 um.

length in neurons seeded at high density (50.000), but not at low density (25.000) (***Fig. 14a***).

Similar results were observed another main readout based on SynPAnal namely that of puncta density/µm2 (***Fig. 14a, 14b***). Moreover, assessing the ratio of intensity of Syn+ synaptic puncta and dendritic length or area was assessed. A similar effect on Syn+ synaptic puncta intensity was seen with the treatment of high density seeded neurons with Aβ42- or LPS-pre-treated astrocytes, leading to a significant reduction compared to the control group of neurons (***Fig. 14a, 14b***).

4. DISCUSSION

4.1 Neuron-astrocyte co-cultures give rise to fully differentiated mouse neurons amenable to experimental manipulations

In this thesis a protocol was established allowing to obtain cultures of properly differentiated primary mouse hippocampal neurons. We were able to maintain neurons regularly up to three weeks *in vitro* with co-cultured astrocyte feeder cells providing trophic paracrine support (***Fig. 1, 2***). Before inversion of neurons over feeder cells marking the onset of co-cultures, rapid and efficient adhesion of primary hippocampal neurons took place within one hour of plating of freshly dissected CNS cells (***Fig. 8***). Additionally, we implemented a glial depletion step by means of single administration of FUDR of co-cultures in the protocol in order to further curb overgrowth of glial cells in the lower part of the co-culture (lower coverslip with feeder astrocytes) (***Fig. 2, 10***). Similar to previous research, we observed that the effect of FUDR in curbing glial proliferation is specific to the upper coverslip, where glial cells (that may have managed to adhere within one hour after plating together with neurons

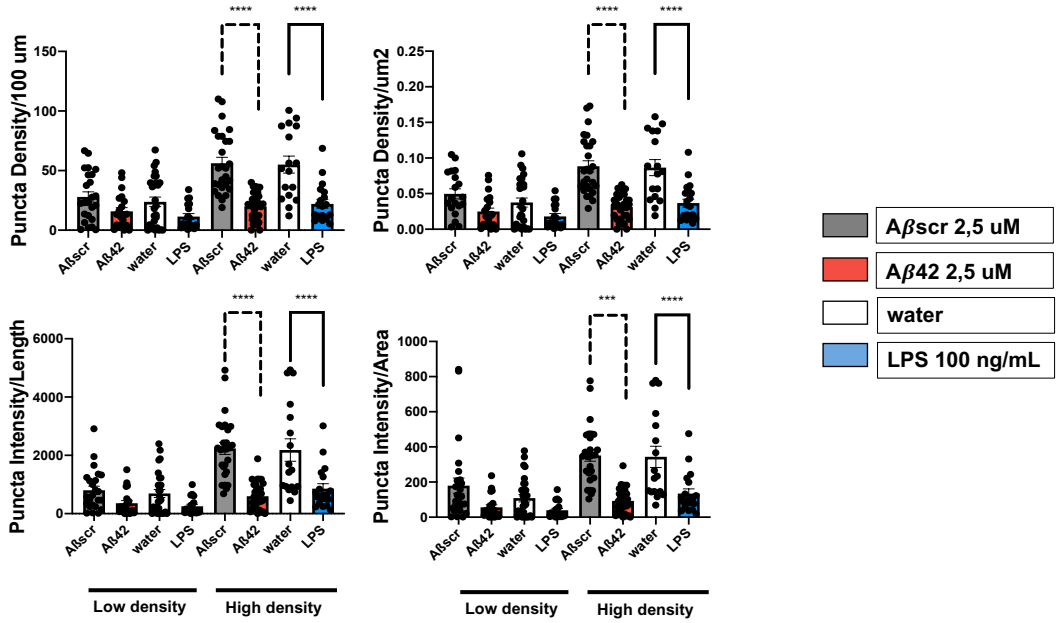

Fig. 14b Probing the effect of astrocytes on synaptic puncta in neurons co-cultured with pre-treated astrocytes: Neurons were exposed to paracrine interactions of pre-treated astrocytes by means of co-culture for 24h. Subsequently neurons were stained for IF and analyzed with SynPAnal. Data analysis was performed using GraphPad Prism 8 (GraphPad Software Inc, La Jolla, CA), statistical comparison was performed using an ordinary one-way ANOVA followed by a post-hoc Tukey's multiple comparison test. Data is shown as mean ± SEM, scale bar = 50 um.

subsequently being inverted with their coverslip over the feeder layer) may initiate growth due to lack of contact inhibition cues emanating from nearby cells and become expansive (74, 75). Conversely, the lower coverslip where glial cells (astrocytes) already have reached near confluence before co-cultures are initiated, will be less likely be impacted by FUDR treatment. In theory, inhibition of thymidylate synthase, preferentially affects mitotic or actively dividing cells, whereas post-mitotic neurons should be spared (74, 75). Importantly, we compared FUDR to another commonly used mitotic inhibitor, namely AraC. In our hands, AraC was found to exert more neurotoxicity in our cultures (data not shown). This is in line with other reports (68, 74, 75). Comparison of monocultured with co-cultured neurons at 9 *DIV* suggested a significant overall increase in indices that reflect neuronal health status (soma size, Syn IntDen, MAP2 IntDen) as well as dendritic complexity (mean intersections, sum of intersections, mean value, critical radius and intersecting radii) (***Fig. 11a, 11b***). Importantly, these observations are in accordance with previous results reported by other groups (74, 75). However, our study provided a more comprehensive comparison of mono-cultured and co-cultured neurons with different relations of seeded neurons and astrocytes with a clear positive impact of astrocytes on neuronal growth. Here, an effect-dose relationship of feeder cells in regard of neurotrophic effects could be observed (***Fig. 11a, 11b, 14a, 14b***). After 14 days of co-culture neurons show proper signs of differentiation by means of dendrite formation and presence of synaptic puncta, which is seen by many researchers as the time point *in vitro,* at which proper neuronal differentiation and maturation is apparent (65, 74, 116, 123, 137, 171, 173, 192) (***Fig. 8***). Yet, other studies in the field performed experiments with primary neuronal cultures maintained for less than two weeks *in vitro* (189, 191). Certainly, one caveat of this study is the small panel of specific markers that has been used for imaging, only showing data for Vglut1 and Synaptophysin as synaptic markers. Although other common synaptic marker proteins such as PSD-95 and Vgat have been tested in this work (data not shown) with co-cultured neurons showing positivity for those markers, lack of sufficient amount of samples and material allowed to perform replicates only for a limited combination of markers for IF and subsequent imaging (***Fig. 2, 11a, 11b***). Future studies should address a more versatile combination of IF markers and not be limited to staining only for DAPI-MAP2-Synaptophysin using for example other triple IF staining protocols (e.g. DAPI-Vglut1-MAP2 or DAPI-PSD95-MAP2) which would allow co-localization analyses (196). Additionally, future studies should leverage more sophisticated imaging modalities for spine classification and qRT-PCR and Western blotting for both cell layers could add additional value and informative readouts to this assay. Accordingly, this

would facilitate dissection of mechanisms and cellular signaling pathways underlying paracrine cross-talk between astrocytes and neurons in AD. Lastly, it would be interesting to determine whether the beneficial effect of astrocytes in only limited to paracrine support.

4.2 Astrocyte-mediated synaptotoxicity can be modelled using *in vitro* primary neuron-astrocyte co-cultures

Readouts used in this work that reflect overall neuronal health status include soma size, CTCF or IntDen of MAP2 stained neurons. Dendritic complexity was evaluated by means of Sholl analysis that produces readouts such as mean number of intersections, sum of intersections and so forth. Synaptic puncta-associated readouts included readouts such as number of Syn+ puncta per 100 µm. These readouts are common in studies testing pharmacological compounds with respect to neurotoxicity and synaptotoxicity, but also found in research aimed at characterizing und comparing phenotypes in different mouse models such as AD mouse models (94, 172, 173). Due to small sample size and the necessity to provide enough technical replicates for each co-culture experiment, we decided to work with 4 different conditions comparing the effects of pre-treatment of astrocytes either with Aβ42 or its control Aβscr and LPS or its correspondent control water (***Fig. 12a, 12b, 13***). In previous studies, it has been shown that glial cells represent key elements in neurodegenerative and neuroinflammatory conditions with astrocytes attaining a reactive phenotype or A1 phenotype as shown only recently by Liddelow et al. (83, 183, 185). To study reactiveness of astrocytes or synaptotoxicity and neurotoxicity in the case of neurons *in vitro,* a common practice is administration of agents such as Aβ42 or LPS at similar concentrations as we used to treat our primary cells. For instance, Fai-Lau et al. used Aβ42 at 5 µM to probe direct synaptotoxic effects of Aβ42 on primary hippocampal rat neurons (173). Likewise, we used LPS and Aβ42 to treat primary astrocytes at concentrations that were published earlier by other groups (83, 99, 186-188, 195) (***Fig. 12a, b, c***). To the best of our knowledge no study probed the indirect effects of LPS and Aβ42 on synaptic puncta readouts in a setting as we did. Still, biological effects seen in our treatment groups need to be verified more systematically, in the context of dose-effect relationships and incorporate also additional negative control conditions for all experiments such as DMSO in the context of Aβ42 treatment. Since our treatments were aimed at assessing the indirect toxic effect of Aβ42 or LPS we decided to maintain relatively low concentrations of for instance Aβ42, which were known to produce no overt toxicity to astrocytes but could result in more subtle

effects such as loss of neurotrophic effects (83). We suspected that this in turn could alter dendritic spines rather than impacting more gross readouts such as soma size, or dendritic complexity. Here, we focused of the presynaptic marker Syn i.e. Syn+ synaptic puncta, a commonly used readout to study synaptotoxicity in primary neurons (94). Concretely, in our study, treatment of co-cultured neurons with Aβ42 showed an no overt effects on Sholl analysis-associated readouts. However, key metrics were affected suggesting some minor effects of neuronal dendritic complexity. More importantly, synaptic puncta readouts by means of Sholl analysis were significantly changed in the Aβ42 treatment group as compared to the Aβscr control group. Although we tested different programmes to analyze and quantify synaptic puncta in our experiments such as simple manual analysis using ImageJ, finally the semi-automatic analysis software SynPAnal provided a straightforward, efficient and a more unambiguous way to detect and quantify puncta (137). Interestingly, our co-cultured neurons showed similar numbers of synaptic puncta as other groups reported for neurons in co-culture (116, 137). Counterintuitively, compared to neurons seeded in higher numbers, in our study, neurons seeded at lower density were not able to distinguish and disclose biological effects resulting from different treatments on Syn+ puncta readouts (***Fig. 14a, 14b***). This might be owing to the fact that neurons in vitro, independently of being co-cultured, rely on direct interactions with neighbouring neurons. Consequently, in neurons seeded at low densities biological effects due to treatment might be more difficult to detect since because neurons show more variability in growth and differentiation.

4.3 Neuron-astrocyte co-cultures can serve as a model to study paracrine interactions between neurons and astrocytes in neurodegeneration

Our modified Banker co-culture assay with two coverslips is modular and amenable to various modifications: Firstly, it allows to incorporate other cell types of interest such as microglia (data not shown), OPCs, or oligodendrocytes, by substituting one cell type or even adding a cell type (triple cultures), thus providing an accessible and versatile model to study cell-cell interactions in the CNS in various disease settings (75, 183, 191, 193-195). Secondly, neurons being suspended and cultured over a feeder layer can be inverted over other astrocytes that were pre-treated with compounds to study the phenotype and impact of astrocytes on neuronal growth. Pre-treatment of astrocytes either with Aβ42 or LPS in serum-free media was associated with signs of activation such as upregulation of GFAP as compared to control settings, which is similar to previous research (***Fig 12a, b, c***).

Furthermore, the modularity of the assay permitted treatment or co-culture of naive differentiated neurons with pre-treated astrocytes (***Fig 13, 14a, b***). Interestingly, astrocytes maintained their phenotype of upregulation of GFAP upon co-culture with neurons and hippocampal neurons cultured with astrocytes pre-exposed to agents known to induce an A1 astrocyte phenotype, namely Aβ42 and LPS, resulted in reduced Syn+ synaptic puncta. This is in accordance to similar observations made by Liddelow and colleagues (83). Astrocytes were cultured in FBS-containing media before any treatment or use for co-cultures. This could potentially provoke some reactive changes in astrocytes destined for co-cultures. Serum-free conditions during the time of co-cultures likely lowered impact of previous serum-induced activation of astrocytes and prevented further activation of astrocytes as shown by repetitive IF stainings for GFAP in our cultured astrocytes (***Fig. 6***). Yet, other (prospective) astrocyte isolation methods such as immunopanning or FACS-based isolation would be superior to our method of astrocyte enrichment. This is based on Pozzi et al. reporting that astrocytes cultured in FBS-containing media showed a flat, cobble-stone morphology and with reduced complex morphology as compared to those astrocytes cultured in serum-free media (121). Furthermore, Zhang et al., as delineated above, argued that single exposure of astrocytes towards serum might already provoke genomic and phenotypic changes (33). Nevertheless, with our co-culture protocol we were able to show consistent, dose-dependent responses of astrocytes upon Aβ treatment of co-cultures, typically up-regulating GFAP when being exposed to Aβ, similar to other pathological conditions such as stroke and SCI, with signs of hypertrophy (***Fig. 14***). Further studies for instance with FITC-labeled Aβ could provide further insights into the response of co-cultures astrocyte feeder cells upon Aβ treatment (33, 100). Last but not least, the co-culture model presented in this work also follows the principle of the 3Rs by this aiding in reducing *in vivo* testing whenever possible and feasible from an experimental perspective (145). Our modified Banker co-culture assay integrates the impact astrocytes and non-cell autonomous paracrine effects have into the role of neurons in the context of AD and might provide more a realistic scenario in vitro AD model as compared to mere addition of astrocytic conditioned media or studying effects of various treatments on neurons in isolation (185, 191).

4.4 A technical note: considerations for optimizing our modified Banker co-culture assay

Regarding further refinements of the presented protocol, several parameters could be modified to further improve our assay, which are as follows:

1) **Age of pups:** Embryonal tissue has several advantages over postnatal tissue. Firstly, culturing mouse postnatal neurons is more challenging than the culture of embryonal mouse neurons given the lower susceptibility of embryonal neurons to damage provoked by the harsh conditions during tissue dissection and trituration (67). As a consequence, postnatal neurons tend to be less robust and maintaining these cells in a healthy state is more difficult. Additionally, postnatal neurons display a higher proportion of non-neuronal cells because gliogenesis peaks around the neonatal period with the highest number of astrocytes around E18 (67, 192). In contrast to this, cultures of postnatal neurons clearly reduce the quantitiy of animals that need to be euthanized since fewer animals per litter are required. Remaining animals can be used for further breeding (67). Lastly, at our institution logistic efforts, timing and costs were more favorable when working with postnatal neuronal cultures as compared to embryonal neuronal cultures.

2) **Enzymatic digestion:** Some groups propagated the use of papain since it has been shown to be less destructive with certain tissues such as retinal neurons, whereas other groups in the field use of DNase I for enzymatic digestion (67, 74). We tested either a combination of trypsin and DNase I or Trypsin without DNase I with similar results for both. Future studies could compare different combinations of enzymatic digestion (e.g. papain with DNase I and trypsin).

3) **Trituration:** Many authors in the field argue that trituration of freshly dissected hippocampal or cortical tissue marks the most crucial step to obtain consistent neuronal *in vitro* cultures (67, 68, 70, 74, 75, 115). We tested different trituration protocols and noticed that a combination of intermittent use of an electronic pipette, fire-polished, sterile Pasteur pipettes and a 1000 µL plastic pipette produced more constant, less variable results in terms of viability and cell number as compared to other settings, e.g. where solely sterile Pasteur pipettes were employed (***Fig. 4***). This is *per se* similar to protocols published by other groups in the field (68, 74).

4) **Cell counting:** Viability as well as cell number of acutely dissected cells derived from hippocampi or cortices was measured with the trypan blue dye exclusion method using a semi-automatic cell counter. A sufficient viability of freshly dissected single cells in suspension with each dissection was essential for the maintenance of co-cultures and downstream experiments. When comparing semi-automatic with manual, hemocytometer-based cell counting, we observed an advantage of time-to-count using the cell counter (data not shown). This in turn, contributes to an overall reduction in assay duration as well as stress and damage of cells in suspension before being plated on

glass coverslips. Additionally, these factors likely resulted in an average increase in the quality of our primary cultures. Again, our viability and number of cells dissected per mouse brain was comparable to established protocols and published work (74, 75).

5) **Seeding density of neurons:** Density of neurons represents another essential variable that has to be taken into account, as insufficient amounts of neurons seeded will likely result in suboptimal growth and differentiation of neurons (68, 74). For both, the feeder layer (lower coverslip) and neuronal layer (upper coverslip) we found optimal seeding densities after having tested different densities based on literature research (74, 75). Feeder cells were seeded at either at a density of 40.000 or 80.000 feeder cells per well per 12 mm glass coverslip, whereas the amount of neuronal cells seeded on the upper coverslip was set to 25.000 (221 cells/mm2) or 50.000 (442 cells/µm2) neurons per well per 12 mm nitric acid-treated, poly-L-lysin-coated glass coverslip. Although we tested even “ultra-low” densities e.g. 5000 cells resulting in autaptic-like neuronal cultures (data not shown), seeding 50.000 neurons was associated with best possible long-term quality of cultures and more constant results. We managed to seed less neurons per coverslips and keeping seeding density lower than that of other studies deploying monocultures of neurons. This effect is most likely due to astrocyte-mediated paracrine support that compensates for low neuron densities. Hence, astrocyte paracrine support clearly seems to render neurons more stable and durable in *in vitro* conditions.

6) **Pre-conditioning of astrocytes:** The time allowed for pre-conditioning of the feeder cells (we regularly pre-conditioned astrocytes for 48-72 hours) represents another example and adjustable parameter that certainly impacts the propagation of neuronal cultures and could be modified (68, 74, 75). Pre-conditioning lasted for two days.

7) **Time to inversion of the upper coverslip:** Time-to-inversion of the neuronal coverslip has been compared during the process of establishment of the co-culture assay, where we compared three hours of time-to-inversion as done by Kaech and Banker vs. one hour time-to-inversion and noticed that neurons regularly adhere and form first dendritic projections already after one hour (***Fig. 8***).

8) **Other minor factors:** Other aspects that could be changed to improve our protocol, involve the duration of co-cultures until experimental manipulation, concentration of FUDR used for glial depletion, incorporating neuronal transfection, duration of experimental manipulation as such, etc. pp. (73, 119). As described earlier, there is the notion shared by many groups that data encompassing experiments with primary

neurons cultured *in vitro* should ideally be derived from neurons cultured at least for two weeks *in vitro*. This allows to perform experiments on properly differentiated neurons. However, using a co-culture approach as in this work, neurons *per se* reach the state of differentiation and expression of synaptic proteins earlier than neurons in monocultures. A more detailed comparison at the gene expression and protein level of neurons in regard to differentiation status in co-cultures and monocultures could provide further insights into the signaling pathways specific to astrocytic support of neurons *in vitro*.

9) **Throughput:** Without increasing pup numbers used for co-cultures one could use smaller wells and coverslips to increase technical replicates per experiment or number of different treatment conditions with one dissection. We used both formats for our co-cultures 24-well plates with 12 mm coverslips and 12-well plates with 18mm coverslips. Even proof-of-principle experiments with a 96-well format and 5 mm coverslips for co-cultures were performed. However, the workload and technical skills to establish the assay in this small format exceeded the potential benefits that could be derived from this kind of experiment since a 96-well co-culture format would be largely limited to MTT and LDH assays without any possibility to perform imaging (data not shown; 154, 155).

10) **Imaging:** Superior imaging methods have been stated already above and could facilitate to track changes in co-cultures and to perform spine classification (69, 196).

11) **Prospective cell isolation:** Additionally, purity of cognate cell types, i.e. lower coverslip for astrocytes and upper coverslips for neurons could be improved by introducing immunopanning or FACS-based approaches (83).

5. SUMMARY

Current AD models have provided valuable insights into disease mechanisms. Yet, there is a substantial lack of effective and targeted disease-modifying therapeutic modalities. One reason for the disappointing clinical trials throughout the last years is based on the shortage of validated pre-clinical AD models. Clearly, *in vivo* mouse models mark the gold-standard in AD research. However, they complicate investigation of cell-cell interactions and its mechanisms (14). On the other hand, cell lines or primary cells may be too reductionistic to study AD-related processes or to test drugs. In contrast to emerging and novel iPS cell-derived or 3D cultures of CNS cells, our modified Banker “sandwich” assay provides a more straightforward, less time-consuming and cost-intensive *in vitro* assay to model AD in a dish format (61, 62, 74, 75). We demonstrate that neurons co-cultured with astrocytes in a paracrine fashion are maintained in a healthy state at least two weeks *in vitro*. Additionally,

co-cultured neurons show accelerated growth and differentiation as compared to neurons in monocultures. Importantly, co-cultures are amenable to experimental manipulations as demonstrated in this work *via* the use of pre-treated astrocytes with Aβ42 and LPS. Hence, our model integrates classic aspects of AD such as the Aβ hypothesis as well as the role of astrocytes. Different readouts for neurons and astrocytes can be exploited to assess biologic alterations in our system. Thus, our approach provides a simple, yet reasonably complex and modular system, that has been reproduced independently by other members of our laboratory and that reflects some aspects of AD pathogenesis, involving cell-autonomous and non-cell autonomous effects on the neuronal phenotype. Finally, our co-culture assay may facilitate dissection of non-neuronal pathways causing neurotoxicity and synaptotoxicity in different diseases (185, 191, 194). To sum up, the work presented in this thesis shows that:

1. Neurons co-cultured with Astrocytes show signs of growth and differentiation
2. Manipulation of co-cultures allows modeling both synaptotoxicity and neurotoxicity
3. Our co-culture system is of potential use to dissect cell-autonomous and non-cell-autonomous effects on neuronal phenotypes
4. Our co-culture system is a cost-effective and reproducible method that has been taught to and performed in our group with published results (e.g. *Mohamadi et al., Mol. Neurobiol., 2020; Rojas Charry et al. (submitted manuscript)*.
5. The system has been shown in our lab to be of value in the characterization of transgenic mouse models (ongoing projects).

Aktuelle AD-Modelle liefern Einblicke in Krankheitsmechanismen. Jedoch existiert ein Mangel wirksamer, gezielter krankheitsmodifizierender Therapien. Ein Grund für bisher enttäuschende Ergebnisse klinischer Studien sind unzureichend validierte präklinischen Modelle. *In-vivo*-Mausmodelle repräsentieren derzeit den Goldstandard in der Alzheimer-Forschung. Die Untersuchung von Zell-Zell-Wechselwirkungen gestaltet sich hierbei als schwierig (14). Hingegen können Zelllinien oder primäre Zellkulturen zu reduktionistisch sein, um Alzheimer-bezogene Prozesse zu untersuchen oder Medikamente zu testen. Im Gegensatz zu neuartigen iPS- oder 3D-Kulturen von ZNS-Zellen stellt unser modifizierter Banker-Assay eine simple, weniger zeitaufwendige und kostenintensive Methode zur Modellierung von AD dar (61, 62, 74, 75). Neuronen in Ko-Kultur mit Astrozyten, *in vitro* überleben zwei Wochen lang in einem gesunden Zustand und zeigen beschleunigtes

Wachstum und Differenzierung im Vergleich zu Neuronen in Monokulturen. Zudem sind Ko-Kulturen experimentellen Manipulationen zugänglich, wie in dieser Arbeit unter Verwendung vorbehandelter Astrozyten mit Aβ42 und LPS dargelegt. Daher integriert unser Modell klassische Aspekte wie die Aβ-Hypothese sowie die Rolle der Astrozyten. Verschiedene Indizes für Neuronen und Astrozyten ermöglichen biologische Veränderungen in unserem System zu bewerten. Somit bietet unser Ansatz ein simples, modulares System, das von mehreren Mitgliedern unseres Labors getestet wurde und Aspekte der Alzheimer-Pathogenese widerspiegelt, wie etwa zell-autonome und nicht-zell-autonome Effekte auf den neuronalen Phänotyp. Der vorgestellte Assay kann einen Beitrag leisten im Kontext verschiedener Pathologien Neuro- und Synaptotoxizität zu untersuchen (185, 191, 194). Zusammenfassend zeigt die vorgestellte Arbeit, dass:

1. Mit Astrozyten ko-kultivierte Neuronen zeigen Anzeichen des Wachstums und der Differenzierung *in vitro*

2. Manipulation von Ko-Kulturen ermöglicht Modellierungen sowohl der Synaptotoxizität als auch der Neurotoxizität

3. Unser Ko-Kultursystem helfen kann zellautonome und nicht zellautonome Effekte auf neuronale Phänotypen untersuchen

4. Unser Ko-Kultursystem ist kostengünstig, reproduzierbar und wurde von mehreren angelernten Mitarbeitern getestet mit publikationswürdigen Resultaten (e.g. *Mohamadi et al., Mol. Neurobiol., 2020* oder *Rojas Charry et al. (eingereichtes Manuskript)*.

5. Das System hat sich in unserem Labor als wertvoll für die Charakterisierung transgener Mausmodelle erwiesen (laufende Projekte).

6. APPENDIX

6.1 Abbreviations

Important abbreviations are introduced and mentioned separately throughout this work. More common abbreviations are not introduced within the text as such but can be found in the list of abbreviations.

Ab	Antibody
Aβ	Amyloid-β
aCM	Astrocyte conditioned medium
AD	Alzheimer's disease
APP	Amyloid precursor protein
et al.	Et alii
BACE-1	ß-site amyloid precursor protein-leaving enzyme 1
°C	Degrees Celcius
C3	Complement 3
Ca2+	Calcium 2+ ion
cat#	Catalog number
CNS	Central nervous system
CM	Conditioned medium
C3R	Complement 3 receptor
CTCF	Corrected total cell fluorescence
cv	Coverslip
d	Day
DAPI	4',6-Diamidino-2-phenylindole
DAPI+	DAPI-positive

DIV	Day *in vitro*
DM	Dissection medium
DMEM	Dulbecco’s modified Eagle’s medium
DMSO	Dimethyl sulfoxide
e.g.	Exemplia gratiae
ELISA	Enzyme linked immunosorbent assay
FACS	Fluorescence-activated cell sorting
FBS	Fetal bovine serum
FDA	Federal drug administration
Fig.	Figure
FUDR	5-Fluoro-2′-deoxyuridine
GFAP	Glial fibrillary acidic protein
GFAP+	GFAP-positive
GGM	Glial growth medium
h	Hour
HBSS	Hank's Balanced Salt Solution
HEPES	Hydroxyethylpiperazine-ethanesulfonic acid
i.e.	id est
IF	Immunofluorescence
IHC	Immunohistochemistry
IOD	Integrated optical density
iPS	Induced pluripotent stem cells
Lot#	Lot number
LPS	lipopolysaccharide

LTP	Long-term potentiation
MAP2	Microtubuli-associated protein 2
MAP2+	MAP2-positive
max. intersections	Maximum of intersections
mg	Miligramm
mL	Mililiter
Model#	Model number
MTT	3-(4,5-Dimethylthiazol-2-yl)-2,5-diphenyltetrazolium bromide
Nav	Mean value
Nm	Critical value
NMM	Neuronal maintenance medium
PLL hydrobromide	Poly-L-lysine hydrobromide
P0	Postnatal 0 day *in vitro*
PSEN1/2	Presinilin 1/2
µL	Microliter
ug	Microgramm
OPCs	Oligodendrocyte precursor cells
RAs	Reactive astrocytes
Rc	Critical radius
Rpm	Rounds per minute
RT	Room temperature
SEM	Standard error of the mean

Syn	Synaptophysin
Syn+	Synaptophysin
TNF-α	Tumor necrosis factor-α
3D	Three-dimensional
µm	Micrometer
UKE	University Medical Center Hamburg Eppendorf
UV light	Ultraviolet light
vs.	Versus
w/v	Weight per volume

Table 5: Abbreviations

6.2 List of figures

6.3. List of tables

7. REFERENCES

1. Advances in the prevention of Alzheimer's Disease. Sindi S, Mangialasche F, Kivipelto M. F1000Prime Rep. 2015 May 12;7:50. doi: 10.12703/P7-50. eCollection 2015. Review. PMID: 26097723

2. The amyloid hypothesis of Alzheimer's disease at 25 years. Selkoe DJ, Hardy J. EMBO Mol Med. 2016 Jun 1;8(6):595-608. doi: 10.15252/emmm.201606210. Print 2016 Jun. Review. PMID: 27025652

3. Alzheimer's disease: the challenge of the second century. Holtzman DM, Morris JC, Goate AM. Sci Transl Med. 2011 Apr 6;3(77):77sr1. doi: 10.1126/scitranslmed.3002369. Review. PMID: 21471435

4. The global prevalence of dementia: a systematic review and metaanalysis. Prince M, Bryce R, Albanese E, Wimo A, Ribeiro W, Ferri CP. Alzheimers Dement. 2013 Jan;9(1):63-75.e2. doi: 10.1016/j.jalz.2012.11.007. Review. PMID: 23305823

5. The price of progress: Funding and financing Alzheimer's disease drug development. Cummings J, Reiber C, Kumar P. Alzheimers Dement (N Y). 2018 Jun 13;4:330-343. doi: 10.1016/j.trci.2018.04.008. eCollection 2018. PMID: 30175227

6. Defeating Alzheimer’s disease and other dementias: a priority for European science and society. Winblad B, Amouyel P, Andrieu S, Ballard C, Brayne C, Brodaty H, Cedazo-Minguez A, Dubois B, Edvardsson D, Feldman H, Fratiglioni L, Frisoni GB, Gauthier S, Georges J, Graff C, Iqbal K, Jessen F, Johansson G, Jönsson L, Kivipelto M, Knapp M, Mangialasche F, Melis R, Nordberg A, Rikkert MO, Qiu C, Sakmar TP, Scheltens P, Schneider LS, Sperling R, Tjernberg LO, Waldemar G, Wimo A, Zetterberg H. Lancet Neurol. 2016 Apr;15(5):455-532. doi: 10.1016/S1474-4422(16)00062-4. Review. PMID: 26987701

7. The neuropsychological profile of Alzheimer disease. Weintraub S, Wicklund AH, Salmon DP.Cold Spring Harb Perspect Med. 2012 Apr;2(4):a006171. doi: 10.1101/cshperspect.a006171. Review. PMID: 22474609

8. Clinical significance of focal ß-amyloid deposition measured by $_{18}$F-flutemetamol PET. Kim SE, Lee B, Park S, Cho SH, Kim SJ, Kim Y, Jang H, Jeong JH, Yoon SJ, Park KW, Kim EJ, Jung NY, Yoon B, Jang JW, Hong JY, Hwang J, Na DL, Seo SW, Choi SH, Kim HJ. Alzheimers Res Ther. 2020 Jan 4;12(1):6. doi: 10.1186/s13195-019-0577-x. PMID: 31901233

9. Role of genes and environments for explaining Alzheimer disease. Gatz M, Reynolds CA, Fratiglioni L, Johansson B, Mortimer JA, Berg S, Fiske A, Pedersen NL. Arch Gen Psychiatry. 2006 Feb;63(2):168-74. PMID: 16461860

10. Environmental risk factors for dementia: a systematic review. Killin LO, Starr JM, Shiue IJ, Russ TC. BMC Geriatr. 2016 Oct 12;16(1):175. Review. PMID: 27729011

11. Molecular genetics of early-onset Alzheimer's disease revisited. Cacace R, Sleegers K, Van Broeckhoven C. Alzheimers Dement. 2016 Jun;12(6):733-48. doi: 10.1016/j.jalz.2016.01.012. Epub 2016 Mar 24. Review. PMID: 27016693

12. Cloning of a gene bearing missense mutations in early-onset familial Alzheimer's disease. Sherrington R, Rogaev EI, Liang Y, Rogaeva EA, Levesque G, Ikeda M, Chi H, Lin C, Li G, Holman K, Tsuda T, Mar L, Foncin JF, Bruni AC, Montesi MP, Sorbi S, Rainero I, Pinessi L, Nee L, Chumakov I, Pollen D, Brookes A, Sanseau P, Polinsky RJ, Wasco W, Da Silva HA, Haines JL, Perkicak-Vance MA, Tanzi RE, Roses AD, Fraser PE, Rommens JM, St George-Hyslop PH. Nature. 1995 Jun 29;375(6534):754-60. PMID: 7596406

13. Alzheimer's Disease Mechanisms and Emerging Roads to Novel Therapeutics. Sala Frigerio C, De Strooper B. Annu Rev Neurosci. 2016 Jul 8;39:57-79. doi: 10.1146/annurev-neuro-070815-014015. Epub 2016 Apr 4. Review. PMID: 27050320

14. Alzheimer's disease: experimental models and reality. Drummond E, Wisniewski T. Acta Neuropathol. 2017 Feb;133(2):155-175. doi: 10.1007/s00401-016-1662-x. Epub 2016 Dec 26. Review. PMID: 28025715

15. The amyloid hypothesis of Alzheimer's disease: progress and problems on the road to therapeutics. Hardy J, Selkoe DJ. Science. 2002 Jul 19;297(5580):353-6. Review. Erratum in: Science 2002 Sep 27;297(5590):2209. PMID: 12130773

16. Altered expression of synaptic proteins occurs early during progression of Alzheimer's disease. Masliah E, Mallory M, Alford M, DeTeresa R, Hansen LA, McKeel DW Jr, Morris JC. Neurology. 2001 Jan 9;56(1):127-9. PMID: 11148253

17. Alzheimer's disease: synaptic dysfunction and Abeta. Shankar GM, Walsh DM. Mol Neurodegener. 2009 Nov 23;4:48. doi: 10.1186/1750-1326-4-48. PMID: 19930651

18. Synaptic alterations in CA1 in mild Alzheimer disease and mild cognitive impairment. Scheff SW, Price DA, Schmitt FA, DeKosky ST, Mufson EJ. Neurology. 2007 May 1;68(18):1501-8. PMID: 17470753

19. Physical basis of cognitive alterations in Alzheimer's disease: synapse loss is the major correlate of cognitive impairment. Terry RD, Masliah E, Salmon DP, Butters N, DeTeresa R, Hill R, Hansen LA, Katzman R. Ann Neurol. 1991 Oct;30(4):572-80. PMID: 1789684

20. Diagnostic yield of brain CT in a limited-access environment. Weiser M, Hendler T, Prohovnik I, Davidson M. Int J Psychiatry Clin Pract. 1998;2(4):279-82. doi: 10.3109/13651509809115374. PMID: 24927092

21. Alzheimer's disease: genes, proteins, and therapy. Selkoe DJ. Physiol Rev. 2001 Apr;81(2):741-66. Review. PMID: 11274343

22. Emerging concepts in Alzheimer's disease. Vinters HV. Annu Rev Pathol. 2015; 10:291-319. doi: 10.1146/annurev-pathol-020712-163927. Epub 2014 Oct 29. Review. PMID: 25387055

23. Naturally secreted oligomers of amyloid beta protein potently inhibit hippocampal long-term potentiation in vivo. Walsh DM, Klyubin I, Fadeeva JV, Cullen WK, Anwyl R, Wolfe MS, Rowan MJ, Selkoe DJ. Nature. 2002 Apr 4;416(6880):535-9. PMID: 11932745

24. LTP inhibits LTD in the hippocampus via regulation of GSK3beta. Peineau S, Taghibiglou C, Bradley C, Wong TP, Liu L, Lu J, Lo E, Wu D, Saule E, Bouschet T, Matthews P, Isaac JT, Bortolotto ZA, Wang YT, Collingridge GL. Neuron. 2007 Mar 1;53(5):703-17. PMID: 17329210

25. Alzheimer's disease-affected brain: presence of oligomeric A beta ligands (ADDLs) suggests a molecular basis for reversible memory loss. Gong Y, Chang L, Viola KL, Lacor PN, Lambert MP, Finch CE, Krafft GA, Klein WL. Proc Natl Acad Sci U S A. 2003 Sep 2;100(18):10417-22. Epub 2003 Aug 18. PMID: 12925731

26. Neurotoxicity of amyloid β-protein: synaptic and network dysfunction. Mucke L, Selkoe DJ. Cold Spring Harb Perspect Med. 2012 Jul;2(7):a006338. doi: 10.1101/cshperspect.a006338. Review. PMID: 22762015

27. The Cellular Phase of Alzheimer's Disease. De Strooper B, Karran E. Cell. 2016 Feb 11;164(4):603-15. doi: 10.1016/j.cell.2015.12.056. Review. PMID: 26871627

28. AlzPathway: a comprehensive map of signaling pathways of Alzheimer's disease. Mizuno S, Iijima R, Ogishima S, Kikuchi M, Matsuoka Y, Ghosh S, Miyamoto T, Miyashita A, Kuwano R, Tanaka H. BMC Syst Biol. 2012 May 30;6:52. doi: 10.1186/1752-0509-6-52. PMID: 22647208

29. Signaling pathway cross talk in Alzheimer's disease. Godoy JA, Rios JA, Zolezzi JM, Braidy N, Inestrosa NC. Cell Commun Signal. 2014 Mar 28; 12:23. doi: 10.1186/1478-811X-12-23. Review. PMID: 24679124

30. Development of a femtomolar-acting humanin derivative named colivelin by attaching activity-dependent neurotrophic factor to its N terminus: characterization of colivelin-mediated neuroprotection against Alzheimer's disease-relevant insults in vitro and in vivo Chiba T, Yamada M, Hashimoto Y, Sato M, Sasabe J, Kita Y, Terashita K, Aiso S, Nishimoto I, Matsuoka M. J Neurosci. 2005 Nov 2;25(44):10252-61. PMID: 16267233

31. Implanted cannula-mediated repetitive administration of Abeta25-35 into the mouse cerebral ventricle effectively impairs spatial working memory. Yamada M, Chiba T, Sasabe

J, Nawa M, Tajima H, Niikura T, Terashita K, Aiso S, Kita Y, Matsuoka M, Nishimoto I. Behav Brain Res. 2005 Nov 7;164(2):139-46. PMID: 16122819

32. Repeated intra-hippocampal injection of beta-amyloid 25–35 induces a reproducible impairment of learning and memory: considering caspase-3 and MAPKs activity. Ghasemi R, Zarifkar A, Rastegar K, Maghsoudi N, Moosavi M. Eur J Pharmacol. 2014 Mar 5;726:33-40. PMID: 24418687

33. Protective effect of melatonin on soluble Aβ1-42-induced memory impairment, astrogliosis, and synaptic dysfunction via the Musashi1/Notch1/Hes1 signaling pathway in the rat hippocampus. Zhang S, Wang P, Ren L, Hu C, Bi J. Alzheimers Res Ther. 2016 Sep 15;8(1):40. doi: 10.1186/s13195-016-0206-x. PMID: 27630117

34. Soluble forms of tau are toxic in Alzheimer's disease. Kopeikina KJ, Hyman BT, Spires-Jones TL. Transl Neurosci. 2012 Sep;3(3):223-233. PMID: 23029602

35. Inflammatory changes parallel the early stages of Alzheimer disease. Parachikova A, Agadjanyan MG, Cribbs DH, Blurton-Jones M, Perreau V, Rogers J, Beach TG, Cotman CW. Neurobiol Aging. 2007 Dec;28(12):1821-33. Epub 2006 Oct 18. PMID: 17052803

36. Monocyte chemoattractant protein-1 plays a dominant role in the chronic inflammation observed in Alzheimer's disease. Sokolova A, Hill MD, Rahimi F, Warden LA, Halliday GM, Shepherd CE. Brain Pathol. 2009 Jul;19(3):392-8. doi: 10.1111/j.1750-3639.2008.00188.x. Epub 2008 Jul 10. PMID: 18637012

37. Amyloid burden, neuroinflammation, and links to cognitive decline after ischemic stroke. Thiel A, Cechetto DF, Heiss WD, Hachinski V, Whitehead SN. Stroke. 2014 Sep;45(9):2825-9. doi: 10.1161/STROKEAHA.114.004285. Epub 2014 Jul 8. Review. No abstract available. PMID: 25005439

38. Neuroinflammation in Alzheimer's disease. Heneka MT, Carson MJ, El Khoury J, Landreth GE, Brosseron F, Feinstein DL, Jacobs AH, Wyss-Coray T, Vitorica J, Ransohoff RM, Herrup K, Frautschy SA, Finsen B, Brown GC, Verkhratsky A, Yamanaka K, Koistinaho J, Latz E, Halle A, Petzold GC, Town T, Morgan D, Shinohara ML, Perry VH,

Holmes C, Bazan NG, Brooks DJ, Hunot S, Joseph B, Deigendesch N, Garaschuk O, Boddeke E, Dinarello CA, Breitner JC, Cole GM, Golenbock DT, Kummer MP. Lancet Neurol. 2015 Apr;14(4):388-405. doi: 10.1016/S1474-4422(15)70016-5. Review. PMID: 25792098

39. The role of astroglia in Alzheimer's disease: pathophysiology and clinical implications. Arranz AM, De Strooper B. Lancet Neurol. 2019 Apr;18(4):406-414. doi: 10.1016/S1474-4422(18)30490-3. Epub 2019 Feb 19. Review. PMID: 30795987

40. Deciphering the Astrocyte Reaction in Alzheimer's Disease. Perez-Nievas BG, Serrano-Pozo A. Front Aging Neurosci. 2018 Apr 25;10:114. doi: 10.3389/fnagi.2018.00114. eCollection 2018. Review. PMID: 29922147

41. Microglia in Alzheimer Disease: Well-Known Targets and New Opportunities. Hemonnot AL, Hua J, Ulmann L, Hirbec H. Front Aging Neurosci. 2019 Aug 30;11:233. doi: 10.3389/fnagi.2019.00233. eCollection 2019. Review. PMID: 31543810

42. Neuro-inflammation induced by lipopolysaccharide causes cognitive impairment through enhancement of beta-amyloid generation. Lee JW, Lee YK, Yuk DY, Choi DY, Ban SB, Oh KW, Hong JT. J Neuroinflammation. 2008 Aug 29;5:37. doi: 10.1186/1742-2094-5-37. PMID: 18759972

43. Microbiome-Derived Lipopolysaccharide Enriched in the Perinuclear Region of Alzheimer's Disease Brain. Zhao Y, Cong L, Jaber V, Lukiw WJ. Front Immunol. 2017 Sep 4;8:1064. doi: 10.3389/fimmu.2017.01064. eCollection 2017. PMID: 28928740

44. Lipopolysaccharide (LPS) Accumulates in Neocortical Neurons of Alzheimer's Disease (AD) Brain and Impairs Transcription in Human Neuronal-Glial Primary Co-cultures. Zhao Y, Cong L, Lukiw WJ. Front Aging Neurosci. 2017 Dec 12;9:407. doi: 10.3389/fnagi.2017.00407. eCollection 2017.PMID: 29311897

45. Neuropathology of Alzheimer's disease. Perl DP. Mt Sinai J Med. 2010 Jan-Feb;77(1):32-42. doi: 10.1002/msj.20157. Review. PMID: 20101720

46. Modeling Alzheimer's disease: from past to future. Saraceno C, Musardo S, Marcello E, Pelucchi S, Di Luca M. Front Pharmacol. 2013 Jun 19;4:77. doi: 10.3389/fphar.2013.00077. eCollection 2013. PMID: 23801962

47. Neurodegeneration: From cellular concepts to clinical applications. Katsnelson A, De Strooper B, Zoghbi HY. Sci Transl Med. 2016 Nov 9;8(364):364ps18. Review. No abstract available. PMID: 27831899

48. A phase 3 trial of semagacestat for treatment of Alzheimer's disease. Doody RS, Raman R, Farlow M, Iwatsubo T, Vellas B, Joffe S, Kieburtz K, He F, Sun X, Thomas RG, Aisen PS; Alzheimer's Disease Cooperative Study Steering Committee, Siemers E, Sethuraman G, Mohs R; Semagacestat Study Group.N Engl J Med. 2013 Jul 25;369(4):341-50. doi: 10.1056/NEJMoa1210951. PMID: 23883379

49. Two phase 3 trials of bapineuzumab in mild-to-moderate Alzheimer's disease. Salloway S, Sperling R, Fox NC, Blennow K, Klunk W, Raskind M, Sabbagh M, Honig LS, Porsteinsson AP, Ferris S, Reichert M, Ketter N, Nejadnik B, Guenzler V, Miloslavsky M, Wang D, Lu Y, Lull J, Tudor IC, Liu E, Grundman M, Yuen E, Black R, Brashear HR; Bapineuzumab 301 and 302 Clinical Trial Investigators. N Engl J Med. 2014 Jan 23;370(4):322-33. doi: 10.1056/NEJMoa1304839. PMID: 24450891

50. Phase 3 trials of solanezumab for mild-to-moderate Alzheimer's disease. Doody RS, Thomas RG, Farlow M, Iwatsubo T, Vellas B, Joffe S, Kieburtz K, Raman R, Sun X, Aisen PS, Siemers E, Liu-Seifert H, Mohs R; Alzheimer's Disease Cooperative Study Steering Committee; Solanezumab Study Group. N Engl J Med. 2014 Jan 23;370(4):311-21. doi: 10.1056/NEJMoa1312889. PMID: 24450890

51.Trial of Solanezumab for Mild Dementia Due to Alzheimer's Disease. Honig LS, Vellas B, Woodward M, Boada M, Bullock R, Borrie M, Hager K, Andreasen N, Scarpini E, Liu-Seifert H, Case M, Dean RA, Hake A, Sundell K, Poole Hoffmann V, Carlson C, Khanna R, Mintun M, DeMattos R, Selzler KJ, Siemers E. N Engl J Med. 2018 Jan 25;378(4):321-330. doi: 10.1056/NEJMoa1705971. PMID: 29365294

52. Randomized Trial of Verubecestat for Prodromal Alzheimer's Disease. Egan MF, Kost J, Voss T, Mukai Y, Aisen PS, Cummings JL, Tariot PN, Vellas B, van Dyck CH, Boada M, Zhang Y, Li W, Furtek C, Mahoney E, Harper Mozley L, Mo Y, Sur C, Michelson D. N Engl J Med. 2019 Apr 11;380(15):1408-1420. doi: 10.1056/NEJMoa1812840. PMID: 30970186

53. Anti-amyloid failures stack up as Alzheimer antibody flops. Mullard A. Nat Rev Drug Discov. 2019 Apr 5. doi: 10.1038/d41573-019-00064-1. [Epub ahead of print] No abstract available. PMID: 31048802

54. The diagnosis of dementia due to Alzheimer's disease: recommendations from the National Institute on Aging-Alzheimer's Association workgroups on diagnostic guidelines for Alzheimer's disease. McKhann GM, Knopman DS, Chertkow H, Hyman BT, Jack CR Jr, Kawas CH, Klunk WE, Koroshetz WJ, Manly JJ, Mayeux R, Mohs RC, Morris JC, Rossor MN, Scheltens P, Carrillo MC, Thies B, Weintraub S, Phelps CH. Alzheimers Dement. 2011 May;7(3):263-9. doi: 10.1016/j.jalz.2011.03.005. Epub 2011 Apr 21. PMID: 21514250

55. NIA-AA Research Framework: Toward a biological definition of Alzheimer's disease. Jack CR Jr, Bennett DA, Blennow K, Carrillo MC, Dunn B, Haeberlein SB, Holtzman DM, Jagust W, Jessen F, Karlawish J, Liu E, Molinuevo JL, Montine T, Phelps C, Rankin KP, Rowe CC, Scheltens P, Siemers E, Snyder HM, Sperling R; Contributors. Alzheimers Dement. 2018 Apr;14(4):535-562. doi: 10.1016/j.jalz.2018.02.018. Review. PMID: 29653606

56. Can we prevent Alzheimer's disease? Secondary "prevention" trials in Alzheimer's disease. Carrillo MC, Brashear HR, Logovinsky V, Ryan JM, Feldman HH, Siemers ER, Abushakra S, Hartley DM, Petersen RC, Khachaturian AS, Sperling RA. Alzheimers Dement. 2013 Mar;9(2):123-131.e1. doi: 10.1016/j.jalz.2012.12.004. Epub 2013 Feb 12. Review. PMID: 23411394

57. Advancing research diagnostic criteria for Alzheimer's disease: the IWG-2 criteria. Dubois B, Feldman HH, Jacova C, Hampel H, Molinuevo JL, Blennow K, DeKosky ST, Gauthier S, Selkoe D, Bateman R, Cappa S, Crutch S, Engelborghs S, Frisoni GB, Fox NC, Galasko D, Habert MO, Jicha GA, Nordberg A, Pasquier F, Rabinovici G, Robert P,

Rowe C, Salloway S, Sarazin M, Epelbaum S, de Souza LC, Vellas B, Visser PJ, Schneider L, Stern Y, Scheltens P, Cummings JL. Lancet Neurol. 2014 Jun;13(6):614-29. doi: 10.1016/S1474-4422(14)70090-0. Erratum in: Lancet Neurol. 2014 Aug;13(8):757. PMID: 24849862

58. Testing the right target and right drug at the right stage. Sperling RA, Jack CR Jr, Aisen PS. Sci Transl Med. 2011 Nov 30;3(111):111cm33. doi: 10.1126/scitranslmed.3002609. Review. PMID: 22133718

59. Studying neurodegenerative diseases in culture models. Schlachetzki JC, Saliba SW, Oliveira AC. Braz J Psychiatry. 2013;35 Suppl 2:S92-100. doi: 10.1590/1516-4446-2013-1159. Review. PMID: 24271231

60. A three-dimensional human neural cell culture model of Alzheimer's disease. Choi SH, Kim YH, Hebisch M, Sliwinski C, Lee S, D'Avanzo C, Chen H, Hooli B, Asselin C, Muffat J, Klee JB, Zhang C, Wainger BJ, Peitz M, Kovacs DM, Woolf CJ, Wagner SL, Tanzi RE, Kim DY. Nature. 2014 Nov 13;515(7526):274-8. doi: 10.1038/nature13800. Epub 2014 Oct 12. PMID: 25307057

61. Functional cortical neurons and astrocytes from human pluripotent stem cells in 3D culture. Paşca AM, Sloan SA, Clarke LE, Tian Y, Makinson CD, Huber N, Kim CH, Park JY, O'Rourke NA, Nguyen KD, Smith SJ, Huguenard JR, Geschwind DH, Barres BA, Paşca SP. Nat Methods. 2015 Jul;12(7):671-8. doi: 10.1038/nmeth.3415. Epub 2015 May 25. PMID: 26005811

62. Building Models of Brain Disorders with Three-Dimensional Organoids. Amin ND, Paşca SP. Neuron. 2018 Oct 24;100(2):389-405. doi: 10.1016/j.neuron.2018.10.007. Review. PMID: 30359604

63. An in vitro model for neuroscience: differentiation of SH-SY5Y cells into cells with morphological and biochemical characteristics of mature neurons. Agholme L, Lindström T, Kågedal K, Marcusson J, Hallbeck M. J Alzheimers Dis. 2010;20(4):1069-82. doi: 10.3233/JAD-2010-091363. PMID: 20413890

64. Neuronal properties and trophic activities of immortalized hippocampal cells from embryonic and young adult mice. Lee HJ, Hammond DN, Large TH, Roback JD, Sim JA, Brown DA, Otten UH, Wainer BH. J Neurosci. 1990 Jun;10(6):1779-87. PMID: 2113086

65. HT22 hippocampal neuronal cell line possesses functional cholinergic properties. Liu J, Li L, Suo WZ. Life Sci. 2009 Feb 27;84(9-10):267-71. doi: 10.1016/j.lfs.2008.12.008. Epub 2008 Dec 16. PMID: 19135458

66. Mixed-culture assays for analyzing neuronal synapse formation. Biederer T, Scheiffele P. Nat Protoc. 2007;2(3):670-6. PMID: 17406629

67. Culturing pyramidal neurons from the early postnatal mouse hippocampus and cortex. Beaudoin GM 3rd, Lee SH, Singh D, Yuan Y, Ng YG, Reichardt LF, Arikkath J. Nat Protoc. 2012 Sep;7(9):1741-54. doi: 10.1038/nprot.2012.099. Epub 2012 Aug 30. PMID: 22936216

68. Isolation and culture of hippocampal neurons from prenatal mice. Seibenhener ML, Wooten MW. J Vis Exp. 2012 Jul 26;(65). pii: 3634. doi: 10.3791/3634. PMID: 22871921

69. Imaging dendritic spines of rat primary hippocampal neurons using structured illumination microscopy. Schouten M, De Luca GM, Alatriste González DK, de Jong BE, Timmermans W, Xiong H, Krugers H, Manders EM, Fitzsimons CP. J Vis Exp. 2014 May 4;(87). doi: 10.3791/51276. PMID: 24835130

70. Single-cell axotomy of cultured hippocampal neurons integrated in neuronal circuits. Gomis-Rüth S, Stiess M, Wierenga CJ, Meyn L, Bradke F. Nat Protoc. 2014 May;9(5):1028-37. doi: 10.1038/nprot.2014.069. Epub 2014 Apr 3. PMID: 24705599

71. All Together Now: Modeling the Interaction of Neural With Non-neural Systems Using Organoid Models. Chukwurah E, Osmundsen A, Davis SW, Lizarraga SB. Front Neurosci. 2019 Jun 21;13:582. doi: 10.3389/fnins.2019.00582. eCollection 2019. Review. PMID: 31293366

72. In vitro identification and electrophysiological characterization of dopamine neurons in the ventral tegmental area. Zhang TA, Placzek AN, Dani JA. Neuropharmacology. 2010 Nov;59(6):431-6. doi: 10.1016/j.neuropharm.2010.06.004. Epub 2010 Jun 18. PMID: 20600174

73. In vitro modelling of Alzheimer's disease: degeneration and cell death induced by viral delivery of amyloid and tau. Stoppelkamp S, Bell HS, Palacios-Filardo J, Shewan DA, Riedel G, Platt B. Exp Neurol. 2011 Jun;229(2):226-37. doi: 10.1016/j.expneurol.2011.01.018. Epub 2011 Feb 2. PMID: 21295028

74. Culturing hippocampal neurons. Kaech S, Banker G. Nat Protoc. 2006;1(5):2406-15. Epub 2007 Jan 11. PMID: 17406484

75. A neuron-astrocyte co-culture system to investigate astrocyte-secreted factors in mouse neuronal development. Jones EV, Cook D, Murai KK. Methods Mol Biol. 2012;814:341-52. doi: 10.1007/978-1-61779-452-0_22. PMID: 22144317

76. Isolation and culture of mouse cortical astrocytes. Schildge S, Bohrer C, Beck K, Schachtrup C. J Vis Exp. 2013 Jan 19;(71). pii: 50079. doi: 10.3791/50079. PMID: 23380713

77. Diversity of astrocyte functions and phenotypes in neural circuits. Khakh BS, Sofroniew MV. Nat Neurosci. 2015 Jul;18(7):942-52. doi: 10.1038/nn.4043. Review. PMID: 261087

78. Astrocytes: biology and pathology. Sofroniew MV, Vinters HV. Acta Neuropathol. 2010 Jan;119(1):7-35. doi: 10.1007/s00401-009-0619-8. Epub 2009 Dec 10. Review. PMID: 20012068

79. Reactive Astrocytes: Production, Function, and Therapeutic Potential. Liddelow SA, Barres BA. Immunity. 2017 Jun 20;46(6):957-967. doi: 10.1016/j.immuni.2017.06.006. Review. PMID: 28636962

80. Astrocytes mediate synapse elimination through MEGF10 and MERTK pathways. Chung WS, Clarke LE, Wang GX, Stafford BK, Sher A, Chakraborty C, Joung J, Foo LC,

Thompson A, Chen C, Smith SJ, Barres BA. Nature. 2013 Dec 19;504(7480):394-400. doi: 10.1038/nature12776. Epub 2013 Nov 24. PMID:24270812

81. Serpins promote cancer cell survival and vascular co-option in brain metastasis. Valiente M, Obenauf AC, Jin X, Chen Q, Zhang XH, Lee DJ, Chaft JE, Kris MG, Huse JT, Brogi E, Massagué J. Cell. 2014 Feb 27;156(5):1002-16. doi: 10.1016/j.cell.2014.01.040. PMID: 24581498

82. Astrocyte scar formation aids central nervous system axon regeneration. Anderson MA, Burda JE, Ren Y, Ao Y, O'Shea TM, Kawaguchi R, Coppola G, Khakh BS, Deming TJ, Sofroniew MV. Nature. 2016 Apr 14;532(7598):195-200. doi: 10.1038/nature17623. Epub 2016 Mar 30. PMID: 27027288

83. Neurotoxic reactive astrocytes are induced by activated microglia. Liddelow SA, Guttenplan KA, Clarke LE, Bennett FC, Bohlen CJ, Schirmer L, Bennett ML, Münch AE, Chung WS, Peterson TC, Wilton DK, Frouin A, Napier BA, Panicker N, Kumar M, Buckwalter MS, Rowitch DH, Dawson VL, Dawson TM, Stevens B, Barres BA. Nature. 2017 Jan 26;541(7638):481-487. doi: 10.1038/nature21029. Epub 2017 Jan 18. PMID: 28099414

84. Inhibition of astrocytic activity alleviates sequela in acute stages of intracerebral hemorrhage. Chiu CD, Yao NW, Guo JH, Shen CC, Lee HT, Chiu YP, Ji HR, Chen X, Chen CC, Chang C. Oncotarget. 2017 Oct 24;8(55):94850-94861. doi: 10.18632/oncotarget.22022. eCollection 2017 Nov 7. PMID: 29212271

85. Author Correction: STAT3 labels a subpopulation of reactive astrocytes required for brain metastasis. Priego N, Zhu L, Monteiro C, Mulders M, Wasilewski D, Bindeman W, Doglio L, Martínez L, Martínez-Saez E, Ramón Y Cajal S, Megías D, Hernández-Encinas E, Blanco-Aparicio C, Martínez L, Zarzuela E, Muñoz J, Fustero-Torre C, Piñeiro-Yáñez E, Hernández-Laín A, Bertero L, Poli V, Sanchez-Martinez M, Menendez JA, Soffietti R, Bosch-Barrera J, Valiente M. Nat Med. 2018 Sep;24(9):1481. doi: 10.1038/s41591-018-0108-5. PMID: 29921958

86. Tumor-associated reactive astrocytes aid the evolution of immunosuppressive environment in glioblastoma. Henrik Heiland D, Ravi VM, Behringer SP, Frenking JH, Wurm J, Joseph K, Garrelfs NWC, Strähle J, Heynckes S, Grauvogel J, Franco P, Mader I, Schneider M, Potthoff AL, Delev D, Hofmann UG, Fung C, Beck J, Sankowski R, Prinz M, Schnell O. Nat Commun. 2019 Jun 11;10(1):2541. doi: 10.1038/s41467-019-10493-6. PMID: 31186414

87. Brain regulatory T cells suppress astrogliosis and potentiate neurological recovery. Ito M, Komai K, Mise-Omata S, Iizuka-Koga M, Noguchi Y, Kondo T, Sakai R, Matsuo K, Nakayama T, Yoshie O, Nakatsukasa H, Chikuma S, Shichita T, Yoshimura A. Nature. 2019 Jan;565(7738):246-250. doi: 10.1038/s41586-018-0824-5. Epub 2019 Jan 2. PMID: 30602786

88. Genomic analysis of reactive astrogliosis. Zamanian JL, Xu L, Foo LC, Nouri N, Zhou L, Giffard RG, Barres BA. J Neurosci. 2012 May 2;32(18):6391-410. doi: 10.1523/JNEUROSCI.6221-11.2012. PMID: 22553043

89. Elusive roles for reactive astrocytes in neurodegenerative diseases. Ben Haim L, Carrillo-de Sauvage MA, Ceyzériat K, Escartin C. Front Cell Neurosci. 2015 Aug 3;9:278. doi: 10.3389/fncel.2015.00278. eCollection 2015. Review. PMID:26283915

90. Astrocytes: a central element in neurological diseases. Pekny M, Pekna M, Messing A, Steinhäuser C, Lee JM, Parpura V, Hol EM, Sofroniew MV, Verkhratsky A. Acta Neuropathol. 2016 Mar;131(3):323-45. doi: 10.1007/s00401-015-1513-1. Epub 2015 Dec 15. Review. PMID: 26671410

91. Astrocyte heterogeneity across the brain and spinal cord occurs developmentally, in adulthood and in response to demyelination. Yoon H, Walters G, Paulsen AR, Scarisbrick IA. PLoS One. 2017 Jul 10;12(7):e0180697. doi: 10.1371/journal.pone.0180697. eCollection 2017. PMID: 28700615

92. Astrocyte phenotype in relation to Alzheimer-type pathology in the ageing brain. Simpson JE, Ince PG, Lace G, Forster G, Shaw PJ, Matthews F, Savva G, Brayne C, Wharton SB; MRC Cognitive Function and Ageing Neuropathology Study Group.

Neurobiol Aging. 2010 Apr;31(4):578-90. doi: 10.1016/j.neurobiolaging.2008.05.015. Epub 2008 Jun 30. PMID: 18586353

93. GABA from reactive astrocytes impairs memory in mouse models of Alzheimer's disease. Jo S, Yarishkin O, Hwang YJ, Chun YE, Park M, Woo DH, Bae JY, Kim T, Lee J, Chun H, Park HJ, Lee DY, Hong J, Kim HY, Oh SJ, Park SJ, Lee H, Yoon BE, Kim Y, Jeong Y, Shim I, Bae YC, Cho J, Kowall NW, Ryu H, Hwang E, Kim D, Lee CJ. Nat Med. 2014 Aug;20(8):886-96. doi: 10.1038/nm.3639. Epub 2014 Jun 29. PMID: 24973918

94. NFκB-activated astroglial release of complement C3 compromises neuronal morphology and function associated with Alzheimer's disease. Lian H, Yang L, Cole A, Sun L, Chiang AC, Fowler SW, Shim DJ, Rodriguez-Rivera J, Taglialatela G, Jankowsky JL, Lu HC, Zheng H. Neuron. 2015 Jan 7;85(1):101-115. doi: 10.1016/j.neuron.2014.11.018. Epub 2014 Dec 18. PMID: 25533482

95. Evidence for astrocytosis in prodromal Alzheimer disease provided by 11C-deuterium-L-deprenyl: a multitracer PET paradigm combining 11C-Pittsburgh compound B and 18F-FDG. Carter SF, Schöll M, Almkvist O, Wall A, Engler H, Långström B, Nordberg A. J Nucl Med. 2012 Jan;53(1):37-46. doi: 10.2967/jnumed.110.087031. PMID: 22213821

96. A reduced astrocyte response to β-amyloid plaques in the ageing brain associates with cognitive impairment. Mathur R, Ince PG, Minett T, Garwood CJ, Shaw PJ, Matthews FE, Brayne C, Simpson JE, Wharton SB; MRC Cognitive Function and Ageing Neuropathology Study Group. PLoS One. 2015 Feb 23;10(2):e0118463. doi: 10.1371/journal.pone.0118463. eCollection 2015. PMID: 25707004

97. Glial scar borders are formed by newly proliferated, elongated astrocytes that interact to corral inflammatory and fibrotic cells via STAT3-dependent mechanisms after spinal cord injury. Wanner IB, Anderson MA, Song B, Levine J, Fernandez A, Gray-Thompson Z, Ao Y, Sofroniew MV. J Neurosci. 2013 Jul 31;33(31):12870-86. doi: 10.1523/JNEUROSCI.2121-13.2013. PMID: 23904622

98. Attenuating astrocyte activation accelerates plaque pathogenesis in APP/PS1 mice. Kraft AW, Hu X, Yoon H, Yan P, Xiao Q, Wang Y, Gil SC, Brown J, Wilhelmsson U,

Restivo JL, Cirrito JR, Holtzman DM, Kim J, Pekny M, Lee JM. FASEB J. 2013 Jan;27(1):187-98. doi: 10.1096/fj.12-208660. Epub 2012 Oct 4. PMID: 23038755

99. Adult mouse astrocytes degrade amyloid-beta in vitro and in situ. Wyss-Coray T, Loike JD, Brionne TC, Lu E, Anankov R, Yan F, Silverstein SC, Husemann J. Nat Med. 2003 Apr;9(4):453-7. Epub 2003 Mar 3. PMID: 12612547

100. GFAP and vimentin deficiency alters gene expression in astrocytes and microglia in wild-type mice and changes the transcriptional response of reactive glia in mouse model for Alzheimer's disease. Kamphuis W, Kooijman L, Orre M, Stassen O, Pekny M, Hol EM. Glia. 2015 Jun;63(6):1036-56. doi: 10.1002/glia.22800. Epub 2015 Mar 2. PMID: 25731615

101. CXCR4-activated astrocyte glutamate release via TNFalpha: amplification by microglia triggers neurotoxicity. Bezzi P, Domercq M, Brambilla L, Galli R, Schols D, De Clercq E, Vescovi A, Bagetta G, Kollias G, Meldolesi J, Volterra A. Nat Neurosci. 2001 Jul;4(7):702-10. PMID: 11426226

102. Astrocytes are important mediators of Aβ-induced neurotoxicity and tau phosphorylation in primary culture. Garwood CJ, Pooler AM, Atherton J, Hanger DP, Noble W. Cell Death Dis. 2011 Jun 2;2:e167. doi: 10.1038/cddis.2011.50. PMID: 21633390

103. Tumor necrosis factor-alpha production by astrocytes. Induction by lipopolysaccharide, IFN-gamma, and IL-1 beta. Chung IY, Benveniste EN. J Immunol. 1990 Apr 15;144(8):2999-3007. PMID: 2109008

104. Human astrocytes: secretome profiles of cytokines and chemokines. Choi SS, Lee HJ, Lim I, Satoh J, Kim SU. PLoS One. 2014 Apr 1;9(4):e92325. doi: 10.1371/journal.pone.0092325. eCollection 2014. PMID: 24691121

105. The dual roles of cytokines in Alzheimer's disease: update on interleukins, TNF-α, TGF-β and IFN-γ. Zheng C, Zhou XW, Wang JZ. Transl Neurodegener. 2016 Apr 5;5:7. doi: 10.1186/s40035-016-0054-4. eCollection 2016. Review. PMID: 27054030

106. Preparation of separate astroglial and oligodendroglial cell cultures from rat cerebral tissue. McCarthy KD, de Vellis J. J Cell Biol. 1980 Jun;85(3):890-902. PMID: 6248568

107. Development of a method for the purification and culture of rodent astrocytes. Foo LC, Allen NJ, Bushong EA, Ventura PB, Chung WS, Zhou L, Cahoy JD, Daneman R, Zong H, Ellisman MH, Barres BA. Neuron. 2011 Sep 8;71(5):799-811. doi: 10.1016/j.neuron.2011.07.022. PMID: 21903074

108. Purification and Characterization of Progenitor and Mature Human Astrocytes Reveals Transcriptional and Functional Differences with Mouse. Zhang Y, Sloan SA, Clarke LE, Caneda C, Plaza CA, Blumenthal PD, Vogel H, Steinberg GK, Edwards MS, Li G, Duncan JA 3rd, Cheshier SH, Shuer LM, Chang EF, Grant GA, Gephart MG, Barres BA. Neuron. 2016 Jan 6;89(1):37-53. doi: 10.1016/j.neuron.2015.11.013. Epub 2015 Dec 10. PMID: 26687838

109. Culturing microglia from the neonatal and adult central nervous system. Bronstein R, Torres L, Nissen JC, Tsirka SE. J Vis Exp. 2013 Aug 9;(78):50647. doi: 10.3791/50647. PMID: 23962915

110. Dissection, plating, and maintenance of cortical astrocyte cultures. Albuquerque C, Joseph DJ, Choudhury P, MacDermott AB. Cold Spring Harb Protoc. 2009 Aug;2009(8):pdb.prot5273. doi: 10.1101/pdb.prot5273. No abstract available. PMID: 20147249

111. Primary cultures of astrocytes: their value in understanding astrocytes in health and disease. Lange SC, Bak LK, Waagepetersen HS, Schousboe A, Norenberg MD. Neurochem Res. 2012 Nov;37(11):2569-88. doi: 10.1007/s11064-012-0868-0. Epub 2012 Aug 28. Review. PMID: 22926576

112. Rat hippocampal neurons in dispersed cell culture. Banker GA, Cowan WM. Brain Res. 1977 May 13;126(3):397-42. PMID: 861729

113. Past, Present, and Future of Neuronal Models In Vitro. Keller JM, Frega M. Adv Neurobiol. 2019;22:3-17. doi: 10.1007/978-3-030-11135-9_1. Review. PMID: 31073930

114. Protocol for culturing low density pure rat hippocampal neurons supported by mature mixed neuron cultures. Yang Q, Ke Y, Luo J, Tang Y. J Neurosci Methods. 2017 Feb 1;277:38-45. doi: 10.1016/j.jneumeth.2016.12.002. Epub 2016 Dec 10. PMID: 27956052

115. New neurons and new memories: how does adult hippocampal neurogenesis affect learning and memory? Deng W, Aimone JB, Gage FH. Nat Rev Neurosci. 2010 May;11(5):339-50. doi: 10.1038/nrn2822. Epub 2010 Mar 31. Review. PMID: 20354534

116. Simultaneous analysis of dendritic spine density, morphology and excitatory glutamate receptors during neuron maturation in vitro by quantitative immunocytochemistry. Nwabuisi-Heath E, LaDu MJ, Yu C. J Neurosci Methods. 2012 Jun 15;207(2):137-47. doi: 10.1016/j.jneumeth.2012.04.003. Epub 2012 Apr 10. PMID: 22521963

117. Characterization of GABAergic neurons in hippocampal cell cultures. Benson DL, Watkins FH, Steward O, Banker G. J Neurocytol. 1994 May;23(5):279-95. PMID: 8089704

118. Culturing hippocampal and cortical neurons. Meberg PJ, Miller MW. Methods Cell Biol. 2003;71:111-27. PMID: 12884689

119. An improved method for growing neurons: Comparison with standard protocols. Pozzi D, Ban J, Iseppon F, Torre V. J Neurosci Methods. 2017 Mar 15;280:1-10. doi: 10.1016/j.jneumeth.2017.01.013. Epub 2017 Jan 27. PMID: 28137433

120. An Autaptic Culture System for Standardized Analyses of iPSC-Derived Human Neurons. Rhee HJ, Shaib AH, Rehbach K, Lee C, Seif P, Thomas C, Gideons E, Guenther A, Krutenko T, Hebisch M, Peitz M, Brose N, Brüstle O, Rhee JS. Cell Rep. 2019 May 14;27(7):2212-2228.e7. doi: 10.1016/j.celrep.2019.04.059. PMID: 31091457

121. Dysregulation of neuronal calcium homeostasis in Alzheimer's disease - A therapeutic opportunity? Popugaeva E, Pchitskaya E, Bezprozvanny I. Biochem Biophys Res Commun. 2017 Feb 19;483(4):998-1004. doi: 10.1016/j.bbrc.2016.09.053. Epub 2016 Sep 15. Review. PMID: 27641664

122. Optimized survival of hippocampal neurons in B27-supplemented Neurobasal, a new serum-free medium combination. Brewer GJ, Torricelli JR, Evege EK, Price PJ. J Neurosci Res. 19

123. Serum-Based Culture Conditions Provoke Gene Expression Variability in Mouse Embryonic Stem Cells as Revealed by Single-Cell Analysis. Guo G, Pinello L, Han X, Lai S, Shen L, Lin TW, Zou K, Yuan GC, Orkin SH. Cell Rep. 2016 Feb 2;14(4):956-965. doi: 10.1016/j.celrep.2015.12.089. Epub 2016 Jan 21. PMID: 26804902

124. NS21: re-defined and modified supplement B27 for neuronal cultures. Chen Y, Stevens B, Chang J, Milbrandt J, Barres BA, Hell JW. J Neurosci Methods. 2008 Jun 30;171(2):239-47. doi: 10.1016/j.jneumeth.2008.03.013. Epub 2008 Apr 1. PMID: 18471889

125. A plea to reduce or replace fetal bovine serum in cell culture media. Gstraunthaler G, Lindl T, van der Valk J. Cytotechnology. 2013 Oct;65(5):791-3. doi: 10.1007/s10616-013-9633-8. Epub 2013 Aug 22. No abstract available. PMID: 23975256

126. An inverted method for culturing dissociated mouse hippocampal neurons. Chen WS, Yueh CY, Huang YA, Hwang E. Neurosci Res. 2011 May;70(1):118-23. doi: 10.1016/j.neures.2011.01.002. Epub 2011 Jan 15. PMID: 21241744

127. Serum and depolarizing agents cause acute neurotoxicity in cultured cerebellar granule cells: role of the glutamate receptor responsive to N-methyl-D-aspartate. Schramm M, Eimerl S, Costa E. Proc Natl Acad Sci U S A. 1990 Feb;87(3):1193-7. PMID: 2153974

128. FACS-array profiling of striatal projection neuron subtypes in juvenile and adult mouse brains. Lobo MK, Karsten SL, Gray M, Geschwind DH, Yang XW. Nat Neurosci. 2006 Mar;9(3):443-52. Epub 2006 Feb 19. PMID: 16491081

129. Synapse-to-neuron ratio is inversely related to neuronal density in mature neuronal cultures. Cullen DK, Gilroy ME, Irons HR, Laplaca MC. Brain Res. 2010 Nov 4;1359:44-55. doi: 10.1016/j.brainres.2010.08.058. Epub 2010 Aug 25. PMID: 20800585

130. The establishment of polarity by hippocampal neurons in culture. Dotti CG, Sullivan CA, Banker GA. J Neurosci. 1988 Apr;8(4):1454-68. PMID: 3282038

131. Dendritic discrimination of temporal input sequences in cortical neurons. Branco T, Clark BA, Häusser M. Science. 2010 Sep 24;329(5999):1671-5. doi: 10.1126/science.1189664. Epub 2010 Aug 12. PMID: 20705816

132. Dendritic spines: structure, dynamics and regulation. Hering H, Sheng M. Nat Rev Neurosci. 2001 Dec;2(12):880-8. Review. PMID: 11733795

133. Analyzing dendritic spine pathology in Alzheimer's disease: problems and opportunities. Dorostkar MM, Zou C, Blazquez-Llorca L, Herms J. Acta Neuropathol. 2015 Jul;130(1):1-19. doi: 10.1007/s00401-015-1449-5. Epub 2015 Jun 11. Review. PMID: 26063233

134. Dissecting spatial knowledge from spatial choice by hippocampal NMDA receptor deletion. Bannerman DM, Bus T, Taylor A, Sanderson DJ, Schwarz I, Jensen V, Hvalby Ø, Rawlins JN, Seeburg PH, Sprengel R. Nat Neurosci. 2012 Jul 15;15(8):1153-9. doi: 10.1038/nn.3166. PMID: 22797694

135. Automated analysis of neuronal morphology, synapse number and synaptic recruitment. Schmitz SK, Hjorth JJ, Joemai RM, Wijntjes R, Eijgenraam S, de Bruijn P, Georgiou C, de Jong AP, van Ooyen A, Verhage M, Cornelisse LN, Toonen RF, Veldkamp WJ. J Neurosci Methods. 2011 Feb 15;195(2):185-93. doi: 10.1016/j.jneumeth.2010.12.011. Epub 2010 Dec 15. Erratum in: J Neurosci Methods. 2011 Apr 15;197(1):190. Veldkamp, Wouter [corrected to Veldkamp, Wouter J H]. PMID: 21167201

136. Neuron tracing in perspective. Meijering E. Cytometry A. 2010 Jul;77(7):693-704. doi: 10.1002/cyto.a.20895. Review. PMID: 20583273

137. SynPAnal: software for rapid quantification of the density and intensity of protein puncta from fluorescence microscopy images of neurons. Danielson E, Lee SH. PLoS

One. 2014 Dec 22;9(12):e115298. doi: 10.1371/journal.pone.0115298. eCollection 2014. Erratum in: PLoS One. 2015;10(3):e0118657. PMID: 25531531

138. Synaptophysin regulates activity-dependent synapse formation in cultured hippocampal neurons. Tarsa L, Goda Y. Proc Natl Acad Sci U S A. 2002 Jan 22;99(2):1012-6. Epub 2002 Jan 15. PMID: 11792847

139. Clinical neuropathology practice guide 5-2013: markers of neuronal maturation. Sarnat HB. Clin Neuropathol. 2013 Sep-Oct;32(5):340-69. doi: 10.5414/NP300638. Review. PMID: 23883617

140. Long-term culture of rat hippocampal neurons at low density in serum-free medium: combination of the sandwich culture technique with the three-dimensional nanofibrous hydrogel PuraMatrix. Kaneko A, Sankai Y. PLoS One. 2014 Jul 17;9(7):e102703. doi: 10.1371/journal.pone.0102703. eCollection 2014. PMID: 25032834

141. Neurite outgrowth in individual neurons of a neuronal population is differentially regulated by calcium and cyclic AMP. Mattson MP, Taylor-Hunter A, Kater SB. J Neurosci. 1988 May;8(5):1704-11. PMID: 2835450

142. Astrocytic neuroligins control astrocyte morphogenesis and synaptogenesis. Stogsdill JA, Ramirez J, Liu D, Kim YH, Baldwin KT, Enustun E, Ejikeme T, Ji RR, Eroglu C. Nature. 2017 Nov 8;551(7679):192-197. doi: 10.1038/nature24638. PMID: 29120426

143. Cell Biology of Astrocyte-Synapse Interactions. Allen NJ, Eroglu C. Neuron. 2017 Nov 1;96(3):697-708. doi: 10.1016/j.neuron.2017.09.056. Review. PMID: 29096081

144. Human Co-culture Model of Neurons and Astrocytes to Test Acute Cytotoxicity of Neurotoxic Compounds. De Simone U, Caloni F, Gribaldo L, Coccini T. Int J Toxicol. 2017 Nov/Dec;36(6):463-477. doi: 10.1177/1091581817739428. Epub 2017 Nov 19. PMID: 29153031

145. Evaluation of in vitro neuronal platforms as surrogates for in vivo whole brain systems. Belle AM, Enright HA, Sales AP, Kulp K, Osburn J, Kuhn EA, Fischer NO,

Wheeler EK. Sci Rep. 2018 Jul 17;f8(1):10820. doi: 10.1038/s41598-018-28950-5. PMID: 30018409

146. The use of ex Vivo Rodent Platforms in Neuroscience Translational Research with Attention to the 3Rs Philosophy. Lossi L, Merighi A. Front Vet Sci. 2018 Jul 19;5:164. doi: 10.3389/fvets.2018.00164. eCollection 2018. Review. PMID: 30073174

147. GSK-3β -induced Tau pathology drives hippocampal neuronal cell death in Huntington's disease: involvement of astrocyte-neuron interaction. L'Episcopo F, Drouin-Ouellet J, Tirolo C, Pulvirenti A, Giugno R, Testa N, Caniglia S, Serapide MF, Cisbani G, Barker RA, Cicchetti F, Marchetti B. Cell Death Dis. 2016 Apr 28;7:e2206. doi: 10.1038/cddis.2016.104. PMID: 27124580

148. Glia-neuron interactions in neurological diseases: Testing non-cell autonomy in a dish. Meyer K, Kaspar BK. Brain Res. 2017 Feb 1;1656:27-39. doi: 10.1016/j.brainres.2015.12.051. Epub 2016 Jan 9. Review. PMID: 26778174

149. Neuroprotective Effects of the Herbal Formular B401 in Both Cell and Mouse Models of Alzheimer's Disease. Hsu CH, Wang SE, Lin CL, Hsiao CJ, Sheu SJ, Wu CH. Evid Based Complement Alternat Med. 2016;2016:1939052. Epub 2016 Sep 28. PMID: 27761145

150. Role of IFN-γ and LPS on neuron/glial co-cultures infected by Neospora caninum. De Jesus EE, Santos AB, Ribeiro CS, Pinheiro AM, Freire SM, El-Bachá RS, Costa SL, de Fatima Dias Costa M. Front Cell Neurosci. 2014 Oct 27;8:340. doi: 10.3389/fncel.2014.00340. eCollection 2014. PMID: 25386119

151. Inflammatory processes induce beta-amyloid precursor protein changes in mouse brain. Brugg B, Dubreuil YL, Huber G, Wollman EE, Delhaye-Bouchaud N, Mariani J. Proc Natl Acad Sci U S A. 1995 Mar 28;92(7):3032-5. PMID: 7708769

152. The role of astrocytes in amyloid production and Alzheimer's disease.Frost GR, Li YM. Open Biol. 2017 Dec;7(12). pii: 170228. doi: 10.1098/rsob.170228. Review. PMID: 29237809

153. Porphyromonas gingivalis in Alzheimer's disease brains: Evidence for disease causation and treatment with small-molecule inhibitors. Dominy SS, Lynch C, Ermini F, Benedyk M, Marczyk A, Konradi A, Nguyen M, Haditsch U, Raha D, Griffin C, Holsinger LJ, Arastu-Kapur S, Kaba S, Lee A, Ryder MI, Potempa B, Mydel P, Hellvard A, Adamowicz K, Hasturk H, Walker GD, Reynolds EC, Faull RLM, Curtis MA, Dragunow M, Potempa J. Sci Adv. 2019 Jan 23;5(1):eaau3333. doi: 10.1126/sciadv.aau3333. eCollection 2019 Jan. PMID: 30746447

154. High-content screening of primary neurons: ready for prime time. Daub A, Sharma P, Finkbeiner S. Curr Opin Neurobiol. 2009 Oct;19(5):537-43. doi: 10.1016/j.conb.2009.10.002. Epub 2009 Nov 4. Review. PMID: 19889533

155. High-throughput screening in primary neurons. Sharma P, Ando DM, Daub A, Kaye JA, Finkbeiner S. Methods Enzymol. 2012;506:331-60. doi: 10.1016/B978-0-12-391856-7.00041-X. PMID: 22341232

156. A model for neural development and treatment of Rett syndrome using human induced pluripotent stem cells. Marchetto MC, Carromeu C, Acab A, Yu D, Yeo GW, Mu Y, Chen G, Gage FH, Muotri AR. Cell. 2010 Nov 12;143(4):527-39. doi: 10.1016/j.cell.2010.10.016. PMID: 21074045

157. Physiological maturation and drug responses of human induced pluripotent stem cell-derived cortical neuronal networks in long-term culture. Odawara A, Katoh H, Matsuda N, Suzuki I. Sci Rep. 2016 May 18;6:26181. doi: 10.1038/srep26181. PMID: 27188845

158. Thiamine metabolism is critical for regulating correlated growth of dendrite arbors and neuronal somata. Liu H, Sang S, Lu Y, Wang Z, Yu X, Zhong C. Sci Rep. 2017 Jul 13;7(1):5342. doi: 10.1038/s41598-017-05476-w. PMID: 28706281

159. Methylferulate from Tamarix aucheriana inhibits growth and enhances chemosensitivity of human colorectal cancer cells: possible mechanism of action. Abaza MS, Afzal M, Al-Attiyah RJ, Guleri R. BMC Complement Altern Med. 2016 Oct 1;16(1):384. PMID: 27716288

160. Loss of human Greatwall results in G2 arrest and multiple mitotic defects due to deregulation of the cyclin B-Cdc2/PP2A balance. Burgess A, Vigneron S, Brioudes E, Labbé JC, Lorca T, Castro A. Proc Natl Acad Sci U S A. 2010 Jul 13;107(28):12564-9. doi: 10.1073/pnas.0914191107. Epub 2010 Jun 10. PMID: 20538976

161. Quantitative immunofluorescence assay to measure the variation in protein levels at centrosomes. Majumder S, Fisk HA. J Vis Exp. 2014 Dec 20;(94). doi: 10.3791/52030. PMID: 25548932

162. Src tyrosine kinase signaling antagonizes nuclear localization of FOXO and inhibits its transcription factor activity. Bülow MH, Bülow TR, Hoch M, Pankratz MJ, Jünger MA. Sci Rep. 2014 Feb 11;4:4048. doi: 10.1038/srep04048. Erratum in: Sci Rep. 2014;4:5137. PMID: 24513978

163. Partial inhibition of Cdk1 in G2 phase overrides the SAC and decouples mitotic events. McCloy RA, Rogers S, Caldon CE, Lorca T, Castro A, Burgess A. Cell Cycle. 2014;13(9):1400-12. doi: 10.4161/cc.28401. Epub 2014 Mar 6. PMID: 24626186

164. Pericytes control key neurovascular functions and neuronal phenotype in the adult brain and during brain aging. Bell RD, Winkler EA, Sagare AP, Singh I, LaRue B, Deane R, Zlokovic BV. Neuron. 2010 Nov 4;68(3):409-27. doi: 10.1016/j.neuron.2010.09.043. PMID: 21040844

165. Variable expression levels of keratin and vimentin reveal differential EMT status of circulating tumor cells and correlation with clinical characteristics and outcome of patients with metastatic breast cancer. Polioudaki H, Agelaki S, Chiotaki R, Politaki E, Mavroudis D, Matikas A, Georgoulias V, Theodoropoulos PA. BMC Cancer. 2015 May 13;15:399. doi: 10.1186/s12885-015-1386-7. PMID: 25962645

166. Semiautomated Sholl analysis for quantifying changes in growth and differentiation of neurons and glia. Gensel JC, Schonberg DL, Alexander JK, McTigue DM, Popovich PG. J Neurosci Methods. 2010 Jun 30;190(1):71-9. doi: 10.1016/j.jneumeth.2010.04.026. Epub 2010 May 11. PMID: 20438758

167. Automated analysis of neurite branching in cultured cortical neurons using HCA-Vision.Vallotton P, Lagerstrom R, Sun C, Buckley M, Wang D, De Silva M, Tan SS, Gunnersen JM. Cytometry A. 2007 Oct;71(10):889-95. PMID: 17868085

168. Neuronal morphometry directly from bitmap images. Ferreira TA, Blackman AV, Oyrer J, Jayabal S, Chung AJ, Watt AJ, Sjöström PJ, van Meyel DJ. Nat Methods. 2014 Oct;11(10):982-4. doi: 10.1038/nmeth.3125. No abstract available. PMID: 25264773

169. A fast and accurate procedure for deriving the Sholl profile in quantitative studies of neuronal morphology. Gutierrez H, Davies AM. J Neurosci Methods. 2007 Jun15;163(1):24-30. Epub 2007 Feb 11. PMID: 17367866

170. Quantifying synapses: an immunocytochemistry-based assay to quantify synapse number. Ippolito DM, Eroglu C. J Vis Exp. 2010 Nov 16;(45). pii: 2270. doi: 10.3791/2270. PMID: 21113117

171. ImageJ for microscopy. Collins TJ. Biotechniques. 2007 Jul;43(1 Suppl):25-30. Review. PMID: 17936939

172. Protective effects of testosterone on presynaptic terminals against oligomeric β-amyloid peptide in primary culture of hippocampal neurons. Lau CF, Ho YS, Hung CH, Wuwongse S, Poon CH, Chiu K, Yang X, Chu LW, Chang RC. Biomed Res Int. 2014;2014:103906. doi: 10.1155/2014/103906. Epub 2014 Jun 18. PMID: 25045655

173. Exosomal cellular prion protein drives fibrillization of amyloid beta and counteracts amyloid beta-mediated neurotoxicity. Falker C, Hartmann A, Guett I, Dohler F, Altmeppen H, Betzel C, Schubert R, Thurm D, Wegwitz F, Joshi P, Verderio C, Krasemann S, Glatzel M. J Neurochem. 2016 Apr;137(1):88-100. doi: 10.1111/jnc.13514. Epub 2016 Mar 2. PMID: 26710111

174. Dendritic organization in the neurons of the visual and motor cortices of the cat. SHOLL DA. J Anat. 1953 Oct;87(4):387-406. No abstract available. PMID: 13117757

175. Rapid colorimetric assay for cellular growth and survival: application to proliferation and cytotoxicity assays. Mosmann T. J Immunol Methods. 1983 Dec 16;65(1-2):55-63. PMID: 6606682

176. Ammonia-containing dimethyl sulfoxide: an improved solvent for the dissolution of formazan crystals in the 3-(4,5-dimethylthiazol-2-yl)-2,5-diphenyl tetrazolium bromide (MTT) assay. Wang H, Wang F, Tao X, Cheng H. Anal Biochem. 2012 Feb 1;421(1):324-6. doi: 10.1016/j.ab.2011.10.043. Epub 2011 Nov 3. PMID: 22100715

177. Plate reader-based assays for measuring cell viability, neuroprotection and calcium in primary neuronal cultures. Burroughs SL, Duncan RS, Rayudu P, Kandula P, Payne AJ, Clark JL, Koulen P, Kaja S. J Neurosci Methods. 2012 Jan 15;203(1):141-5. doi: 10.1016/j.jneumeth.2011.09.007. Epub 2011 Sep 24. PMID: 21968036

178. Differentiation of human adipose-derived stem cells into neuron-like cells which are compatible with photocurable three-dimensional scaffolds. Gao S, Zhao P, Lin C, Sun Y, Wang Y, Zhou Z, Yang D, Wang X, Xu H, Zhou F, Cao L, Zhou W, Ning K, Chen X, Xu J. Tissue Eng Part A. 2014 Apr;20(7-8):1271-84. doi: 10.1089/ten.TEA.2012.0773. PMID: 24251600

179. Use of multiple assay endpoints to investigate the effects of incubation time, dose of toxin and plating density in cell-based cytotoxicity assays. Riss TL, Moravec RA. Assay Drug Dev Technol. 2004 Feb;2(1):51-62. PMID: 15090210

180. Psychedelics Promote Structural and Functional Neural Plasticity. Ly C, Greb AC, Cameron LP, Wong JM, Barragan EV, Wilson PC, Burbach KF, Soltanzadeh Zarandi S, Sood A, Paddy MR, Duim WC, Dennis MY, McAllister AK, Ori-McKenney KM, Gray JA, Olson DE. Cell Rep. 2018 Jun 12;23(11):3170-3182. doi: 10.1016/j.celrep.2018.05.022. PMID: 29898390

181. An Autaptic Culture System for Standardized Analyses of iPSC-Derived Human Neurons. Rhee HJ, Shaib AH, Rehbach K, Lee C, Seif P, Thomas C, Gideons E, Guenther A, Krutenko T, Hebisch M, Peitz M, Brose N, Brüstle O, Rhee JS. Cell Rep. 2019 May 14;27(7):2212-2228.e7. doi: 10.1016/j.celrep.2019.04.059. PMID: 31091457

181. Astrocytes usurp neurons as a disease focus. Liddelow SA, Sofroniew MV. Nat Neurosci. 2019 Apr;22(4):512-513. doi: 10.1038/s41593-019-0367-6. No abstract available. PMID: 30858602

182. NeuronGlia Interactions Increase Neuronal Phenotypes in Tuberous Sclerosis Complex Patient iPSC-Derived Models. Nadadhur AG, Alsaqati M, Gasparotto L, Cornelissen-Steijger P, van Hugte E, Dooves S, Harwood AJ, Heine VM. Stem Cell Reports. 2019 Jan 8;12(1):42-56. doi: 10.1016/j.stemcr.2018.11.019. Epub 2018 Dec 20. PMID: 30581017

183. Astrocytes and microglia: Models and tools. Guttenplan KA, Liddelow SA. J Exp Med. 2019 Jan 7;216(1):71-83. doi: 10.1084/jem.20180200. Epub 2018 Dec 12. Review. PMID: 30541903

184. Astrocytes are important mediators of Aβ-induced neurotoxicity and tau phosphorylation in primary culture. Garwood CJ, Pooler AM, Atherton J, Hanger DP, Noble W. Cell Death Dis. 2011 Jun 2;2:e167. doi: 10.1038/cddis.2011.50. PMID: 21633390

185. Notch signaling in astrocytes mediate their morphological response to an inflammatory challenge. Acaz-Fonseca E, Ortiz-Rodriguez A, Azcoitia I, Garcia-Segura LM, Arevalo MA. Cell Death Discov. 2019 Apr 3;5:85. doi: 10.1038/s41420-019-0166-6. eCollection 2019. PMID: 30962951

186. In vitro evaluation of reactive astrocyte migration, a component of tissue remodeling in glaucomatous optic nerve head. Tezel G, Hernandez MR, Wax MB. Glia. 2001 May;34(3):178-89. PMID: 11329180

187. Lithium Ameliorates LPS Induced Astrocytes Activation Partly via Inhibition of Toll-Like Receptor 4 Expression. Li N, Zhang X, Dong H, Zhang S, Sun J, Qian Y. Cell Physiol Biochem. 2016;38(2):714-25. doi: 10.1159/000443028. Epub 2016 Feb 15. PMID: 26870942

188. In vitro and in vivo activation of astrocytes by amyloid-beta is potentiated by pro-oxidant agents. García-Matas S, de Vera N, Aznar AO, Marimon JM, Adell A, Planas AM, Cristòfol R, Sanfeliu C. J Alzheimers Dis. 2010;20(1):229-45. doi: 10.3233/JAD-2010-1365. PMID: 20164580

189. Phenotypic polarization of activated astrocytes: the critical role of lipocalin-2 in the classical inflammatory activation of astrocytes. Jang E, Kim JH, Lee S, Kim JH, Seo JW, Jin M, Lee MG, Jang IS, Lee WH, Suk K. J Immunol. 2013 Nov 15;191(10):5204-19. doi: 10.4049/jimmunol.1301637. Epub 2013 Oct 2. PMID: 24089194

190. Neuronal mTORC1 Is Required for Maintaining the Nonreactive State of Astrocytes. Zhang Y, Xu S, Liang KY, Li K, Zou ZP, Yang CL, Tan K, Cao X, Jiang Y, Gao TM, Bai XC. J Biol Chem. 2017 Jan 6;292(1):100-111. doi: 10.1074/jbc.M116.744482. Epub 2016 Nov 28. PMID: 27895121

191. The Regulatory Machinery of Neurodegeneration in In Vitro Models of Amyotrophic Lateral Sclerosis. Ikiz B, Alvarez MJ, Ré DB, Le Verche V, Politi K, Lotti F, Phani S, Pradhan R, Yu C, Croft GF, Jacquier A, Henderson CE, Califano A, Przedborski S. Cell Rep. 2015 Jul 14;12(2):335-45. doi: 10.1016/j.celrep.2015.06.019. Epub 2015 Jul 2. PMID: 26146077

192. Timing is everything: making neurons versus glia in the developing cortex. Miller FD, Gauthier AS. Neuron. 2007 May 3;54(3):357-69. Review. PMID: 17481390

193. Generation and assembly of human brain region-specific three-dimensional cultures. Sloan SA, Andersen J, Pașca AM, Birey F, Pașca SP. Nat Protoc. 2018 Sep;13(9):2062-2085. doi: 10.1038/s41596-018-0032-7. PMID: 30202107

194. A 3D human triculture system modeling neurodegeneration and neuroinflammation in Alzheimer's disease. Park J, Wetzel I, Marriott I, Dréau D, D'Avanzo C, Kim DY, Tanzi RE, Cho H. Nat Neurosci. 2018 Jul;21(7):941-951. doi: 10.1038/s41593-018-0175-4. Epub 2018 Jun 27. PMID: 29950669

195. Beyond the neuron-cellular interactions early in Alzheimer disease pathogenesis. Henstridge CM, Hyman BT, Spires-Jones TL. Nat Rev Neurosci. 2019 Feb;20(2):94-108. doi: 10.1038/s41583-018-0113-1. Review. PMID: 30643230

196. Image-Based Profiling of Synaptic Connectivity in Primary Neuronal Cell Culture. Verstraelen P, Van Dyck M, Verschuuren M, Kashikar ND, Nuydens R, Timmermans JP, De Vos WH. Front Neurosci. 2018 Jun 26;12:389. doi: 10.3389/fnins.2018.00389. eCollection 2018. Review. PMID: 29997468

8. ACKNOWLEDGEMENTS

I am indebted to:

Prof. Dr. med. Markus Glatzel who gave me the unique opportunity to work in a scientifically excellent environment, provided research funding, supervision and support to me.

PD Dr. rer. nat. Susanne Krasemann and Dr. med. Diego Sepulveda-Falla for dedicating their time and effort to supervise me, provide me with scientific advice and helping with troubleshooting, offering valuable and motivational discussions, and regular support throughout research and writing. Thank you both for your patience!

Beata Szalay for her help including introduction into laboratory techniques and excellent technical assistance.

The whole team and staff of the Institute of Neuropathology for the motivation, the support as well as interesting and fruitful scientific discussions, particularly Behnam Mohammadi, Liliana Rojas Charry, Christian Linnenberg, who showed patience, who were cooperative and willing to apply the co-culture assay in their work.

Dr. Antononio Virgilio Failla and Dr. Bernd Zobiak from the UKE Microscopy Imaging Facility for confocal microscopy-related assistance and help.

The whole staff of the animal facility at the UKE for support throughout mouse work.

Furthermore, I would like to thank Dr. rer. nat. Dorthe Labonté and Prof. Dr. rer. nat. Thomas Braulke for giving me the chance to be part of the Research Training Group (RTG) 1459/Graduiertenkolleg (GRK) 1459, the scholarship provided by the programme and their effort to organize all the seminars, workshops, symposia and retreats.

9. CURRICULUM VITAE

Der Lebenslauf wurde aus datenschutzrechtlichen Gründen in der elektronischen Version nicht veröffentlicht.

10. EIDESSTAATLICHE ERKLÄRUNG

[als letztes Blatt in die Dissertation einzubinden]

Ich versichere ausdrücklich, dass ich die Arbeit selbstständig und ohne fremde Hilfe verfasst, andere als die von mir angegebenen Quellen und Hilfsmittel nicht benutzt und die aus den benutzten Werken wörtlich oder inhaltlich entnommenen Stellen einzeln nach Ausgabe (Auflage und Jahr des Erscheinens), Band und Seite des benutzten Werkes kenntlich gemacht habe.

Ferner versichere ich, dass ich die Dissertation bisher nicht einem Fachvertreter an einer anderen Hochschule zur Überprüfung vorgelegt oder mich anderweitig um Zulassung zur Promotion beworben habe.

Ich erkläre mich einverstanden, dass meine Dissertation vom Dekanat der Medizinischen Fakultät mit einer gängigen Software zur Erkennung von Plagiaten überprüft werden kann.

Unterschrift: David Wasilewski